

# **Application of the Geostatistical Program NOMAD-KRIBS to Geoenvironmental Problems**

by

**Maria – Aikaterini Nikolinakou**

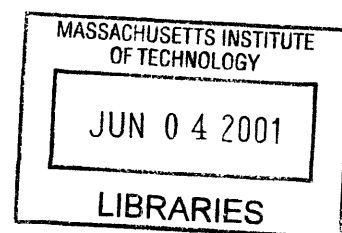
Diploma, Civil Engineering (1999)  
National Technical University of Athens, Greece

Submitted to the Department of Civil and Environmental Engineering  
in Partial Fulfillment of the Requirements for the degree of  
Master of Science in Civil and Environmental Engineering

at the

Massachusetts Institute of Technology  
June 2001

© 2001 Massachusetts Institute of Technology  
All rights reserved



ENG

Signature of Author.....  
Department of Civil and Environmental Engineering  
May 11, 2001

Certified by.....  
Prof. Herbert H. Einstein  
Professor of Civil and Environmental Engineering  
Thesis Supervisor

Accepted by.....  
Prof. Oral Buyukozturk  
Chairman, Departmental Committee on Graduate Studies



Room 14-0551  
77 Massachusetts Avenue  
Cambridge, MA 02139  
Ph: 617.253.2800  
Email: [docs@mit.edu](mailto:docs@mit.edu)  
<http://libraries.mit.edu/docs>

## **DISCLAIMER OF QUALITY**

Due to the condition of the original material, there are unavoidable flaws in this reproduction. We have made every effort possible to provide you with the best copy available. If you are dissatisfied with this product and find it unusable, please contact Document Services as soon as possible.

Thank you.

The images contained in this document are of the best quality available.



# **Application of the Geostatistical Program NOMAD-KRIBS to Geoenvironmental Problems**

by

**Maria – Aikaterini Nikolinakou**

Submitted to the Department of Civil and Environmental Engineering  
on May 11, 2001, in Partial Fulfillment of the Requirements for the degree of  
Master of Science in Civil and Environmental Engineering

## **Abstract**

NOMAD-KRIBS is a computer based 3-D ground profiler that enables one to represent, edit, translate and rotate subsurface information and to interactively produce cross sections. Input data can be any geotechnical information from ground types to Atterberg limits. KRIBS generates geostatistical profiles and it offers the capability of incorporating subjective, and objective information for updating the soil profile.

In this thesis the program was used to study geoenvironmental problems that involve changes of spatial configuration with time. The Wellesley case study showed that NOMAD can indeed illustrate data changing with time. Furthermore, an important feature that the program introduces to geoenvironmental problems is the representation of well logs on the vertical plane. Finally, a theoretical approach was proposed for modifying KRIBS to be able to incorporate non-stationary hydrological data.

Thesis supervisor: Herbert H. Einstein

Title: Professor of Civil and Environmental Engineering, MIT





## Acknowledgments

I am grateful to my supervisor, Prof. Einstein for his input and support during this project, which sometimes seemed not to work. I would like to thank Prof. Culligan and Prof. Veneziano for their help on special topics of this thesis, and Prof. Whittle for his questions about the program.

I would also like to thank the Northeast Hazardous Substance Research Center for their funding, the Massachusetts Highway Department and especially Ann Roche for the Wellesley Depot site data they provided to me.

Special thanks are also due to Patrick Kinnicutt for his distance help on software problems.

Talking about distance, I would like to thank my parents and sisters in Greece for their support.

These first two years at MIT would have been much more difficult without Yannis Chatzigiannelis, and George Kokosalakis-Dominic Assimaki, my classmates with which we tied up so well together, Michalis Aftias and my other Greek friends, Aggeliki Stathopoulou-Yannis Papamichail in London, Fotis Fotopoulos and Ricardo Garcia.

*“No one’s certain what your future will behold” (Nomad)*



# TABLE OF CONTENTS

<b>Chapter 1: Introduction</b>	<b>15</b>
<b>Chapter 2: NOMAD - KRIBS</b>	<b>19</b>
2.1 Introduction	19
2.2 Nomad	19
2.3 KRIBS	23
2.3.1 <i>Description of the program</i>	23
2.3.2 <i>KRIBS algorithm</i>	26
2.4 KRIBS model	27
<b>Chapter 3: Geostatistical concepts</b>	<b>31</b>
3.1 Introduction	31
3.2 Ordinary Kriging	31
3.2.1 <i>Introduction to Ordinary kriging</i>	31
3.2.2 <i>Main principle</i>	32
3.2.3 <i>Comments</i>	34
3.3 Spatial description of a data set	36
3.3.1 <i>Definitions</i>	36
3.3.2 <i>Characteristic parameters of a semi-variogram:</i>	38
3.3.3 <i>Semi-variogram models</i>	39
3.3.4 <i>Effect of Variogram characteristics</i>	44
3.3.5 <i>Conclusion</i>	46
3.4 Anisotropy	46
3.4.1 <i>General</i>	46
3.4.2 <i>Models of anisotropy</i>	46
3.5 CoKriging	49
3.5.1 <i>Introduction</i>	49
3.5.2. <i>Main Principle-CoKriging system for 2 variables.</i>	49
3.5.3. <i>Comments</i>	51
3.6 Block kriging	51
3.6.1 <i>Main principle</i>	51

3.6.2 Comments	52
3.7 Bayesian updating	53
3.7.1 Bayesian Analysis	53
3.7.2 Bayes' Theorem	53
3.7.3 Appropriate PDF functions	54
<b>Chapter 4: Research in geostatistics</b>	<b>55</b>
4.1 Introduction	55
4.2 Covariance Function Determination	55
4.3 Computational Methods	56
4.4 Kriging Methods	57
4.5 Subsurface modeling	58
4.6 Multipoint statistics	60
4.7 Future research	61
4.7.1 Method proposed by Journel	61
4.7.2 3-D Kriging	62
<b>Chapter 5: Application of Nomad-KRIBS to MBTA Red Line extension from Porter Sq. to Davis Sq.</b>	<b>65</b>
5.1 Introduction	65
5.2. Interpretation of the geological information.	65
5.3 Nomad	65
5.4. KRIBS	69
5.5 Educational part	77
<b>Chapter 6: Data changing with time: The Wellesley Maintenance Depot Site</b>	<b>79</b>
6.1 Introduction	79
6.2 History of the site	80
6.3 Geologic representation of the site.	81
6.3.1 Geology and geological profiles	81
6.3.2 Geostatistical profiles	86
6.3.3 Interpretation of the geology with respect to expected permeabilities	93
6.4 Hydrogeological data	94
6.4.1 Early years: 1993-1996	96
6.4.2 Later years: 1997-2000	100
6.4.3 Review of NOMAD representation	109

6.4.4 Application of KRIBS	110
<b>Chapter 7: Conclusions and future recommendations</b>	<b>115</b>
<b>References</b>	<b>117</b>
<b>Appendix 1: Creating profiles with NOMAD</b>	<b>121</b>
I.1 Nomad	123
I.2 General	123
I.3 Creating the input file	123
I.4 Program's environment	124
<b>APPENDIX II: Borehole data for MBTA Porter Sq.–Davis Sq. case study</b>	<b>129</b>
<b>APPENDIX III: Geostatistical profiles for the MBTA Porter Sq. to Davis Sq. case study</b>	<b>137</b>
III.1 Exponential model - Coarse grid: (x,y,z)=(50,50,5) (ft)	139
III.2 Exponential model - Medium grid: (x,y,z)=(5,5,5) (ft)	141
III.3 Exponential model - Fine grid: (x,y,z)=(1,1,1) (ft)	143
III.4 Spherical model - Medium grid: (x,y,z)=(5,5,5) (ft)	146
<b>APPENDIX IV: Borehole and hydrogeological data for the Wellesley Maintenance Depot case study</b>	<b>149</b>
<b>APPENDIX V: Contamination treatment techniques in site remediation: Soil vapor extraction and Air sparging</b>	<b>173</b>
V.1: Soil vapor extraction	175
V.2: Air Sparging	177



## TABLE OF FIGURES

Figure 2.1: Spreadsheet containing input information for NOMAD.	20
Figure 2.2: General view of NOMAD interface.	21
Figure 2.3: Rotational features of NOMAD.	21
Figure 2.4: Edit menu.	24
Figure 2.5: Cross sections in NOMAD.	23
Figure 2.6: Experimental semi-variograms and fitted models.	24
Figure 2.7: Kriged profile (from MBTA Porter Sq. to Davis Sq. case study).	25
Figure 2.8: Kriged profiles with probability threshold 25% and 50%	25
Figure 2.9: The probability wheel.	26
Figure 2.10: KRIBS algorithm.	27
Figure 2.11: Lag angle determining which pairs of data will be examined.	28
Figure 3.1: Pairing of data to obtain an h-scatterplot.	36
Figure 3.2: h-scatterplots capturing spatial distribution of a variable V, for different values of h.	37
Figure 3.3: Sill s and Range a of a semi-variogram.	39
Figure 3.4: Complete variogram surface.	39
Figure 3.5: Relative plot of gaussian, exponential and spherical models.	42
Figure 3.6: Linear model.	43
Figure 3.7: Scale effect.	45
Figure 3.8: Shape effect.	45
Figure 3.9: Nugget effect.	45
Figure 3.10: Range effect.	45
Figure 3.11a: Geometric anisotropy.	47
Figure 3.11b: Zonal anisotropy.	47
Figure 3.11c: Combination of Geometric and Zonal anisotropy.	47
Figure 3.12: Directional variogram models along the axis (x,y,z) of a three-dimensional geometric anisotropy.	48
Figure 3.13: Block Kriging.	51
Figure 4.1: Geologic formations are reconstructed using solid modeling.	59
Figure 4.2: Triangulation Irregular Network (TIN) technique.	60
Figure 4.3: Basic Principles of directional Variograms.	62
Figure 4.4: 18 directional semi-variograms along different directions plotted in the same set of axes.	63
Figure 4.5: Contoured 2-D variogram surface.	63
Figure 5.1a: Map of Porter Sq. to Davis Sq. alignment; Section of Porter Sq.	66
Figure 5.1b: Map of Porter Sq. to Davis Sq. alignment; Section of Davis Sq.	66



Figure 5.2: Borehole locations and alignment between Porter Sq. and Davis Sq.	67
Figure 5.3: Borehole logs inserted into Nomad environment.	67
Figure 5.4 – Porter Sq.: Borehole information and geological profile.	68
Figure 5.5 - Porter Sq.: Geological profile.	69
Figure 5.6a: Profile resulting from a coarse grid, (x-y-z)=(50-50-5) (ft).	70
Figure 5.6b: Profile resulting from a medium grid, (x-y-z)=(5-5-5) (ft).	70
Figure 5.6c: Profile resulting from a fine grid, (x-y-z)=(1-1-1) (ft)	71
Figure 5.7 - Porter Sq.: Experimental semi-variograms and exponential variogram models	72
Figure 5.8 - Porter Sq.: Experimental semi-variograms and spherical variogram models.	73
Figure 5.9: Geostatistical profile from kriging analysis based on an exponential model-Probability threshold 0%	74
Figure 5.10: Geostatistical profile from kriging analysis based on a spherical model-Probability threshold 0%	74
Figures 5.11a: Kriged profile with probability threshold 30%.	75
Figures 5.11b: Kriged profile with probability threshold 50%.	75
Figure 5.12: Semi-variogram models fitting the experimental data with small ranges.	76
Figure 5.13: Kriged profile with small range values-threshold 0%.	77
Figure 6.1: General view of the site.	80
Figure 6.2: Plan view of the site.	82
Figure 6.3: Profile along A-A.	83
Figure 6.4: Colored profile along A-A.	83
Figure 6.5: Profile along B-B.	84
Figure 6.6: Colored profile along B-B.	84
Figure 6.7: Profile along C-C.	85
Figure 6.8: Colored profile along C-C.	85
Figure 6.9: Experimental semi-variograms and semi-variogram models.	87
Figure 6.10: Geostatistical profile along A-A – probability threshold 0%	87
Figure 6.11: Geostatistical profile along A-A – probability threshold 35%	88
Figure 6.12: Geostatistical profile along A-A – probability threshold 50%	88
Figure 6.13: Experimental semi-variograms and variogram models for profile B-B.	89
Figure 6.14: Geostatistical profile along B-B – probability threshold 0%	89
Figure 6.15: Geostatistical profile along B-B – probability threshold 35%	90
Figure 6.16: Geostatistical profile along B-B – probability threshold 50%	90
Figure 6.17: Experimental semi-variograms and variogram models for profile C-C.	91
Figure 6.18: Geostatistical profile along C-C – probability threshold 0%	91
Figure 6.19: Geostatistical profile along C-C – probability threshold 35%	92

Figure 6.20: Geostatistical profile along C-C – probability threshold 50%	92
Figure 6.21: The 25 most frequently detected groundwater contaminants at hazardous waste sites.	94
Figure 6.22: Sample representation of concentrations using NOMAD.	95
Figure 6.23: Acetone, 1993.	96
Figure 6.24: Acetone, 1996.	96
Figure 6.25: Arsenic, 1993.	97
Figure 6.26: Arsenic, 1996.	97
Figure 6.27: Benzene, 1993.	98
Figure 6.28: Benzene, 1996.	98
Figure 6.29: Toluene, 1993.	99
Figure 6.30: Toluene, 1996.	99
Figure 6.31: TCE plume prior to cleaning (April 1997).	100
Figure 6.32: Plan view of the wells monitoring Trichloroethane concentrations during years 1997-2000.	102
Figure 6.33: Tabulated concentrations for Trichloroethane over time.	102
Figure 6.34: Concentrations for Trichloroethane over time at well locations.	103
Figure 6.35: Concentrations for Trichloroethane over time at well locations, excluding the very high ones at ABB-15.	103
Figure 6.36: Trichloroethane, 1997.	105
Figure 6.37: Trichloroethane, February 1998.	105
Figure 6.38: Trichloroethane, April 1998.	106
Figure 6.39: Trichloroethane, May 1998.	106
Figure 6.40: Trichloroethane, July 1998.	107
Figure 6.41: Trichloroethane, September 1998.	107
Figure 6.42: Trichloroethane, 1999.	108
Figure 6.43: Trichloroethane, 2000.	108
Figure 6.44: Representation of TCE concentrations using the conventional contour plot	109
Figure 6.45: True log(c) surface (unknown) and fitted surface.	111
Figure I.1: Example of input spreadsheet.	124
Figure I.2: Nomad menu options.	125
Figure I.3: Nomad main window.	125
Figure I.4: Shortcut buttons.	125
Figure I.5: Explanation of shortcut buttons.	126
Figure I.6: The Edit menu.	126
Figure I.7: Example of a Ground types legend.	126
Figure I.8: Nomad window with imported borehole data.	127
Figure I.9: Rotated profile with layers.	127

Figure I.10: Model with curved lines.	128
Figure III.1: Experimental semi-variograms and exponential semi-variogram models -coarse grid.	139
Figure III.2: Kriged profile - exponential model - coarse grid – threshold 0%	140
Figure III.3: Kriged profile - exponential model - coarse grid – threshold 30%	140
Figure III.4: Kriged profile - exponential model - coarse grid – threshold 50%	141
Figure III.5: Experimental semi-variograms and exponential semi-variogram models -medium grid.	141
Figure III.6: Kriged profile - exponential model - medium grid – threshold 0%	142
Figure III.7: Kriged profile - exponential model - medium grid – threshold 30%	142
Figure III.8: Kriged profile - exponential model - medium grid – threshold 50%	143
Figure III.9: Experimental semi-variograms and exponential semi-variogram models - fine grid.	143
Figure III.10: Kriged profile - exponential model - fine grid – threshold 0%	144
Figure III.11: Kriged profile - exponential model - fine grid – threshold 30%	144
Figure III.12: Kriged profile - exponential model - fine grid – threshold 40%	145
Figure III.13: Kriged profile - exponential model - fine grid – threshold 50%	145
Figure III.14: Experimental semi-variograms and spherical semi-variogram models-medium grid.	146
Figure III.15: Kriged profile - spherical model - medium grid – threshold 0%	146
Figure III.16: Kriged profile - spherical model - medium grid – threshold 30%	147
Figure III.17: Kriged profile - spherical model - medium grid – threshold 50%	147
Figure V.1: Principle of soil vapor extraction.	175
Figure V.2: Examples of extraction wells.	176
Figure V.3: List of contaminants that can be cleaned up using soil vapor extraction.	176
Figure V.4: Principle of air sparging system.	177

## Chapter 1: Introduction

The understanding and representation of the geological subsurface is the essential first step in all major projects in geotechnical and geoenvironmental engineering. Usually the information available for drawing geologic profiles is limited to data coming from boreholes (soil descriptions, SPT data, lithology, or RQD values, depending on the nature of the ground). Given a plan view of the site, alignments of cross sections are specified, and the boreholes, which fall within a certain distance from the alignment, are projected onto the vertical plane containing the alignment.

The procedure of geologic cross-section drawing used to be manual, but now computers are used to automatically create geologic profiles, based on the borehole data that has already been recorded in a spreadsheet. The main disadvantage of these methods is that programs usually do linear interpolation and the geologic judgement is in most cases ignored. Also programs do not often include options for updating the profiles according to changes in the given data, resulting for example from updated subsurface exploration or geologist beliefs.

In this context, geostatistics can provide more formal methods of visualizing the subsurface and they can furthermore offer means of evaluating where additional exploration should be carried out.

Indeed, geostatistics is widely accepted in the geologic, mining and engineering geology community, and it is believed that they should be part of the education of geologists, mining engineers, hydrogeologists and engineering geologists. Furthermore, construction people start realizing the significance of geostatistical profiles in reducing extra costs due to unexpected or misunderstood subsurface geology. However, one should be careful, since problematic results can occur if geostatistics are used without comprehending the concepts of the field, or without being able to recognize bad data.

Another important issue is that the three dimensional nature of the site is not usually extensively reflected. Boreholes are actually projected into 2-D planes and 2-D profiles are drawn. In order to reveal the three-dimensional nature of the site, cross sections in different directions can be drawn. The actual extrapolation into 3-D space depends on the

experience of the geologist or the engineer. Most importantly, the correct directions should be chosen. Furthermore one should simultaneously look at different profiles, critically compare them and remember the significant details. However, in practice, few cross sections are drawn and it is usually difficult to realize the 3-D nature of certain geological features.

Finally, problems of ground and groundwater contamination created the need to study the spatial distribution of pollutant plumes and, more importantly, their changes with time. Until recently only few programs were addressing this need. Moreover there was limited application of geostatistics to the representation of contaminant plumes.

In this context, a geostatistical program, NOMAD-KRIBS, was developed in earlier years at MIT in an effort to provide solutions for the above geological/geotechnical demands. Up to now, the program had not been used for hydroenvironmental data.

The present thesis is based on a research project that aimed at expanding the NOAMD-KRIBS software and at checking its suitability for hydroenvironmental (geoenvironmental) problems.

Specifically, the main objectives of the study were:

- to retain and improve the functionality of the software,
- to apply Nomad-KRIBS to geoenvironmental problems. As described above, these problems, apart from having a 3D spatial nature, involve changes over time, which are of great interest in order to illustrate how pollutants advance and to predict their future distribution. The program, up to now, has been used for geologic cases that do not change with time, so its functionality for time dependent problems will be examined and it will possibly be adapted to other new demands.

Fulfillment of these objectives is presented with two case studies following an introduction to the program environment, to some geostatistical concepts and to previous research:

Chapter 2 presents the basic features of NOMAD-KRIBS, familiarizes the reader with the program's user interface and gives some details of KRIBS geostatistical algorithms.

Chapter 3 provides a review of the basic geostatistical concepts, emphasizing the main principles that were used to develop KRIBS. Among the topics discussed are Ordinary Kriging, variograms and variogram models, the handling of anisotropy, CoKriging, Block Kriging, and Bayesian Analysis.

Chapter 4 presents some previous research performed in geostatistics with main objective to review methods that KRIBS is using or could have used. In addition some new geostatistical concepts are presented and possible fields of future research are discussed.

Chapter 5 reviews the MBTA Porter Sq. to Davis Sq. case study, that was used to check and improve the functionality of the program. Through this case study NOMAD features are presented in detail and decisions required in KRIBS modeling are discussed while comparing the different analysis outputs.

Chapter 6 presents the Wellesley Maintenance Depot case. Here the applicability of NOMAD-KRIBS to geoenvironmental problems, that involve the time parameter is studied and discussed. In parallel geological profiles are generated with NOMAD and compared with the ones statistically reproduced with KRIBS.

Chapter 7 summarizes the work presented in this thesis, discusses the conclusions derived throughout it and summarizes some future recommendations.



## **Chapter 2: NOMAD - KRIBS**

### **2.1 Introduction**

Nomad is a three-dimensional ground profiler using a combination of C, C++, XWindows and Motif on the Unix platform. It was originally developed at Massachusetts Institute of Technology by Noak (1988) [34] and extended by Kinnicutt (1991) [25]. On this graphical basis a geostatistical model, KRIBS, was later added by Kinnicutt (1995) [27] in order to incorporate uncertainty in underground investigation programs.

Below, the basic features of NOMAD-KRIBS are presented. For more detailed information, description of the various features and for the manual of the program, one should refer to Kinnicutt 's Ph.D. Thesis [27], and also to Appendix I.

### **2.2 Nomad**

NOMAD is a three-dimensional ground profiler. This means that spatial data about the ground is stored as nodal information and can be recalled at any time. Cross sections in 2-D planes, usually used in project presentations, are not drawn using directly the borehole data, but they are resulting from the general 3-D profiler.

Input data are imported in .csv (comma separated values) format. Such a format can be exported from any spreadsheet program, which makes the manipulation of initial information easy and conventional. Figure 2.1 shows a spreadsheet containing the input data for a project. Each line in the spreadsheet contains attribute values (location, description, etc) for a certain borehole section. For each such line a NOMAD object, called a node, will be created in the program, and it will store all the above information. Each column is reserved for a different information category. The user can include ground types, SPT or RQD data, Atterberg limits or any other geotechnical information he believes is useful for distinguishing areas of uniform ground behavior, by just defining the category in the first row of that column.



Borehole name	x	y	description	depth	z	ground type	SPT	RGD	layer
ABB-SB-1	680	660.8	Surface	0	100	Surface			
ABB-SB-1	680	660.8	Widely graded	2	98	Widely graded sand	20		
ABB-SB-1	680	660.8	Widely graded	4	96	Widely graded sand	24		
ABB-SB-1	680	660.8	Widely graded	5	95	Widely graded sand			
ABB-SB-1	680	660.8	Widely graded	7	93	Widely graded sand	33		
ABB-SB-1	680	660.8	Widely graded	7.2	92.8	Widely graded sand	38		
ABB-SB-1	680	660.8	Silt	7.5	92.5	Silt			
ABB-SB-1	680	660.8	Widely graded	10	90	Widely graded sand			
ABB-SB-1	680	660.8	Widely graded	12	88	Widely graded sand	38		
ABB-SB-1	680	660.8	Widely graded	15	85	Widely graded sand			
ABB-SB-1	680	660.8	Widely graded	15.2	84.8	Widely graded sand	20		
ABB-SB-1	680	660.8	Silt	16.4	83.6	Silt	20		
ABB-SB-1	680	660.8	Silt	20	80	Silt			
ABB-SB-1	680	660.8	Silt	22	78	Silt	20		
ABB-SB-1	680	660.8	Silt	25	75	Silt	7		
ABB-SB-2/MW-1	1032	710.4	Surface	0	100	Surface			
ABB-SB-2/MW-1	1032	710.4	Widely graded	3	97	Widely graded sand	22		
ABB-SB-2/MW-1	1032	710.4	Widely graded	3.5	96.5	Widely graded sand	13		
ABB-SB-2/MW-1	1032	710.4	sandy Silt	4	96	sandy Silt	13		
ABB-SB-2/MW-1	1032	710.4	sandy Silt	5	95	sandy Silt			
ABB-SB-2/MW-1	1032	710.4	sandy Silt	5.5	94.5	sandy Silt	22		
ABB-SB-2/MW-1	1032	710.4	Widely graded	6.1	93.9	Widely graded sand	22		
ABB-SB-2/MW-1	1032	710.4	Widely graded	10	90	Widely graded sand			

Figure 2.1: Spreadsheet containing input information for NOMAD

NOMAD reads from the imported data the spatial coordinates of all borehole points for which information exists and illustrates them with colored intervals according to the corresponding ground type they define. Nodal data also stores all other information provided (SPT values etc). Figure 2.2 shows a general view of the program's interface with the imported borehole data. The three windows display the site from three orthogonally oriented directions. Each of the three views can be rotated, scaled and translated (Figure 2.3), either simultaneously or independently.

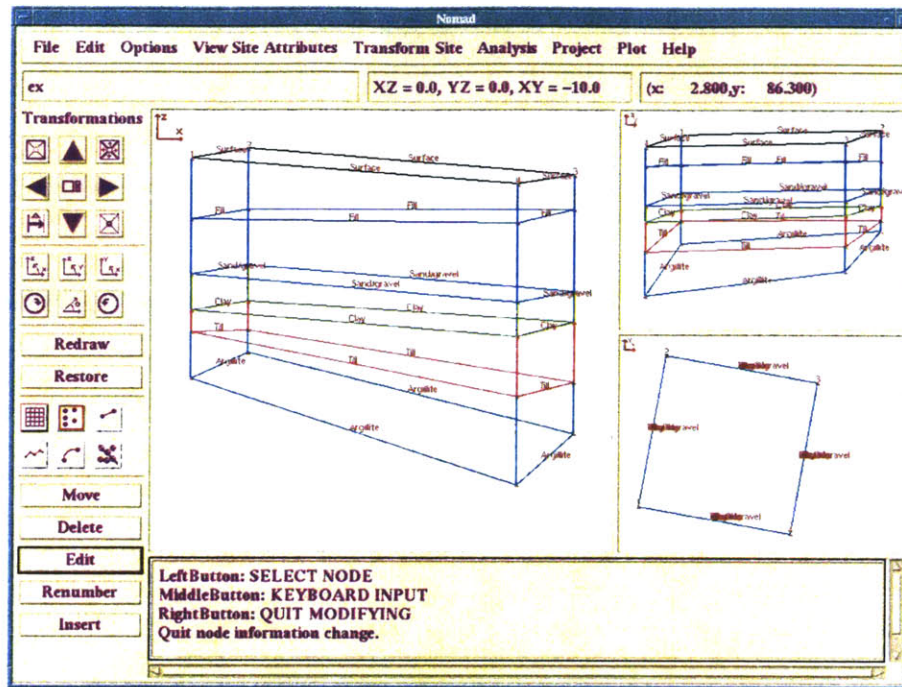


Figure 2.2: General view of NOMAD interface

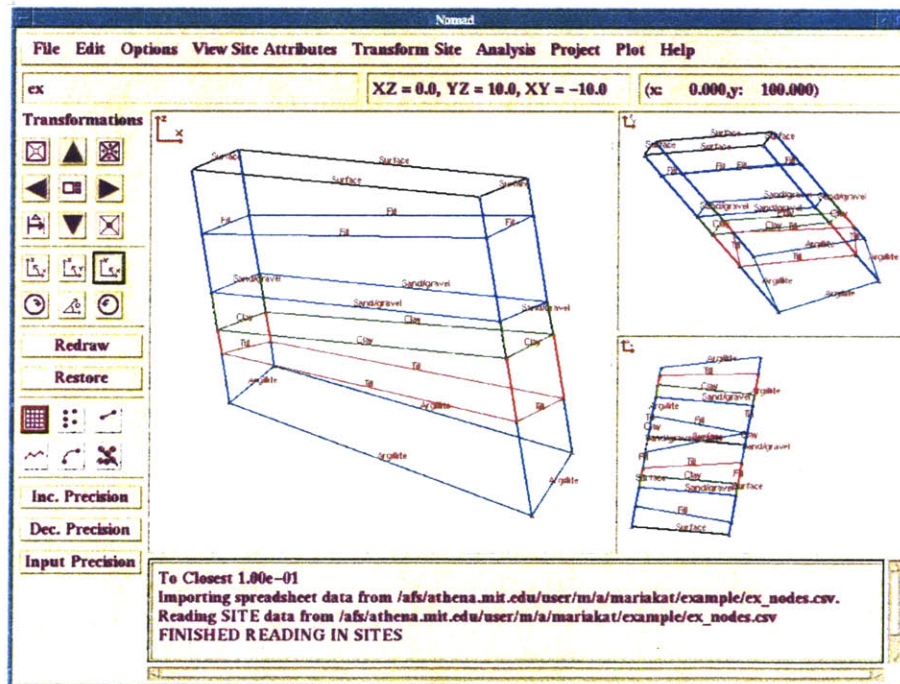


Figure 2.3: Rotational features of NOMAD

Once the input data are imported into NOMAD and a file is created, the user does not have to update the input file each time he wishes to make a change. The user can interactively edit the site data by inserting, deleting and moving nodal, borehole and line data according to his subjective beliefs or additional objective information. Figure 2.4 displays such an interface menu.

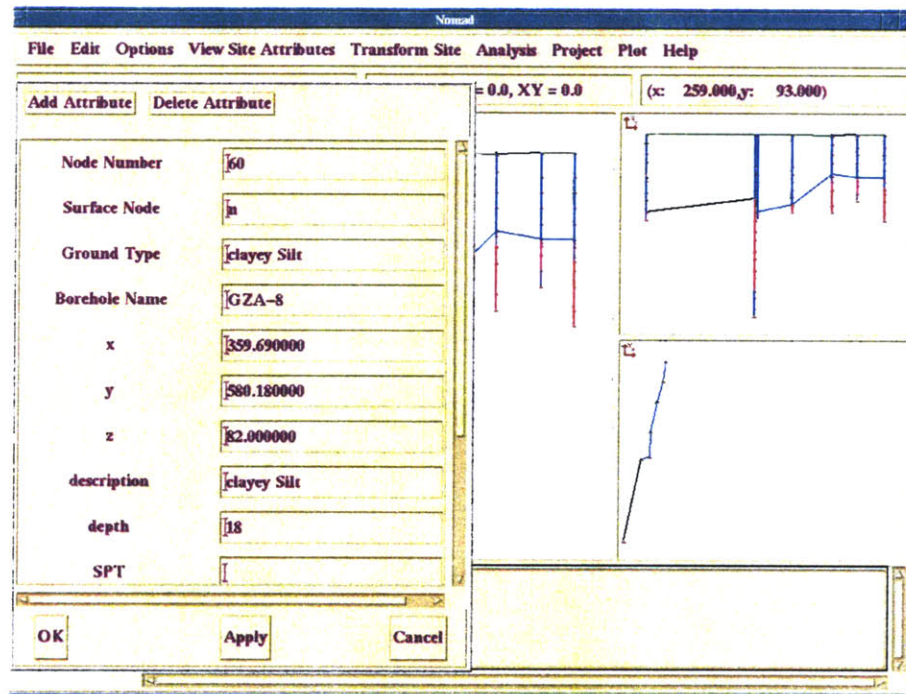
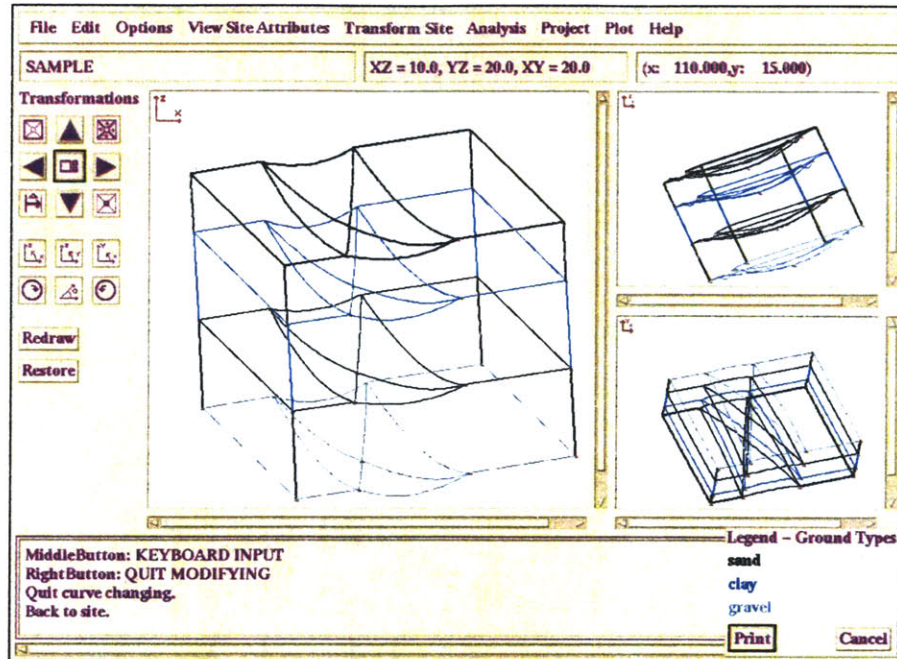


Figure 2.4: Edit menu that allows user to interact with the input data.

Lines and the layers they define are not generated automatically. This forces the user to use geologic judgement to introduce lenses or ignore information that seems to be affected by errors in investigation processes.

The user can also create cross sections and edit them, having the changes automatically propagated to the three-dimensional site model and to intersecting cross sections (Figure 2.5).





*Figure 2.5: Cross sections can be edited, with the changes automatically propagated to the three-dimensional site model and to intersecting cross sections*

## 2.3 KRIBS

### 2.3.1 Description of the program

KRIBS is a Kriging-Bayesian updating model for the creation of geologic profiles using Indicator CoKriging and Bayesian Updating techniques.

The KRIBS model can take into account the three-dimensional nature of the data as stored in the NOMAD files. For geostatistical analysis, the spatial structure of the data is captured with semi-variograms. The available semi-variogram models are the spherical, the exponential and the gaussian one. Because semi-variograms are constructed in 2-D planes, the actual kriging process is not three-dimensional. Figure 2.6 shows a set of experimental semi-variograms along with fitted models. Background information about the definition and modeling of variograms, along with reference to various geostatistical concepts can be found in Chapter 3.

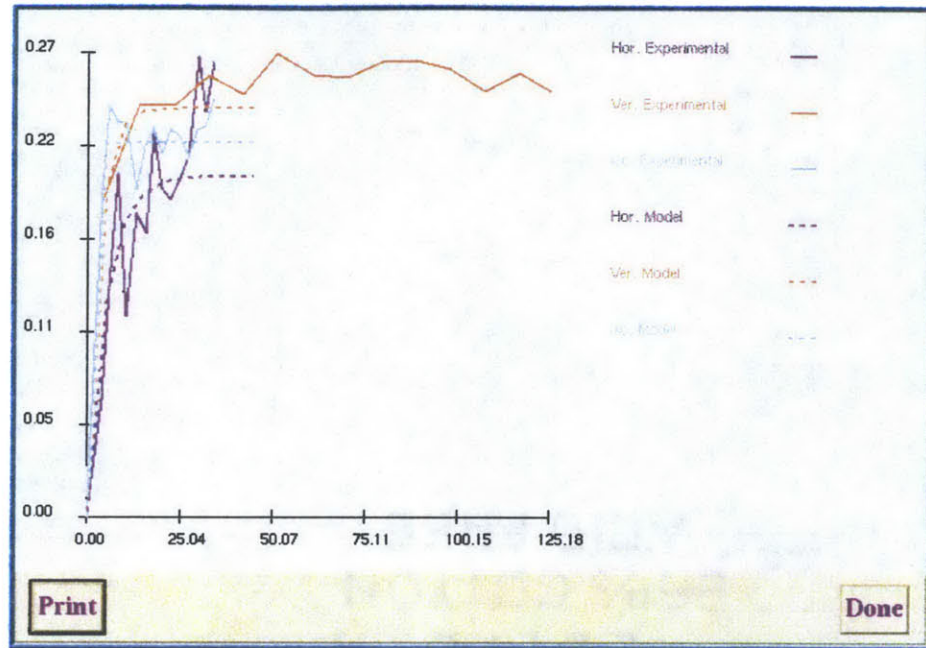


*Figure 2.6: Experimental semi-variograms and fitted models*

The CoKriging feature allows the kriging model to consider two or more input data categories, such as both ground type information and SPT values, in calculating the probability of a ground type to exist in a certain location.

The program's output is a ground profile along with probabilities of each individual ground type occurring spatially in the profile and variances associated with each ground type. In other words, spatial uncertainties are captured. Figure 2.7 shows such a kriged profile. The user can choose a probability threshold when displaying the ground profile; in locations where ground types have been calculated to occur with a probability lower than the threshold the profile is blank, indicating that based on the criteria chosen, further site investigation should be carried out. Figure 2.8 shows the kriged profile with thresholds 25% and 50%. As the threshold increases, more areas are left blank; in those areas uncertainty is higher and further investigation may be required, depending on the significance of the project.



Figure 2.7: Kriged profile (from MBTA Porter Sq. case study).

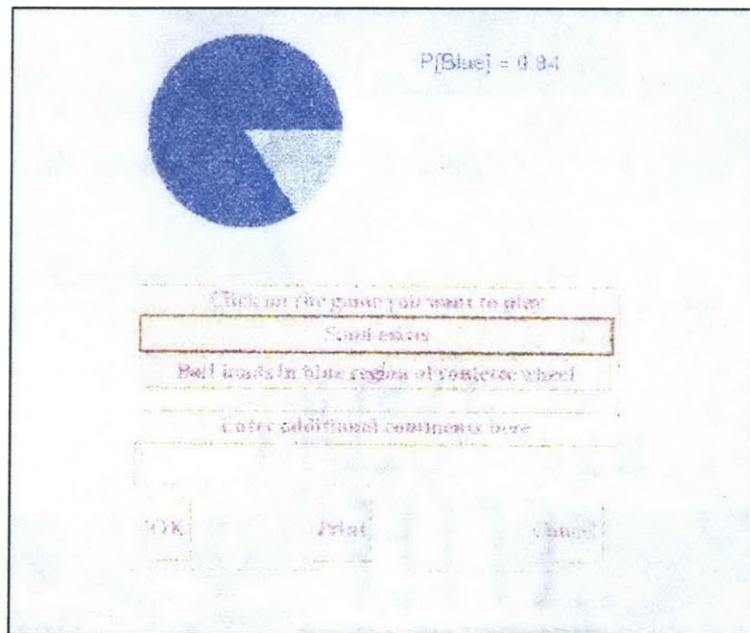


Figure 2.8: Kriged profiles with probability threshold 30% and 50%: Areas that appear blank correspond to ground types predicted to occur with probability less than the threshold (from MBTA Porter Sq. case study).

Furthermore, the Bayesian updating features of KRIBS give the program the ability to incorporate additional objective and subjective knowledge in modeling a site. The kriged profile can be altered and probabilities of occurrence can be recalculated according to the geologist's beliefs or new objective information. Especially as far as personal beliefs are concerned, the user can develop subjective probability with a computerized probability wheel (Figure 2.9). The probability wheel makes use of the gaming theory. In this



“game”, the user is given a choice (Fig. 2.9); either he can bet on the event that a certain ground type (sand) exists in a particular region, or bet that the roulette ball will fall in the blue region of the wheel (with the probability of the ball falling in this region being equal to the area of the region, assuming a total area of 1). User will place his/her bet on the game he is more likely to win; in other words one will bet on sand only when he believes that the probability of sand is greater than the area of the blue region. Until this happens, the user is presented with successive rounds of betting with different refined areas of blue region, so that to bracket his subjective belief that sand exists.



*Figure 2.9: The probability wheel function enables user to input quantitatively subjective beliefs (from Kinnicutt, 1995 [27]).*

These features of KRIBS make NOMAD-KRIBS useful for locating the most suitable positions for new borings and planning efficient further exploration programs.

### 2.3.2 KRIBS algorithm

As described above, site data is organized into an input file, which is then read into NOMAD and modified by the user. The KRIBS model is then initialized: Grid dimensions are specified and the experimental semi-variograms, which capture the spatial

configuration of the data, are calculated. Based on these experimental variograms, the user specifies the semi-variogram models to be used in the CoKriging system. Solution of this system provides the kriged profiles. Furthermore, information can be updated and the system solved again. The procedure is illustrated in Figure 2.10 below:

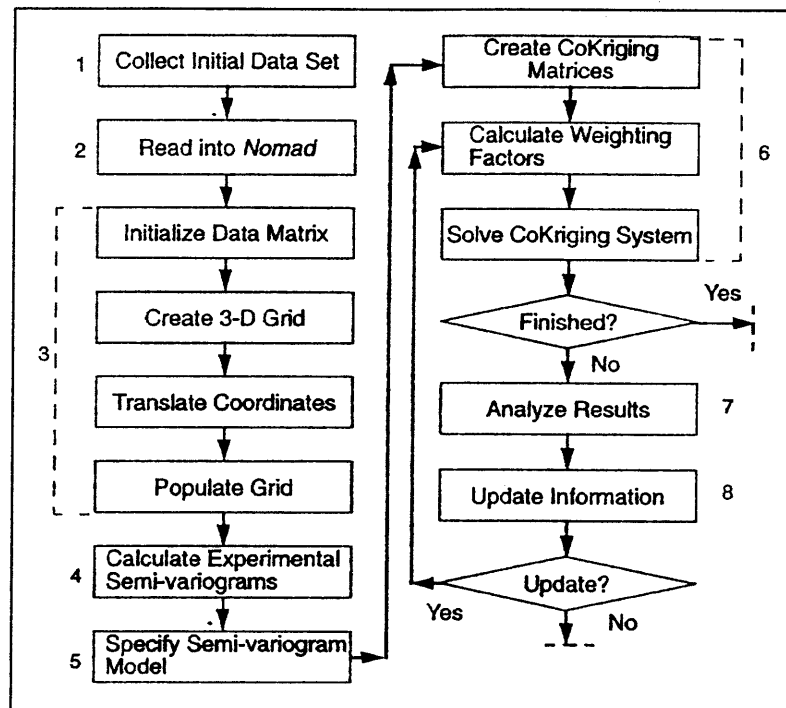


Figure 2.10: KRIBS algorithm (from Kinnicutt, 1995 [27]).

## 2.4 KRIBS model

Below some basic features of KRIBS model are cited for reference purposes. Geostatistical concepts are assumed to be known, but if this is not the case, one should refer to Chapter 3 and the corresponding bibliography.

Experimental semi variograms are calculated from the grided data in the  $x$ ,  $y$ ,  $z$  directions for up to  $300/x_{incr}$  step intervals,  $x_{incr}$  being the grid increment in  $x$  direction. The approximate horizontal distance for correlation between stratigraphic borehole data



has been found to be around 50 feet, therefore 300 ft was used in calculating the step intervals since this is twice the effective range for an exponential model<sup>1</sup>.

The equation for calculating the experimental semi-variograms in KRIBS is

$$\gamma(h,\alpha) = \frac{1}{2N'} \sum_{i=1}^{N'} (z(x_i + h) - z(x_i))^2 \quad (2.1)$$

where  $\gamma(h,\alpha)$  is the semi variogram for a distance  $h$  and a direction  $\alpha$ ,

$N'$  is the number of data pairs encountered a distance  $h$  apart in direction  $\alpha$ ,

$z(x_i+h)$  is the data value at location  $x_i+h$  and

$z(x_i)$  at location  $x_i$ .

This equation corresponds to the mean of the variances of the differences between the experimental values and it assumes the intrinsic hypothesis, which states that the variogram function  $2\gamma(h,\alpha)$  only depends on the distance and direction of  $(h,\alpha)$  and not on the location  $x_i$ .

Currently, the KRIBS model calculates the experimental semi-variograms in the horizontal and vertical directions and also isotropically (all directions).

A lag angle of 22.5 is used to capture pairs of data, which are in the general direction of interest but are offset (Figure 2.11).

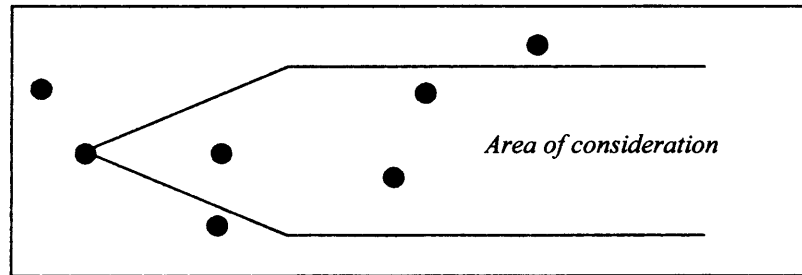


Figure 2.11: Lag angle determining which pairs of data will be examined

---

<sup>1</sup> See Chapter 3. Exponential model is defined in the bibliography either as  $\gamma(h) = 1 - \exp(\frac{-3h}{a})$  or as

$\gamma(h) = 1 - \exp(\frac{-h}{a})$ . KRIBS uses the latter case, so the effective range is  $3a = 3 \times 50\text{ft} = 150\text{ft}$ . Twice the effective range is then 300ft.

The cone terminates into a band after reaching a specified bandwidth; this aims to minimize the effects of variances, due to spatial distances in direction other than the direction of interest.

Ideally experimental semi-variograms would be calculated for each ground type individually, then separate semi variogram models would be specified for each ground type, and different kriging systems would be created and solved. But such a procedure would require too much computational time. Instead, KRIBS specifies a model that captures how the ground types change with distance. Then, based on this one structural model, one kriging system is solved, and the same set of weighting factors are obtained and used for the estimation of the various ground types.

This model is able though of capturing the anisotropic properties in the soil by superimposing several different semi-variogram models, with each model capturing a particular component. More specifically, the semi-variogram model is of the form:

$$\gamma(h_x, h_y, h_z) = \gamma_0(|h|) + \gamma_1(|h_1|) + \gamma_2(|h_2|) + \gamma_3(|h_3|) \quad (2.2)$$

where  $\gamma(h_x, h_y, h_z)$  is the combined model and  $h_i = \sqrt{\left(\frac{h_x}{a_x}\right)^2 + \left(\frac{h_y}{a_y}\right)^2 + \left(\frac{h_z}{a_z}\right)^2}$ , with  $a_i$  accounting for anisotropy. Among the model components,

$\gamma_0(|h|)$  captures the isotropic nugget effect (effect at small distances between data points)

$\gamma_1(|h_1|)$  captures the horizontal behavior of the data – in this case  $a_z=0$

$\gamma_2(|h_2|)$  reflects zonal anisotropy in the vertical direction, so  $a_x = a_y = 0$

$\gamma_3(|h_3|)$  captures the isotropic behavior of the data.



## Chapter 3: Geostatistical concepts

### 3.1 Introduction

In this chapter some basic geostatistical concepts are presented. In more detail, this includes an introduction to Ordinary Kriging, and issues arising from the spatial description of a given data set, such as the definition and discussion of variograms and variogram models, and the handling of Anisotropy. Furthermore, CoKriging, Block Kriging, and Bayesian Analysis are briefly discussed.

The scope of this chapter is not to provide an exhaustive description of the geostatistical field, but rather to discuss the main principles that were used to develop KRIBS.

### 3.2 Ordinary Kriging

#### 3.2.1. *Introduction to Ordinary kriging*

Ordinary Kriging is one of the Point Estimation methods that is also referred as Best Linear Unbiased Estimator (B.L.U.E.). It is considered linear because the estimates are weighted linear combinations of the available data, unbiased because it tries to have the mean residual (error)  $m_R$  zero, and best, because among the other linear methods, it aims to minimize the variance of the errors  $\sigma_R^2$ . The latter is actually the distinguishing feature of the Ordinary Kriging.

In practice, the mean residual  $m_R$  and the variance of errors  $\sigma_R^2$  are unknown. The best approach one can make is to build a model and work with the average error and the average error variance for the model. In other words, to use a probability model in which the bias and error variance can both be calculated. Then, weights for the nearby samples are chosen so that the average error  $\tilde{m}_R$  is exactly 0 and the modeled error variance  $\tilde{\sigma}_R^2$  is minimized.

### 3.2.2. Main principle

At every point where no data exists, the unknown true value is estimated with a weighted linear combination of the available samples:

$$\hat{v} = \sum_{j=1}^n w_j \cdot v_j \quad (3.1)$$

where  $v_j$  are the known values of the available samples

$w_j$  are the weights that need to be determined in order to obtain  $\hat{v}$

and  $\hat{v}$  is the estimation of the unknown true value. Note that the  $\hat{\phantom{x}}$  symbol is used to denote the estimated values.

The weights are allowed to change as we estimate unknown values at different locations.

It can be proven (for example Isaaks, [17]) that in order to ensure unbiasedness, the sum of all the weighting factors should be 1:

$$\sum_{j=1}^n w_j = 1 \quad (3.2)$$

This is the *unbiasedness condition*.

As mentioned above the main aim of ordinary kriging is the *minimization of the variance of the errors*  $\sigma_R^2$ .  $\sigma_R^2$  of a set of  $k$  estimates can be expressed as:

$$\sigma_R^2 = \frac{1}{k} \sum_{i=1}^k (r_i - m_R)^2 \quad (3.3)$$

With  $r_i = \hat{v}_i - v_i$  being the estimation error and

$m_R = \frac{1}{k} \sum_{i=1}^k r_i$  the mean residual error, (3.3) becomes:

$$\sigma_R^2 = \frac{1}{k} \sum_{i=1}^k \left[ \hat{v}_i - v_i - \frac{1}{k} \sum_{i=1}^k (\hat{v}_i - v_i) \right]^2 \quad (3.4)$$

Assuming that the mean error is 0, (3.4) is simplified:

$$\sigma_R^2 = \frac{1}{k} \sum_{i=1}^k [\hat{v}_i - v_i]^2 \quad (3.5)$$

Equation (3.5) gives an expression for  $\sigma_R^2$  but it is practically useless, since it requires the knowledge of the true values  $v_i$ . The probabilistic solution to this problem is to conceptualize the unknown values as the outcome of a random process and then to solve for the conceptual model. At any point where an unknown value is to be estimated, the model is a stationary random function consisting of  $n+1$  random variables,  $n$  being the number of the existing data plus one for the unknown value that has to be estimated.

Introducing a random function model, the error variance can be expressed as:

$$\sigma_R^2 = \tilde{\sigma}^2 + \sum_{i=1}^n \sum_{j=1}^n w_i w_j \tilde{C}_{ij} - 2 \sum_{i=1}^n w_i \tilde{C}_{i0} \quad (3.6)$$

where  $\tilde{\sigma}^2$ ,  $\tilde{C}_{ij}$  are the random function model parameters (variance and covariance) and  $w_i$  are the  $n$  unknown variables (weighting factors). Note again that the  $\sim$  symbol is used to denote the model parameters

The minimization of a function of  $n$  variables is then accomplished by setting the  $n$  partial first derivatives to zero. So a system of  $n$  equations with  $n$  unknowns is produced.

But since the unbiasedness condition (3.2) is also imposed, there is actually one more equation in the system. Not any solution  $w_1, \dots, w_n$  of the  $n \times n$  system satisfies the unbiasedness condition and the problem is actually a constrained optimization with  $n+1$  equations and  $n$  unknowns.

In order to convert the constrained system into an unconstrained one, the Lagrange Parameter technique is used. The Lagrange parameter  $\mu$  is introduced in the system as an extra unknown:

$$\sigma_R^2 = \tilde{\sigma}^2 + \sum_{i=1}^n \sum_{j=1}^n w_i w_j \tilde{C}_{ij} - 2 \sum_{i=1}^n w_i \tilde{C}_{i0} + 2\mu \left( \sum_{i=1}^n w_i - 1 \right) \quad (3.7)$$

Equality is not violated since  $\mu$  is introduced in a term that is overall equal to zero. Furthermore, now by setting the  $n+1$  partial first derivatives to 0 one gets  $n+1$  equations, containing  $n+1$  unknowns.

The system in matrix notation is:

$$\begin{array}{ccc}
 C & W & = D \\
 \begin{bmatrix} \tilde{C}_{11} & \dots & \tilde{C}_{1n} & 1 \\ \vdots & \dots & \vdots & 1 \\ \tilde{C}_{n1} & \dots & \tilde{C}_{nn} & 1 \\ 1 & & 1 & 0 \end{bmatrix} \cdot \begin{bmatrix} w_1 \\ \vdots \\ w_n \\ \mu \end{bmatrix} & = & \begin{bmatrix} \tilde{C}_{10} \\ \vdots \\ \tilde{C}_{n0} \\ 1 \end{bmatrix} \\
 (n+1) \times (n+1) & (n+1) \times 1 & (n+1) \times 1
 \end{array} \quad (3.8)$$

This is referred as the *ordinary kriging system*.

The solution to it is

$$W = C^{-1}D$$

which gives the n values of the weighting factors plus  $\mu$ .

The minimized error variance is then calculated as

$$\tilde{\sigma}_R^2 = \tilde{\sigma}^2 - \left( \sum_{i=1}^n w_i \tilde{C}_{i0} + \mu \right) = \tilde{\sigma}^2 - W \cdot D \quad (3.9)$$

This is referred as the *ordinary kriging variance*.

In terms of the variogram, the ordinary kriging system can be written as:

$$\sum_{j=1}^n w_j \tilde{\gamma}_{ij} - \mu = \tilde{\gamma}_{i0} \quad \forall i = 1, 2, \dots, n. \quad (3.10)$$

$$\sum_{j=1}^n w_j = 1$$

and the modeled error variance

$$\tilde{\sigma}_R^2 = \sum_{i=1}^n w_i \tilde{\gamma}_{i0} + \mu \quad (3.11)$$

### 3.2.3. Comments

1. An important issue is how to take into account the spatial description of the data set.

This will be discussed below in section 3.3

2. One should note C and D matrices require the calculation of the  $(n+1)^2$  covariances  $\tilde{C}_{ij}$  and this is done by choosing a covariance function  $\tilde{C}(\mathbf{h})$ . Actually, what is fitted in the data values is usually the variogram model (section 3.3), then

$$\tilde{C}(\mathbf{h}) = \tilde{\gamma}(\infty) - \tilde{\gamma}(h) \quad (3.12)$$

with  $\tilde{\gamma}(h)$  being the variogram model and  $\tilde{\gamma}(\infty)$  its maximum value (sill).

3. The D matrix provides a weighting scheme similar to that of the various inverse distance methods: the covariance between any sample and the estimated point generally decreases as the distance of the sample from the point increases. Actually the fact that D is formed by covariances makes it possible to consider not only geometric (or in other words physical) distances, but more generally statistical distances. The introduction of statistical distance takes into account both the physical position of the data values, and their spatial continuity. For example, consider two points 10m apart. Their physical or geometric distance is the same (10m), but they will have different correlation if the data concern the elevation of the groundwater table, rather than measuring gold concentration. The statistical distance in the latter case will have a much higher value, because groundwater elevation does not change significantly over a 10m distance, but gold concentration can exhibit very large fluctuations.
4. The C matrix records distances between samples, so it provides the system with information about the clustering of the sample data. Clustered values lead to large values in the C matrix whereas samples far apart result in small values at the corresponding matrix positions. Multiplying D with  $C^{-1}$  adjusts the distance (physical or statistical) weights of the D matrix to account for possible clustering of the sample data.

Summarizing, the success of ordinary kriging is mainly based on the fact that it uses statistical distance instead of geometric distance and that it attempts to decluster the available sample data.

$$\mathbf{W} = \mathbf{C}^{-1} \cdot \mathbf{D}$$

Clustering      Distance



### 3.3 Spatial description of a data set

#### 3.3.1: Definitions

A powerful means of representing the spatial characteristics of a given set of data are semi-variograms. A semi-variogram is defined as a means to summarize the information contained in an h-scatterplot.

An h-scatterplot is a plot showing all possible pairs of data values whose locations are separated by a certain distance in a particular direction (from Isaaks & Srivastava [17]).  $h=(0,1)$  means that each data location is paired with data location whose easting is the same and whose northing is 1 unit larger.  $h=(1,1)$  means that data are paired with the data location whose both easting and northing is 1 unit larger. This is illustrated in Figure 3.1:

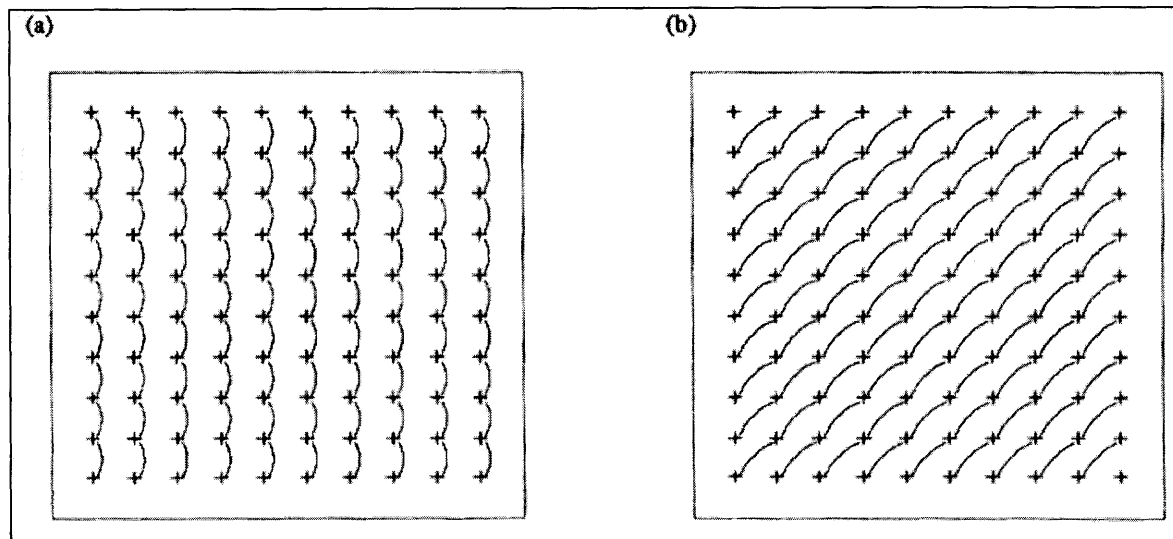


*Figure 3.1: Pairing of data to obtain an h-scatterplot: In the left figure each location is paired with the location being one unit further north than itself; in the right figure, each figure is paired with the location being one unit further north and one further east than itself (from Isaaks & Srivastava [17]).*

If there is no spatial variation, data values in both paired locations will be the same. As spatial variability increases, the difference between the two values will increase. h-scatterplots are thus a cloud of points around the line  $y(x)=x$ . The shape of the cloud indicates how continuous the data values are over a certain distance in a particular

direction; if the data values at locations separated by  $h$  are very similar, the pairs will plot very close to  $y(x)=x$ . Otherwise, and as  $h$  represents greater distances, the cloud becomes more spread out and diffuses. This is illustrated in Figure 3.2.

Quantitative summaries of the information contained in an  $h$ -scatterplot (description of the cloud) can be done with:

- the correlation coefficient (which decreases as the cloud of points spreads out). A correlogram or correlation function plots the relationship between the correlation coefficient of an  $h$ -scatterplot and  $h$ .
- the covariance, and respectively the covariance function
- the moment of inertia of the cloud about the line  $y(x)=x$ .

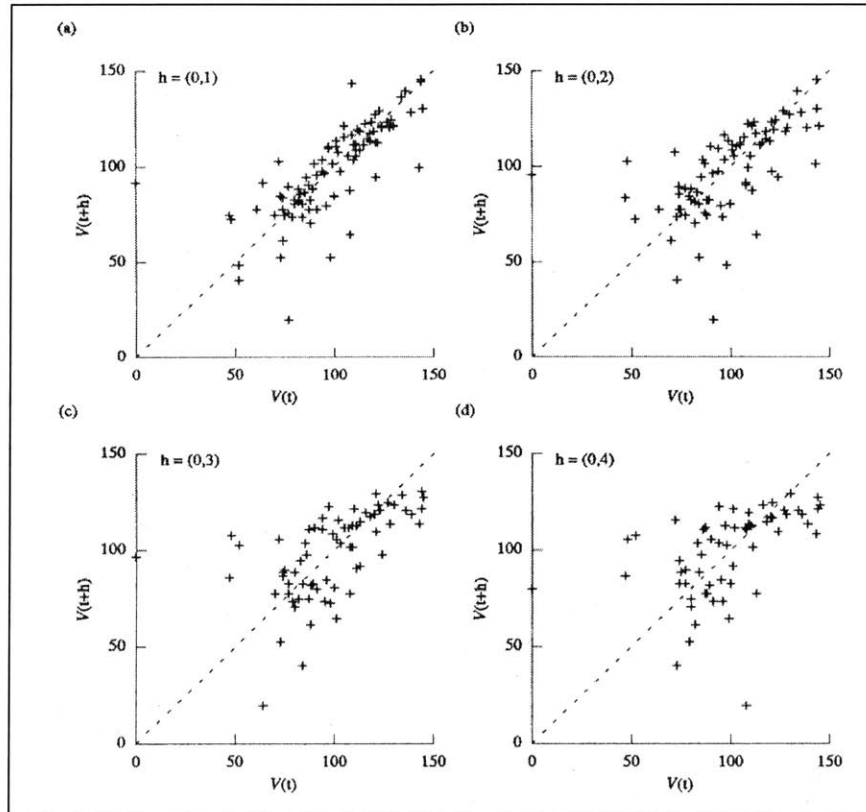


*Figure 3.2:  $h$ -scatterplots capturing spatial distribution of a variable  $V$ , for different values of  $h$ ; as the pairing distance increases, data values become less correlated and the cloud of points spreads out (from Isaaks & Srivastava [17]).*

Considering that for  $h=(0,0)$ , all points of the plot will fall exactly on  $y(x)=x$  (since each value will be paired with itself) and that as  $|h| = \sqrt{h_x + h_y}$  increases the points will drift away from  $y(x)=x$ , this moment of inertia is a measure of how spread out the cloud is. Unlike the other 2 indices, the moment of inertia increases as the cloud drifts away.

The relationship between the moment of inertia of an h-scatter plot and  $h$  is called the semi-variogram (or simply variogram) of the data set.

Should  $Z(\bar{x})$  be a random variable with  $\bar{x} = \{x,y,z\}$ , then the semi-variogram is defined through equation 3.13:

$$\gamma(\bar{x}_1, \bar{x}_2) = \text{Var} \{Z(\bar{x}_1) - Z(\bar{x}_2)\}, \quad (3.13)$$

where  $\text{Var}\{\}$  is the Variance of the random variable

$Z(\bar{x}_i)$  is the value of the random variable  $Z$  at location  $\bar{x}_i = \{x_i, y_i, z_i\}$

$\gamma(\bar{x}_1, \bar{x}_2)$  is the variogram value for variable  $Z$  between the two locations  $\bar{x}_1$  and  $\bar{x}_2$ .

### 3.3.2 Characteristic parameters of a semi-variogram:

As expected, in many cases, after a certain distance  $\alpha$  the two random variables paired are no longer correlated. This distance is called *the range* of the semi-variogram.

At distances greater than  $\alpha$ , the semi-variogram usually converges to a limit value known as the *sill*:

$$\gamma(h \geq \alpha) = \gamma(\infty) = s$$

Finally, at  $h = 0$ , the semi-variogram is defined to be 0; at small distances, however, a discontinuity can exist in the semi-variogram model. The behavior of the semi-variogram at those short distances is captured by what is called the nugget effect.

The above are illustrated in the Figure 3.3 below and a complete variogram surface is shown in Figure 3.4:

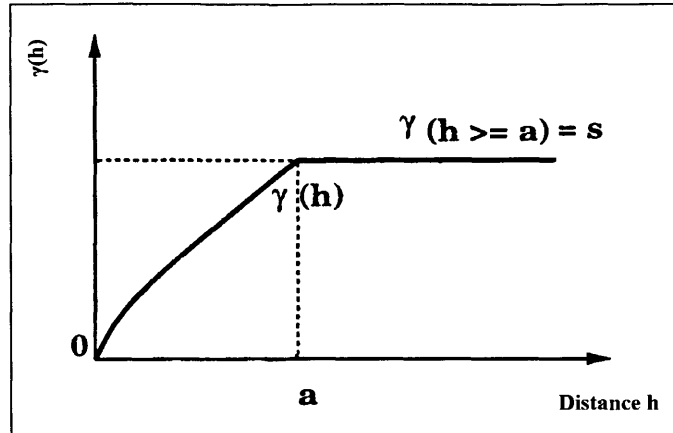


Figure 3.3: Sill  $s$  and Range  $a$  of a semi-variogram

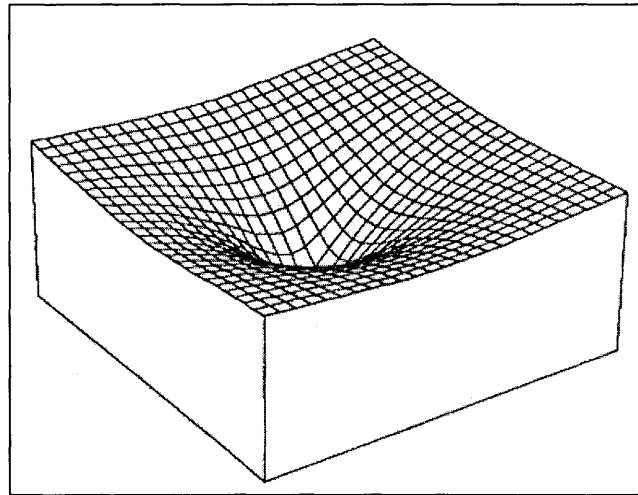


Figure 3.4: Complete variogram surface. The depression at the center of the surface represents the variogram at zero distance (from Isaaks & Srivastava [17]).

### 3.3.3 Semi-variogram models

In geostatistical applications, a sample (or in other words experimental) variogram is calculated using the given data and then a function is fitted to it. This function models the spatial correlations for domains where there are no experimental data and provides a means of estimating the value of a random variable in regions where little or no data are known. A model has to be fitted and used instead of the sample variogram because:

- 1) A continuous relation is needed, since estimation could be required at any point in space (and so the D matrix may call for variogram values for distances that are not available in the sample data).
- 2) The use of the sample variogram does not guarantee the existence and uniqueness of the solution to the ordinary kriging system. To guarantee that the system has *one and only one solution, and that this solution is stable*, one must ensure that it possesses the property of positive definiteness.

Actually, one should ensure that the matrix:

$$C = \begin{bmatrix} \tilde{C}_{00} & \tilde{C}_{01} & \dots & \tilde{C}_{0n} \\ \tilde{C}_{10} & \tilde{C}_{11} & \dots & \tilde{C}_{1n} \\ \vdots & \vdots & \dots & \vdots \\ \tilde{C}_{n0} & \tilde{C}_{n1} & \dots & \tilde{C}_{nn} \end{bmatrix} \quad (n+1) \times (n+1)$$

is positive definite.

A necessary and sufficient condition for this is:

$$w^T C w > 0 \Rightarrow \sum_{i=1}^n \sum_{j=1}^n w_i w_j \text{Cov}(V_i V_j) > 0 \quad (3.14)$$

for any non zero vector w.

Taking into account that the variance of a random variable, defined by a weighted linear combination of other random variables, is given by:

$$\text{Var}\left\{\sum_{i=1}^n w_i V_i\right\} = \sum_{i=1}^n \sum_{j=1}^n w_i w_j \text{Cov}(V_i V_j) \quad (3.15)$$

if in (3.14) w is taken as the vector of weights, the positive definiteness guarantees that the variance of the estimation error,

$$R_0 = \sum_{i=1}^n w_i V_i - V_0$$

will be positive.

In practice, (3.14) is not a useful way to check positive definiteness. For reference, other necessary and sufficient conditions are:

- All eigenvalues of  $C$  are positive.
- All submatrices of  $C$  have positive determinants.
- All the pivots (without row exchanges) are greater than 0.

In geostatistical applications, the positive definiteness is guaranteed by fitting in the experimental variogram a model (function) that is known to possess this property.

Several theoretical models have been developed using the hypothesis of stationarity<sup>1</sup> and positive definite properties. Variogram models can be divided into two basic categories: those that reach a plateau, and those which do not. The former are referred as transition models, the plateau is the sill, and the distance at which they reach the plateau is the range. Some models reach the sill asymptotically; in this case the range is defined as the distance at which 95% of the sill has been reached. Models, which reach no plateau, are representing cases where there is a trend or a drift in the data.

Some commonly used variogram models are the spherical, exponential, gaussian and linear ones:

### ***Spherical model***

$$\gamma(h) = \begin{cases} 1.5 \frac{h}{a} - 0.5 \left(\frac{h}{a}\right)^3, & \text{if } h \leq a \\ 1 & \text{if } h > a \end{cases} \quad (3.16)$$

It is characterized by linear behavior at small separation distances near the origin, but flattens out at larger distances. It reaches the sill at range  $a$  and the tangent at origin intersects the sill at  $2/3$  of the range.

---

<sup>1</sup> *Stationarity*: Stationarity is a concept of geostatistics according to which the covariance and semi-variogram functions do not depend on the two data point locations in space, but rather only on the distance between the two data points. This assumption of stationarity is important in linear geostatistics, since statistical inferences can be made with many fewer data points (realizations of a random variable) than would otherwise be required. Different degrees of stationarity may exist, depending on the assumptions made.

### ***Exponential model***

$$\gamma(h) = 1 - \exp\left(-\frac{3h}{a}\right) \quad (3.17)$$

It is linear at very short distances near the origin, but rises more steeply, and then flattens out more gradually. It reaches the sill asymptotically and the tangent at origin intersects the sill at about 1/5 of the range.

### ***Gaussian model***

$$\gamma(h) = 1 - \exp\left(-\frac{3h^2}{a^2}\right) \quad (3.18)$$

It reaches the sill asymptotically. Its distinguishing factor is the parabolic behavior near the origin. Also it has an inflection point.

The three above-mentioned models are shown at Figure 3.5:

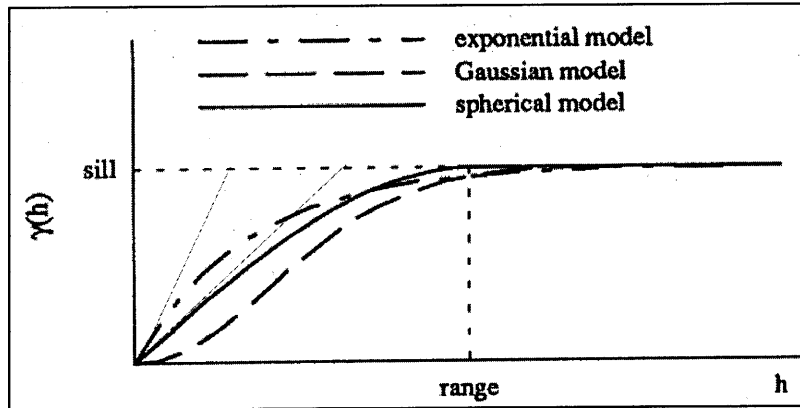


*Figure 3.5: Relative plot of gaussian, exponential and spherical models.*

The suitability of any one of these three models depends mainly on the behavior of the sample data near the origin. If the underlying phenomenon is quite continuous, pairs of data separated by small distances will have very similar values, so  $\gamma(h)$  (which increases as correlation decreases) will have values very close to zero, or it will change at a very slow rate. This means that the tangent through the origin will be almost horizontal and therefore the sample variogram will probably show a parabolic behavior for small

distances. So, the Gaussian model will be the most appropriate. If the behavior near the origin is linear, which means that the data values have weaker correlation than in the parabolic case, even at small distances, a spherical or exponential should be tried. The choice between them depends on what part of the range a straight line drawn tangent near the origin intersects the sill, which again reflects how strong the correlation is at small distances. An exponential model, which has a steeper tangent at the origin, and intersects the sill at a smaller percentage of the range (20%), reflects much weaker correlations than the spherical one, which intersects the sill at 66% of the range. This can be understood when one bears in mind the definition of the variogram; the higher the value for a certain distance  $h$ , the more spread out the data points are, and thus less correlated (section 3.3.1). So, the steeper the slope in the variogram, the faster (in terms of increasing distance  $h$ ) the data become uncorrelated. In any case the physical explanation of the behavior should be examined.

***Linear model:***

$$\gamma(h) = |h| \quad (3.19)$$

It is obvious that it reaches no sill. As mentioned above, this models cases where there is a trend or a drift in the data set. As an example, one can think of mapping the elevation of a bedrock surface, when the bedrock is known to have a constant slope. Note that it is not always positive definite, but it can be if one insists that the weights sum to 0.

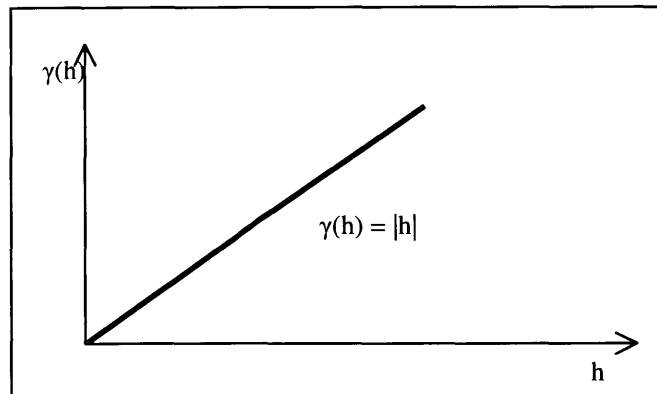


*Figure 3.6: Linear model*



### ***Linear combination of models***

The behavior of a sample data set can be modeled either using one basic model, or a linear combination of more than one of them. This is justified since positive definite variograms have the property that any linear combination of them is positive definite.

A final note would be that the distance  $h$  used in the semi-variogram models does not have to be the physical distance between the points ( $h = \sqrt{x^2 + y^2 + z^2}$ ), but can take into account the geometrical *anisotropies* (different values in different directions),  $a_x$ ,  $a_y$  and  $a_z$  that the region may exhibit.

$$h = \sqrt{(a_x x)^2 + (a_y y)^2 + (a_z z)^2} \quad (3.20)$$

The physical distance can be used in the theoretical model if the ground is believed to be homogenous.

### ***3.3.4 Effect of Variogram characteristics***

- a. Scale: The models have the same shape, but different sills. So correlation over distance does not change, but correlation at the same distance differs by a factor equal to the ratio of the two sills. (Figure 3.7). Thus scale does not affect the weights or the ordinary kriging estimate but only the ordinary kriging variance, which actually changes by the same factor that was used to rescale the variogram.
- b. Shape: It affects how weights are distributed to the various data samples. For example a parabolic behavior near the origin gives more weight to the closest samples. (Figure 3.8). Different shapes can result in negative weights or weights that are greater than 1. This gives the procedure the advantage of being able to give estimates larger than the largest sample value or smaller than the smallest sample value. The disadvantage is that there exists the possibility of creating negative estimates (which should be set to zero). Nevertheless, even if the behavior seems to be parabolic near the origin, such models are avoided because negative weights make the estimation rather erratic.

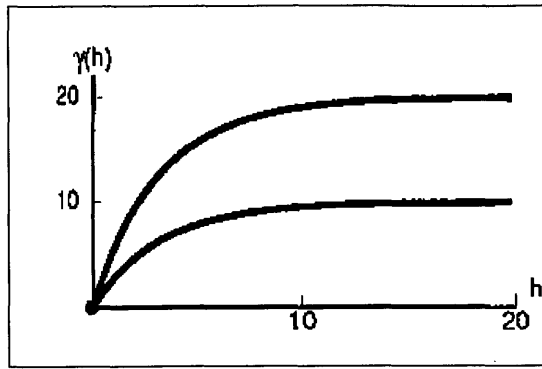


Figure 3.7: Scale effect

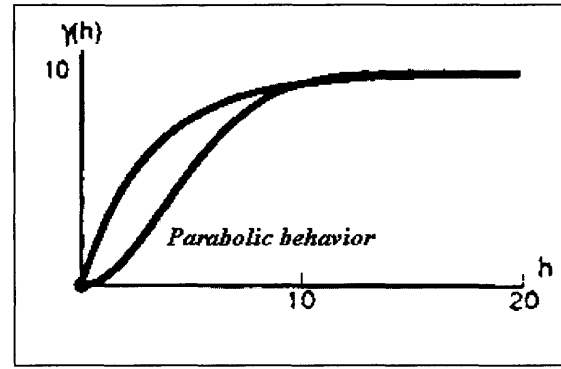


Figure 3.8: Shape effect

- c. Nugget effect: Increasing the nugget effect, (i.e. increasing the starting point of the variogram at  $h=0$ ), results in a more equal distribution of weights, since values close to one another are given a degree of correlation similar to that of values separated by a distance close to the range (Figure 3.9). So the estimation procedure tends to become a simple averaging of the sample data; a pure nugget effect model means that for  $h=0$  the variogram has already a value equal to the sill, and so there is a complete lack of spatial correlation.
- d. Range: it has minor effect on kriging weights, but changes the variance; doubling the range makes the samples to appear twice as close in terms of statistical distance (Figure 3.10). If it becomes very small, all samples appear to be equally far away from the point being estimated, so again the procedure tends to become a simple averaging.

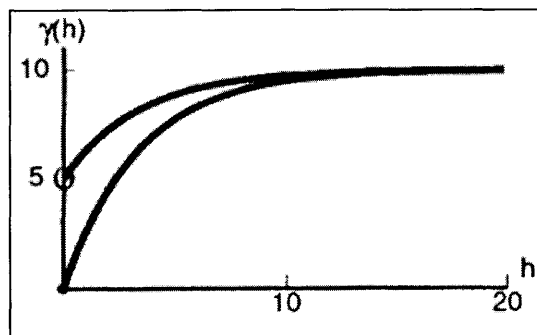


Figure 3.9: Nugget effect

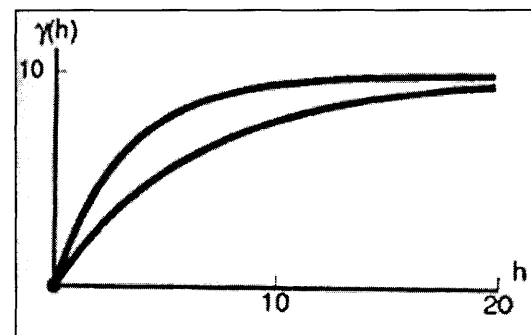


Figure 3.10: Range effect

### **3.3.5 Conclusion**

For any geostatistical application, experimental semi-variograms are calculated based on the existing data and then an appropriate theoretical model is chosen for capturing the spatial structure of the domain.

Before the theoretical model is selected though, the existing data must be studied for different distances and directions to get an idea of its structural configuration.

## **3.4 Anisotropy**

### **3.4.1 General**

In many data sets stronger correlation of the data values along certain directions is observed. In such cases anisotropic models are required to give more weight to the samples that lie along the main axis of anisotropy, despite the fact that some other samples may be closer to the estimation point in terms of geometric distance.

In practice though, many times there is not a uniform continuity throughout the sample area, but rather local fluctuations in the direction and degree of anisotropy. The character of anisotropy in those cases is quite difficult to be captured and so sample variograms may appear isotropic. Under such circumstances, a posteriori updating procedures that can incorporate the subjective believes of the geologist-engineer are a very useful.

### **3.4.2 Models of anisotropy**

Anisotropy may include changes in the range or the sill as the direction changes. The first type is known as *geometric* anisotropy, while the second as *zonal* anisotropy; there can also be a combination of the two. Figure 3.11 shows variogram surfaces with 3 different types of anisotropy.

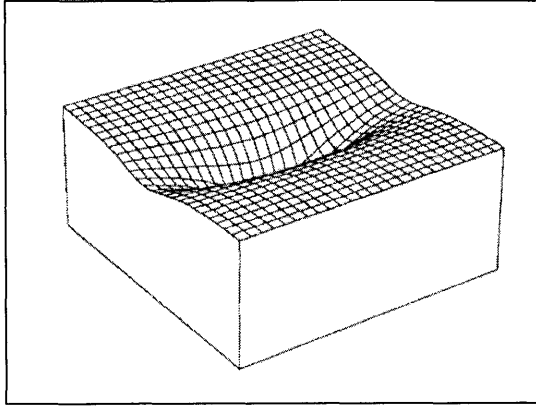


*Figure 3.11a: Geometric anisotropy*

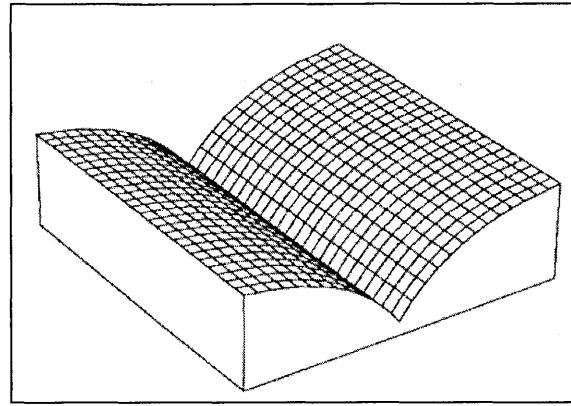


*Figure 3.11b: Zonal anisotropy*

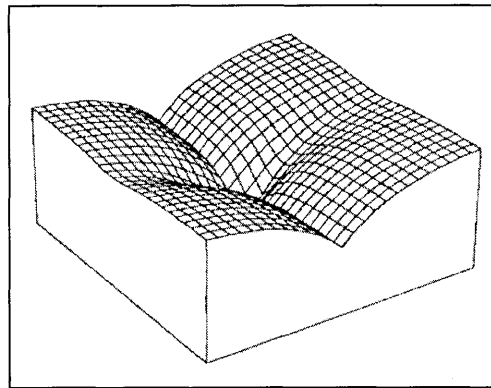


*Figure 3.11c: Combination of Geometric and Zonal anisotropy*

*(from Isaaks & Srivastava [17]).*

Should the sample variograms reveal that the data set is anisotropic, an equivalent model can be built according to the following procedure:

- a) The anisotropy axes should be identified (in other words the directions of the maximum and minimum values of the anisotropic property). Contour maps of the variogram surface, rose diagrams and geologic information/knowledge of the genesis of the phenomena are very useful for this step.
- b) A combined model should be defined that will describe how correlation changes with both the distance and the direction. For changes in the range this can be achieved by defining a transformation that reduces all directional variograms to a common model with a range of 1.

For example, if one sample variogram has a range of  $a$ , it can be transformed to an equivalent of range 1 by reducing the separation distance  $h$  to  $h/a$ . So, in an actual three-dimensional case with ranges  $a_x, a_y, a_z$ , as shown in Figure 3.12, the anisotropic variogram model will be considering an equivalent distance  $h_e$ :

$$h_e = \sqrt{\left(\frac{h_x}{a_x}\right)^2 + \left(\frac{h_y}{a_y}\right)^2 + \left(\frac{h_z}{a_z}\right)^2} \quad (3.21)$$

and so

$$\gamma(\bar{h}) = \gamma(h_x, h_y, h_z) = \gamma(h_e) \quad (3.22)$$

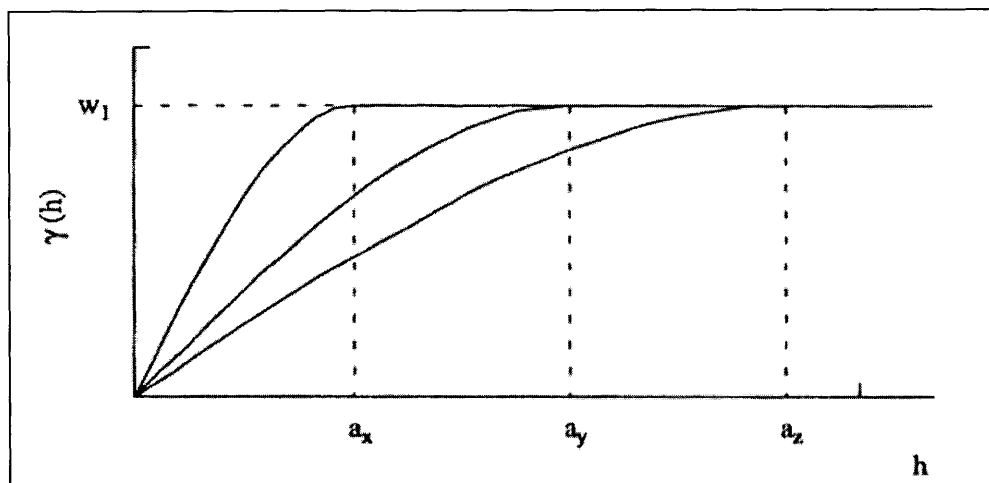


Figure 3.12: Directional variogram models along the axis (x,y,z) of a three-dimensional geometric anisotropy

For changes in the sill one should just combine the isotropic models.

So in the general case the combined model of an anisotropic data set would be:

$$\gamma(h_x, h_y, h_z) = \gamma_1(|h_1|) + \gamma_2(|h_2|) + \gamma_3(|h_3|) + \dots \quad (3.23)$$

where  $\gamma(h_x, h_y, h_z)$  is the combined model

$$h_i = \sqrt{\left(\frac{h_x}{a_x}\right)^2 + \left(\frac{h_y}{a_y}\right)^2 + \left(\frac{h_z}{a_z}\right)^2}$$

is the equivalent distance, with  $a_i$  factors accounting for anisotropy

$\gamma_i(|h_i|)$  are variograms with different sill values (but the same range, since  $h_i$  is the equivalent distance), which reflect different behaviors of the data set (i.e. zonal or geometric anisotropy, isotropic behavior, nugget effect etc).

Finally, one should note that in the above cases the combined variograms should be of the same type.

### 3.5 Cokriging

#### 3.5.1 Introduction

A data set usually contains one or more secondary variables that are spatially cross-correlated with the primary variable of interest, thus containing useful information about it.

CoKriging is a method of estimation that minimizes the variance of estimation error by taking into account the cross correlation between several variables.

The development of the CoKriging system follows the same procedure as the one for Kriging, with the difference that now one has more than one variables and more than one sets of weights.

#### 3.5.2. Main Principle-CoKriging system for 2 variables.

Consider two variables U (primary) and V. The CoKriging estimate of the primary variable at a location 0 is a linear combination of both primary and secondary data values:

$$\hat{u}_0 = \sum_{i=1}^n a_i \cdot u_i + \sum_{j=1}^m b_j \cdot v_j \quad (3.24)$$

where  $u_i$ ,  $i=1,2,\dots,n$  are the primary data samples at  $n$  nearby locations, and  $v_j$ ,  $j=1,2,\dots,m$  are the secondary data samples at  $m$  nearby locations, with  $a_i$ ,  $b_j$  respectively being the CoKriging weights that have to be determined.

It can be shown that a set of unbiased conditions is:

$$\sum_{i=1}^n a_i = 1 \quad (3.25)$$

$$\sum_{j=1}^m b_j = 0 \quad (3.26)$$

These are the most commonly used but other non-bias conditions are possible.

In CoKriging the minimization of the variance of errors is a minimization problem subject to two constraints. This requires the introduction of two Lagrange parameters  $\mu_1$  and  $\mu_2$ . The  $(n+m+2) \times (n+m+2)$  system is acquired by taking the  $n$  partial derivatives of the estimation error variance with respect to  $a$  weights, the  $m$  partial derivatives with respect to  $b$  weights and two with respect to the two Lagrange multipliers. The final form of the system is given below:

$$\sum_{i=1}^n a_i \text{Cov}(U_i U_j) + \sum_{j=1}^m b_j \text{Cov}(V_j U_j) + \mu_1 = \text{Cov}(U_0 U_j), \quad j=1, \dots, n \quad (3.27a)$$

$$\sum_{i=1}^n a_i \text{Cov}(U_i V_j) + \sum_{j=1}^m b_j \text{Cov}(V_j V_j) + \mu_2 = \text{Cov}(U_0 V_j), \quad j=1, \dots, m \quad (3.27b)$$

$$\sum_{i=1}^n a_i = 1 \quad (3.27c)$$

$$\sum_{j=1}^m b_j = 0 \quad (3.27d)$$

The variance of errors is

$$\text{Var}(R) = \text{Cov}(U_0 U_0) + \mu_1 - \sum_{i=1}^n a_i \text{Cov}(U_i U_0) - \sum_{j=1}^m b_j \text{Cov}(V_j U_0) \quad (3.28)$$

Again the spatial continuity is modeled using semi-variograms.

As in kriging, in order for the solution to exist and be unique, the set of auto- and cross-variograms must be positive definite<sup>2</sup>.

---

<sup>2</sup> The use of the linear model of coregionalization with positive definite matrices of coefficients satisfies this condition. This model provides a method for modeling the auto- and cross- covariances of two or more variables so that the variance of any possible linear combination of these variables is always positive. This is achieved when auto- and cross- covariances are constructed using the same basic variogram models.

### 3.5.3. Comments

CoKriging does not always improve the estimate of ordinary kriging. If the primary and secondary variables both exist at all data locations and the auto and cross variograms are proportional to the same basic model, then the CoKriging estimates are identical to the ordinary kriging ones. In practice, if all the variogram models are quite similar in shape and the primary variable is not noticeably undersampled, CoKriging will not improve the estimation.

## 3.6 Block kriging

### 3.6.1 Main principle

Block estimation stands for the estimation of the average value of a variable within a prescribed local area. Then this value represents the block area for correlations with any other data points (block to point correlations) or with other blocks (block to block correlations). Figure 3.13 shows the main principle of block analysis:

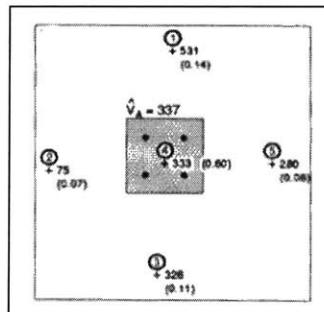


*Figure 3.13: The shaded area represents a block. The mean value of the block is estimated based on the available data, and from then on it represents the block for all other spatial correlations (from Isaaks & Srivastava [17]).*

The theoretical approach for such an estimation would be to discretize the area into blocks, obtain point estimates through ordinary kriging for each sample point in the block and average the individual point values in the block to obtain the estimate for the block. The disadvantage of this procedure in practice is that it requires too much computational



time. A better approach is to modify ordinary kriging so that only one kriging system for each block estimate will have to be solved.

Considering the kriging system described by (3.8) one notices that matrix  $C$  does not contain any information about the location of the estimation point, and so of the block to be estimated. Matrix  $D$  actually consists of covariance values between the random variables at sample locations and the one at the estimation location.

For the purposes of block analysis a random variable  $V_A$  describing the mean value over the block area  $A$  is introduced:

$$V_A = \frac{1}{|A|} \sum_{j: j \in A} v_j \quad (3.29)$$

where  $v_j$  are the available data values at locations in the block (since  $j \in A$ ).

It can easily be shown that the point to block covariances for matrix  $D^{(B)}$  are then:

$$\tilde{C}_{iA} = \frac{1}{|A|} \sum_{j: j \in A} \tilde{C}_{ij} \quad (3.30)$$

and so the block estimation weights can be obtained through the modified system

$$C \cdot W = D^{(B)} \quad (3.31)$$

### 3.6.2 Comments:

- a) The discretization grid should be regular, but anisotropy can be introduced by considering different spacing in different directions (i.e. define rectangular blocks instead of square ones).
- b) Case studies (for example Isaaks [17]) have shown that although point estimates have a better mean error, block estimates have a lower spread and correlate better with the true values.

### 3.7 Bayesian updating

#### 3.7.1 Bayesian Analysis

In a Bayesian analysis, any quantity whose value is not known is a random variable; this random variable can take on various values, and if it is continuous, it may be expressed in the form of a *probability density function (PDF)*. Any data initially known about the random variable is used to form an *a priori* PDF. Any new information obtained is then used to determine a new *a posteriori* PDF, which represents an updated state of knowledge about the random variable. This *a posteriori* PDF can then be used in any future updating or analysis, replacing the *a priori* PDF.

The above justified by Bayes' Theorem (section 3.7.2) and is summarized in equation 3.32:

$$f_{Z|X}(Z_0/x_0) = \frac{f_{x|Z}(x_0/Z_0)f_Z(Z_0)}{\int_{Z_0} f_{x|Z}(x_0/Z_0)f_Z(Z_0)dZ_0} \equiv f_Z(Z_0) \quad (3.32)$$

The procedure is as follows: the a priori PDF  $f_Z(Z_0)$  for the random variable  $Z$  is initially determined. The conditional PDF for a value  $x_0$  given  $Z_0$ ,  $f_{x|Z}(x_0/Z_0)$ , can then be determined. Equation (3.32) provides the a posteriori PDF  $f_Z(Z_0)$  whenever new information is available.

#### 3.7.2 Bayes' Theorem

The updating procedure is justified by Bayes' Theorem: Given an event space  $A$  composed of events  $A_1, A_2, \dots, A_N$ , which are mutually exclusive and collectively exhaustive, that  $P(B) \neq 0$  and that  $B$  occurred, the probability that  $A_i$  given  $B$  occurred can be determined by:

$$P(A_i/B) = \frac{P(A_i)P(B/A_i)}{\sum_{i=1}^N P(A_i)P(B/A_i)} \quad (3.33)$$

### 3.7.3 Appropriate PDF functions

In the Bayesian analysis, it is important to choose an appropriate PDF, so that updating or determining a *posteriori* PDFs will be simple and quick [Drake, 1967].

In general, the *a priori* PDF should be selected based on the following criteria:

- (a) it should describe the state of knowledge fairly well;
- (b) it should be specified by a small number of parameters, since realistically one can not expect to capture accurately the uncertainty believed for an *a priori* PDF.
- (c) updating of the PDF to obtain an *a posteriori* PDF should be as simple as possible.

Since the *a posteriori* PDF will be treated in the future as a new *a priori* PDF, both should be from the same family of PDFs, in order to make calculations easier. Optimally, one should be able to update the parameter values in a PDF, instead of determining a new function for use and updating each time.

Several families of PDFs have been found to satisfy the above criteria. The *normal PDF* is commonly used in mining applications for estimating errors in geostatistical estimations, and provides a powerful family of PDFs upon which to perform Bayesian analysis.

## **Chapter 4: Research in geostatistics**

### **4.1 Introduction:**

In this chapter some references to the research performed in geostatistics are presented, with main objective to review methods that KRIBS is using or could have used, and propose some improvements to the program concepts. Research fields are divided into five categories: covariance function determination, computational methods, research in kriging theory, research in subsurface modelling, and multipoint statistics. Then, possible fields for future research are discussed.

### **4.2 Covariance Function Determination:**

The research in this field intends to develop more accurately calculated covariances, and also covariance functions, which are more robust and insensitive to the data. Such developments are essential as geological or field data are usually not spatially uniform and the values deviate from the true ones due to measurement errors. In addition, it aims to provide means of specifying weighting functions.

Two classic examples of this research field are the following:

- Kitanidas (Kitanidas 1993) described how one may use a generalized covariance function that will be the same for both the original and detrended data (i.e. data which have the drift subtracted from them). Usually, functions are graphically fit using experimental variograms from the detrended data. The generalized covariance is a version of the ordinary one, but it neglects redundant terms, which are captured through the drift of a domain. As a result, the generalized covariance for the original data and the detrended data is the same, even though the ordinary covariance is different between the two. So, one has a unique spatial description.
- Bourgault (Bourgault 1992) proposed the use of a multivariate variogram to deflate similarities between distant samples. This method produces spatial weighting functions, which automatically form spatially homogenous groups, or in other words,

it groups spatial regions into clustered groups. This research is important for providing a means of taking spatial data into account in cluster analysis techniques.

#### **4.3 Computational Methods:**

This research field is aiming at improving the performance of computational systems when solving Kriging systems, by using more effective algorithms and procedures requiring less time and computational effort.

- Carr (Carr-Myers 1993) discussed algorithms for solving the CoKriging system efficiently, either by using an  $mn \times mn$  matrix of scalar entries, where  $n$  is the number of sample entries and  $m$  is the number of variables, or by using an  $n \times n$  matrix, where each entry is an  $m \times m$  matrix. Since CoKriging takes much more computational time than ordinary Kriging, this research attempts to minimize the time required to solve a CoKriging system. It is shown that the use of the scalar matrix formulation with standard Gauss elimination techniques results in significant reductions in computer time.
- Barnes (Barnes-You 1992), (Barnes-Watson 1992) discussed a method for extending ordinary kriging to include bounds on the estimates, and also proposed an efficient method for updating kriging estimates and variances. These methods help to improve the efficiency and accuracy of ordinary kriging, by constraining estimates to reasonable bounds (e.g. probabilities between 0 and 100 percent) and reducing the computational time necessary for multiple kriging.
- Anand (Anand 1993) presented an efficient algorithm for generating three-dimensional contour surfaces by interpolating on a regular grid. The method uses distance-weighted linear interpolation to approximate the surface.
- Cressie, Journel and others (Cressie 1991, Journel 1978) have also discussed computational issues involved in improving the performance of kriging systems.

#### **4.4 Kriging Methods:**

- Carr (Carr-Mao 1993) discussed the use of CoKriging in a probability kriging model. Probability kriging is a special form of CoKriging where one indicator variable is estimated by using two variables, an indicator variable and a uniform variable. This is used for estimating the conditional probability at a cut off. This research enables one to obtain estimates of two variables, the conditional probability and the uniform transform, whereas the original probability kriging model only obtains one estimate, that of the primary variable.
- Goovaerts (Goovaerts 1993) discussed the principal components' analysis. The principal components are linear combinations of the original variables that are uncorrelated and capture the variability in the original data set over small distances. Spatial orthogonality is assumed, but correlation is non-negligible at short distances, so the variability of the original data set over those small distances is captured. It is a method similar to CoKriging but does not capture as much information.
- Pan (Pan 1993) compared CoKriging with Ordinary Kriging for estimating mineral resources in a polymetallic deposit. He concluded that while CoKriging involves more difficulties in modelling cross-variograms and in handling non-stationarity, it produces better estimates of ore resources, reducing the overall estimation error by 15% and the variance of error by 20%.
- Posa (Posa 1992) examined the effect of kriging weights on the non-bias conditions. In particular, 1-D and 2-D analysis using Ordinary Kriging and Universal Kriging were performed and compared, showing that when the nugget effect is small, Ordinary Kriging and Universal Kriging have equivalent interpolation conditions, while when the nugget effect increases, the differences between the two kriging methods become larger.
- Schmitz (Schmitz 1990) compared the Gaussian conditional mean method with Universal Kriging. The Gaussian approach assumes normally or lognormally distributed spatial variation, while in Kriging this is not explicitly imposed by the method, but results from the linear form of the kriging estimator. He showed that both

methods always yield identical results, but Kriging requires fewer assumptions and can take into account that parameters of the regression model can be also estimates.

- Solow (Solow 1993) studied the case of threshold problems (i.e. problems where the value of a variable exceeds a specified threshold value) and showed that the indicator approach is useful when the distribution is normal, because the indicator approach is not very sensitive to extreme values.
- Spikula (Spikula 1983) discussed the use of a best (minimum variance) linear unbiased estimator (BLUE) for estimating soil properties along with lagrangian techniques for minimizing the estimation variance. Spatial correlation is performed in his model using an autocorrelation function to interpolate the exploration data. Case studies showed that a BLUE method, as he describes it, is useful when abundant data exist, but is no panacea and begins to break down when the data is sparse.
- Yates (Yates 1986) continued a discussion on disjunctive Kriging methods, focusing on disjunctive CoKriging. This is a non-linear estimator that yields better estimates than ordinary CoKriging, in terms of accuracy and reduced variance of errors. Its disadvantage is that it requires more computational time (which is not as much of an issue nowadays).
- Journel (Journel 1986) introduced the Soft Kriging (or Bayesian Kriging) approach, in which “hard” data and “soft” data are integrated in a model for estimations. Soft kriging enables “inequality-type” and “soft” data to be considered. This is a classic paper and it is referred to, since it was an important step in geostatistical analysis methods, considering the nature of field information and the importance of including geological beliefs

#### **4.5 Subsurface Modeling:**

- Nobre (Nobre 1992) discussed a Bayesian Kriging technique applied to subsurface characterization. Bayesian Kriging is another kriging method, which uses linear estimators, and allows one to incorporate soft data in the model. The problem he addressed was to determine how to characterize a bedrock surface elevation based on the hard and soft information available. In this case study, he compared Bayesian

Kriging with both Simple Kriging and Universal Kriging, and found that when no uncertainties are associated with the soft data, Bayesian Kriging and Universal Kriging are equivalent, while if no soft data is specified, Bayesian Kriging is equivalent to Simple Kriging. This research also showed that if the soft data has no uncertainties associated with it, the soft data can be incorporated in Universal Kriging in the form of a drift, and produce equivalent results.

- Jones (Jones 1991) discussed the representation of subsurface using solid modeling techniques to create the bodies of ground types and Triangulation Irregular Network (TIN) techniques to generate the surfaces of the layer interfaces. This method creates 3D models, where volume calculations become very easy and cross sections can be very conveniently constructed. It requires critical interference of the engineer, but may provide some formulation for a future geostatistical approach (although layers are created as solid bodies and do not result from point data information, which can form the basis for a geostatistical analysis). Since this technique is quite different from the others discussed, its principles are illustrated in Figures 4.1 and 4.2 below.

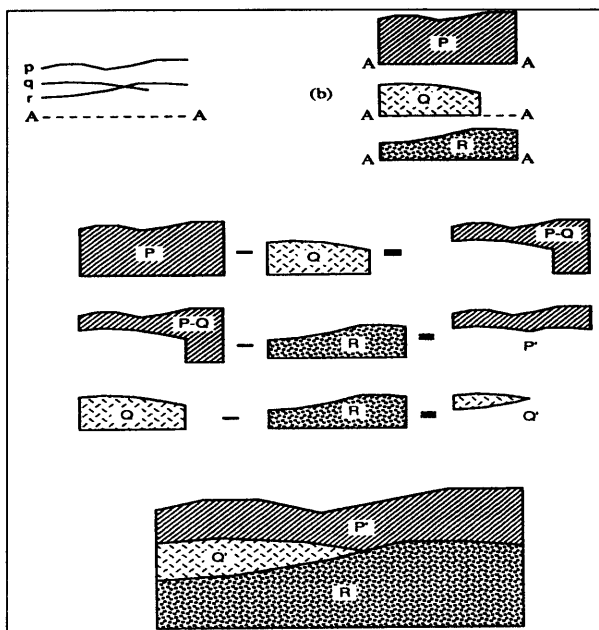


*Figure 4.1: Geologic formations are reconstructed using solid modeling. As a result the ground types are 3D bodies that can be rotated, cut, etc.*



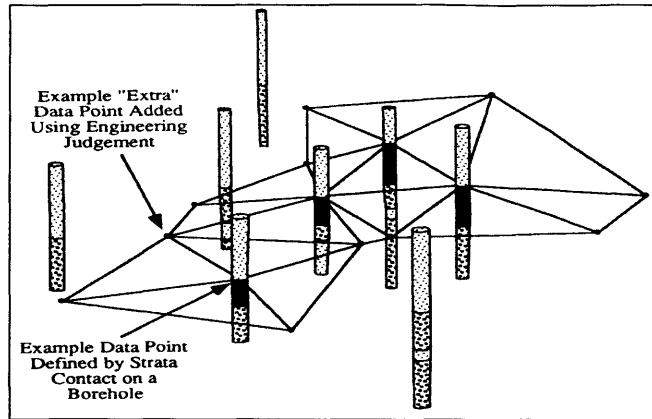


Figure 4.2: Triangulation Irregular Network (TIN) techniques are used to form the surfaces of the layer interfaces between the boreholes.

- *Bayesian techniques* have been used by Halim (Halim 1990), Einstein (Einstein 1991), Ghahreman (Ghahreman 1992), Drake (Drake 1967) and others for modelling problems where more data leads to greater knowledge in quantifying the value of a random variable. As mentioned in previous sections, the Bayesian approach treats all unknown data quantities as random variables, where each one can be described by a probability density function (PDF). Once new information is obtained concerning a random variable, the new data is combined with the existing *a priori* PDF to produce a new *a posteriori* PDF, reflecting the current state of knowledge of the random variable.

In this field, Johnson described an approach to estimate the extents of contamination plumes, using a combination of Bayesian analysis and geostatistics to capture both “soft” and “hard” information. An *a priori* Beta distribution is used to represent the probability for any grid node that contamination is present. This can then be updated using Bayesian analysis to yield to an *a posteriori* Beta distribution. Indicator kriging is used to provide a non-parametric estimation of the contamination probability at a specified location.

#### 4.6 Multipoint statistics:

- Journel (MIT, April 10, 2000) has proposed the use of multipoint statistics instead of variograms, which are 2-point covariances, in order to have an  $n$  point covariance and capture better the spatial character of the field data. His method is

based on a training image, which is a template believed to be suitable for the given data. The image is processed through pattern recognition, its important features are detected and extracted, the resulting data are statistically analyzed and then the image is reconstructed. Thus, the training image in a way replaces Kriging. The method reproduces very well data sets that even have anomalies difficult to model otherwise, because such anomalies are very sensitive to all surrounding data. The training image is important to the effectiveness of the method while its main drawback is that it requires a lot of RAM.

## **4.7 Future research**

### ***4.7.1 Method proposed by Journal***

Kriging is based on variograms, which are constructed with 2-point covariances. Multiple combinations between pairs of all the points with known data can provide a good representation of the subsurface, but still some details are not mapped. Such details are anomalies, clustering, borders between 2 different ground types. This behaviour is due to the fact that prediction of such non-ordinary points is very sensitive to all surrounding data.

In contrast, the new method proposed by Journal is using multipoint statistics which use n-point covariances. As a result estimation is smoother.

The new method should be understood in detail and applicability to the Nomad environment can be examined. Since this method requires an enormous amount of RAM a lot of research is to be done in this direction. Also the criteria for the selection of the training image are an issue that should be further discussed. Since the training image is the initial image that is being analysed, the closer this image is to reality, the more efficient and quick the method will be. Of course, the objective is not to capture all the structural details of the data, because then no further statistical analysis would be required. But should the geologist or the engineer expect any irregular features or anomalies, indication of these structures could be strategically placed in the training image to help the analysis identify information about them in the input data.

#### 4.7.2 3-D Kriging

Kriging in KRIBS is accounting for anisotropy and models are constructed for the horizontal and vertical direction. So actually kriging is limited to the 2-D plane. An approach that will produce kriging results in the 3-D space could be to use rotated 2-D variograms. One could divide the 360 space into equal angles (how small depends on computational capacity), define an origin close to where most of the data is concentrated, define vertical planes, getting away from this origin, and compute and model variograms on those planes. In this way, spatial variation could be captured in greater detail.

As a first step to this development, Hango, J.S. (1998) has added to NOMAD-KRIBS a 2D semi-variogram surface function, which calculates a series of 18 directional experimental variograms, with a five-degree half angle.

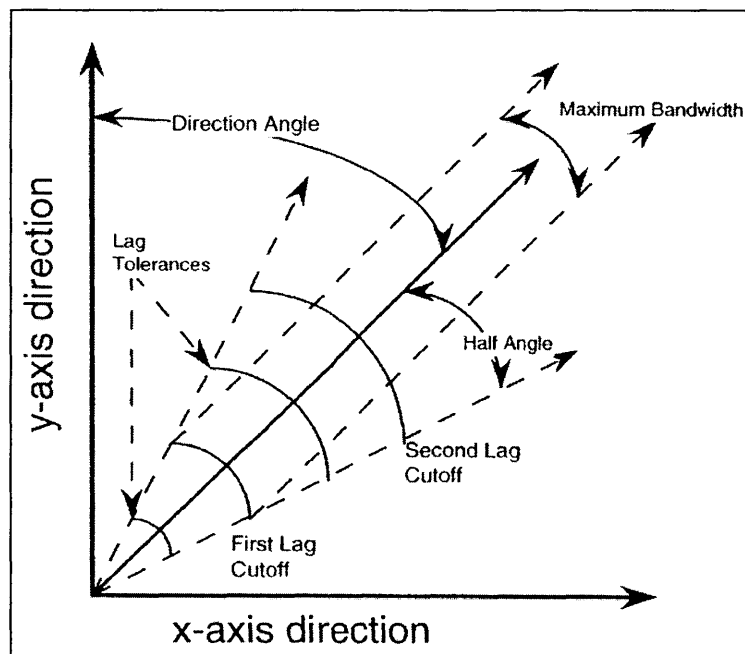


*Figure 4.3: Basic Principles of directional Variograms*

The semi-variogram values are displayed either on the same set of axes (Figure 4.4), or as a contour surface (Figure 4.5).

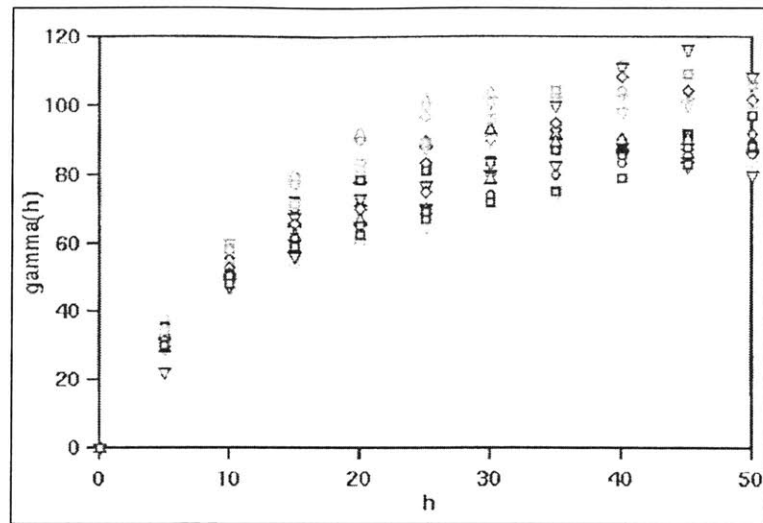


Figure 4.4: 18 directional semi-variograms along different directions plotted in the same set of axes.

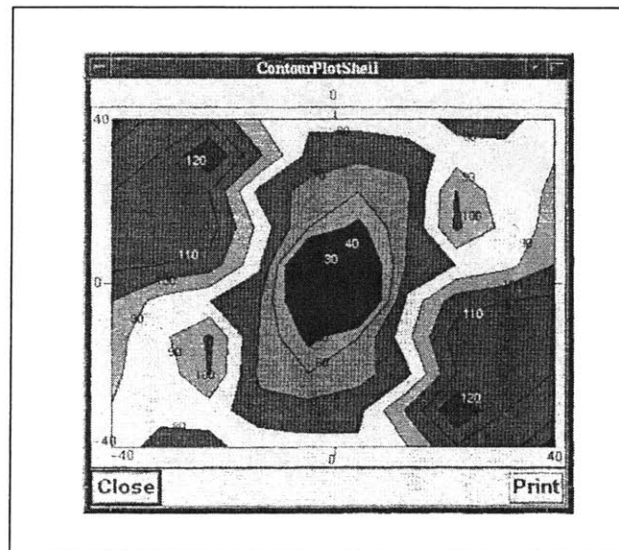


Figure 4.5: Contoured 2-D variogram surface. The darker shadings in the centre of the graph indicate lower  $\gamma(h)$  values, while the contours towards the edges of the graph indicate higher  $\gamma(h)$  values. Any cross section of this surface along a direction will yield to the plot of a semi-variogram (for this direction).

However, as Hango notes, the surface resulting from those 2D variograms is not a continuous one, and so not suitable for Kriging, which as explained in Chapter 3 requires a continuous, positive definite function. This surface in the 3-D space is an equivalent to the experimental semi-variogram in the 2-D space. So, in order to perform kriging in the 3-D space, a continuous smooth surface should be fitted to this “sample” surface connecting the directional 2-D variograms, as in the 2-D case a continuous positive definite function is fitted to the points that form the sample semi-variogram.

## **Chapter 5: Application of Nomad-KRIBS to MBTA Red Line extension from Porter Sq. to Davis Sq.**

### **5.1 Introduction**

Nomad-KRIBS has been developed and operates in the MIT ATHENA computing system. Various updates in the Athena environment during the last years have resulted in the program not being fully functional. A lot of editing features, such as inserting or curving lines, or creating cross sections were not working. Therefore functionality should be re-obtained and the program results checked before proceeding to a case study with additional parameters (time).

For this purpose one needed a well-known geologic profile, but which would also include lenses and similar non-regular geologic formations. Such a profile is the one between Porter Sq. and Davis Sq. along the Red Line. Because of the Red Line tunnel construction, a lot of borehole information exists for this alignment and the profile is well known. In addition the bedrock formation – Argillite – is generally fractured and isolated zones or lenses of different RQD values are quite frequent.

### **5.2. Interpretation of the geological information.**

The geology of the alignment is very typical for the greater Boston area. It consists of Fill, Sand/gravel, Clay, Till, Silt, Argillite and a dike of Basalt. Argillite was divided into 4 categories according to RQD values. These categories are RQD<25%, RQD 25%-50%, RQD 50%-75%, RQD >75%. Apart from the ground type, no other information was used, so only Kriging but not Co-Kriging was applied. Again the reason for this was that principal problems with the software had to be solved first.

### **5.3 Nomad**

Problems in Nomad included misfunctionalities in inserting and editing nodes or lines, creating cross sections and similar actions. In general, the main problems seem to have been successfully solved.

Figure 5.1 shows a map of the Porter Sq. to Davis Sq alignment. Figure 5.2 shows the borehole locations and the actual cross section studied. Borehole information and the actual input file can be found at Appendix II. Figure 5.3 shows the borehole logs as inserted into NOMAD and Figure 5.4 the final geologic profile along the alignment.

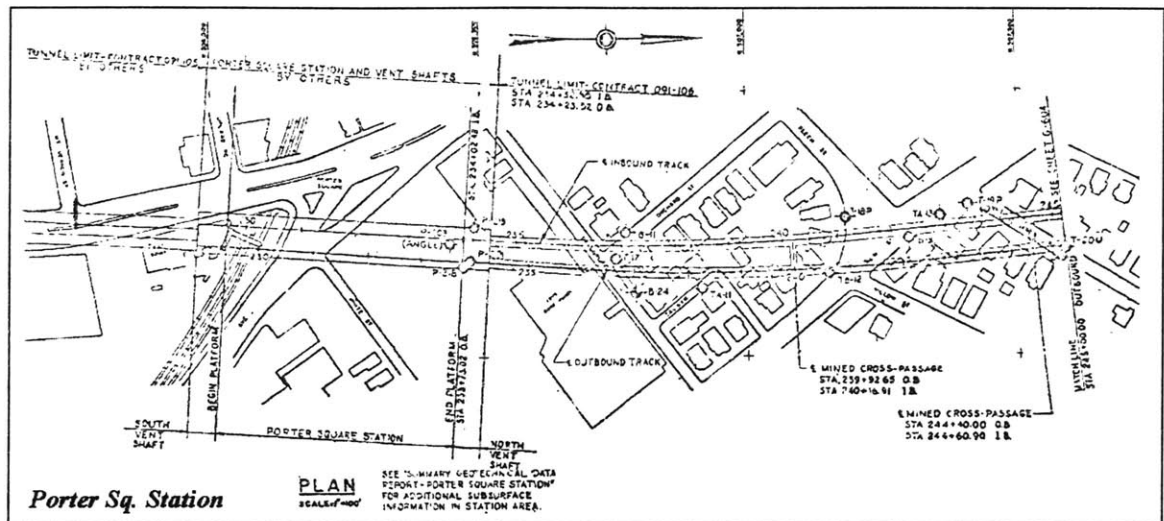


Figure 5.1a: Map of Porter Sq. to Davis Sq. alignment; Section of Porter Sq.

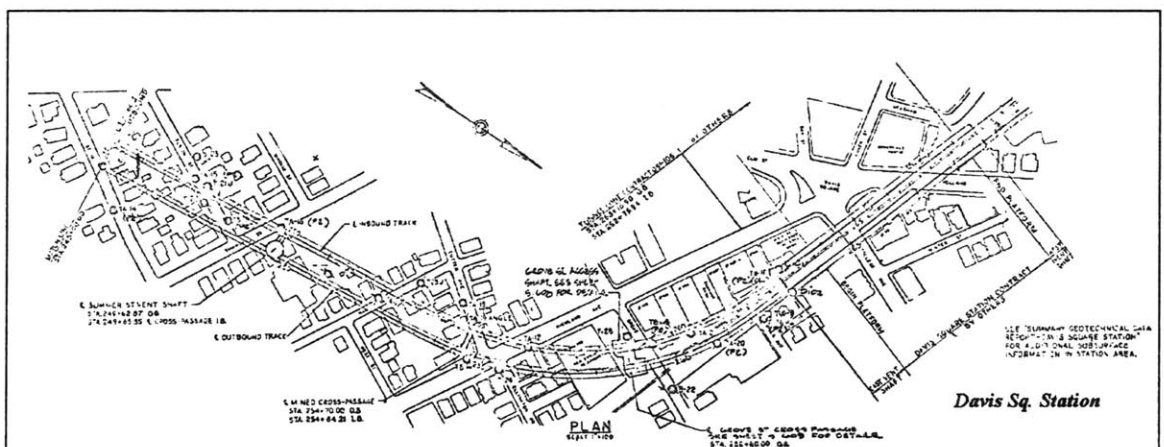


Figure 5.1b: Map of Porter Sq. to Davis Sq. alignment; Section of Davis Sq.

(MBTA maps)

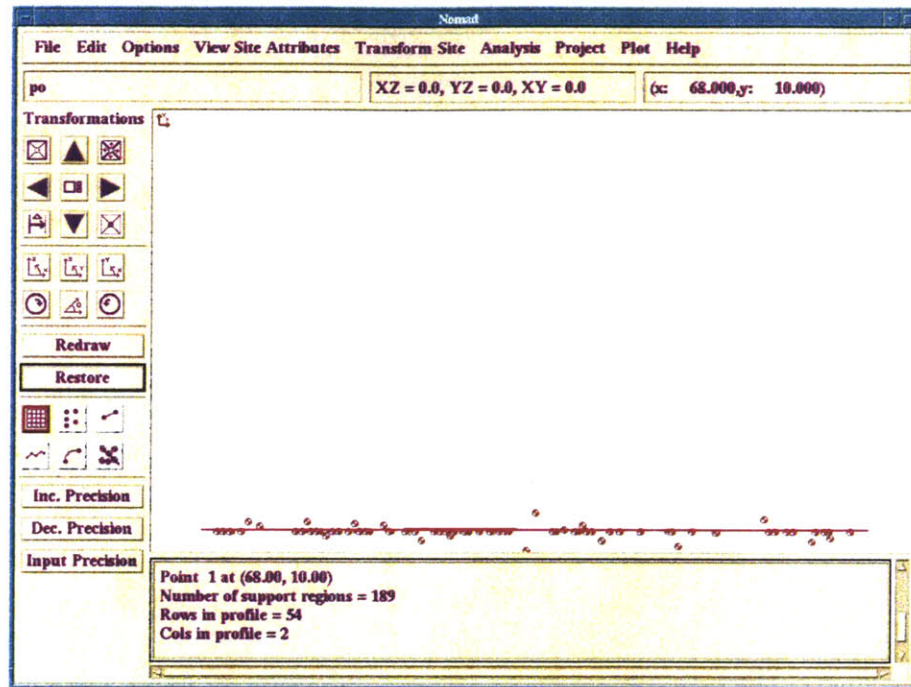


Figure 5.2: Borehole locations and alignment between Porter Sq. and Davis Sq.

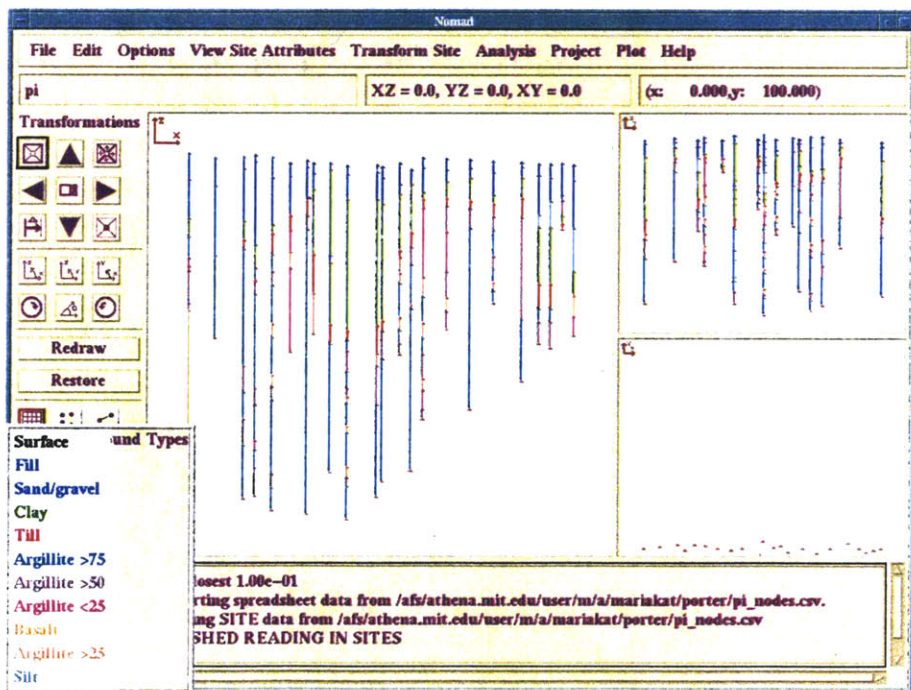


Figure 5.3: Borehole logs inserted into Nomad environment.



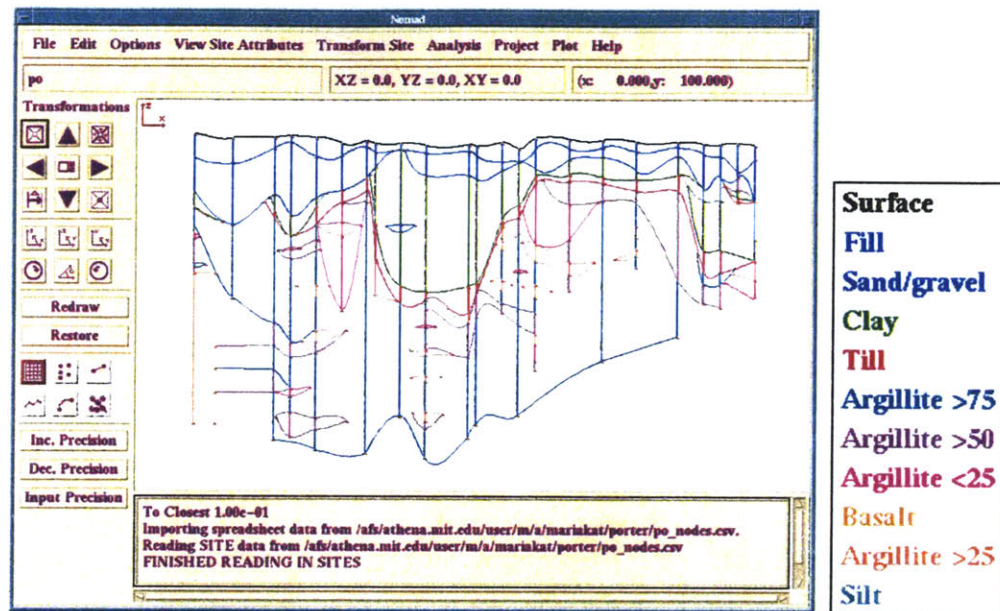
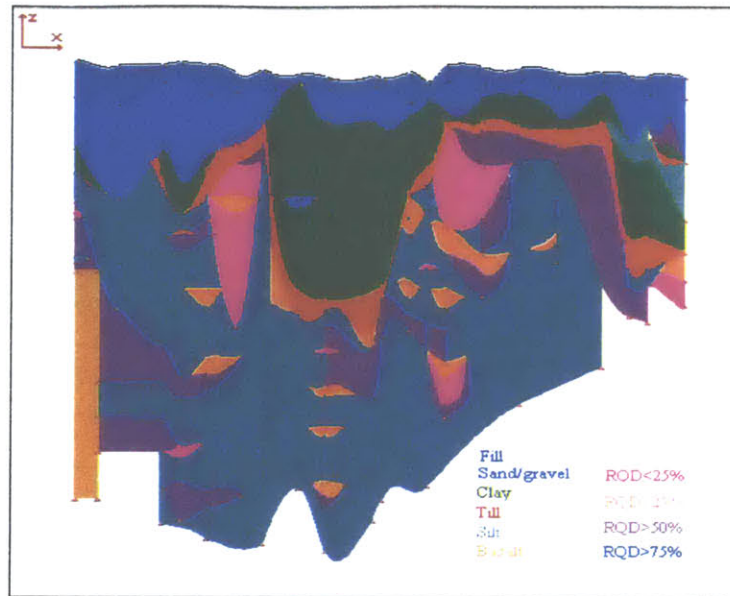


Figure 5.4 – Porter Sq.: Borehole information and geological profile.

This profile is the result of the user's interaction with Nomad's input scheme, which only provides the vertical colored lines representing the borings. Lines have been drawn connecting similar neighboring borehole sections in order to form the ground layers. Furthermore, curving of these lines enables more realistic representation of the natural geologic structures. Additional nodes have been inserted and lenses formed in the locations where borehole data indicated fractured areas in the Argillite, or, more generally, areas of different material. It should be commented though that as recovery from boreholes do not always provide reliable information for RQD, especially for fractured parts, some intervals were ignored when forming lenses of different RQD in the Argillite mass.

Figure 5.5 shows a colored version of Figure 5.4, which will be more illustrative when comparing with the results of kriging analysis.



*Figure 5.5 - Porter Sq.: Geological profile.*

#### 5.4. KRIBS

The initial KRIBS condition included fundamental problems such as the kriging algorithm not being properly called, or previous analysis not being saved each time the program was terminated. Also results had a color shift; where ground type  $i$  was expected, the color of ground type  $i+1$  appeared,  $i$  being the order of ground types in the Nomad ground type list. After improvements, most of the KRIBS features function quite well.

The first step in KRIBS is to choose a suitable grid, to determine how detailed the analysis will be. The Grid size for this case was selected  $(x-y-z)=(5-5-5)$  (ft). The corresponding profile is shown at Figure 5.6b. Less dense grids were leading to meaningless results as small variances were being lost. A profile resulting from a  $(x-y-z)=(50-50-5)$  (ft) can be seen in Figure 5.6a. Denser grids yield very good results but required too much computational time. Figure 5.6c shows the profile for a grid  $(x,y,z) = (1-1-1)$  (ft).



Figure 5.6a: Profile resulting from a coarse grid,  $(x-y-z)=(50-50-5)$  (ft).

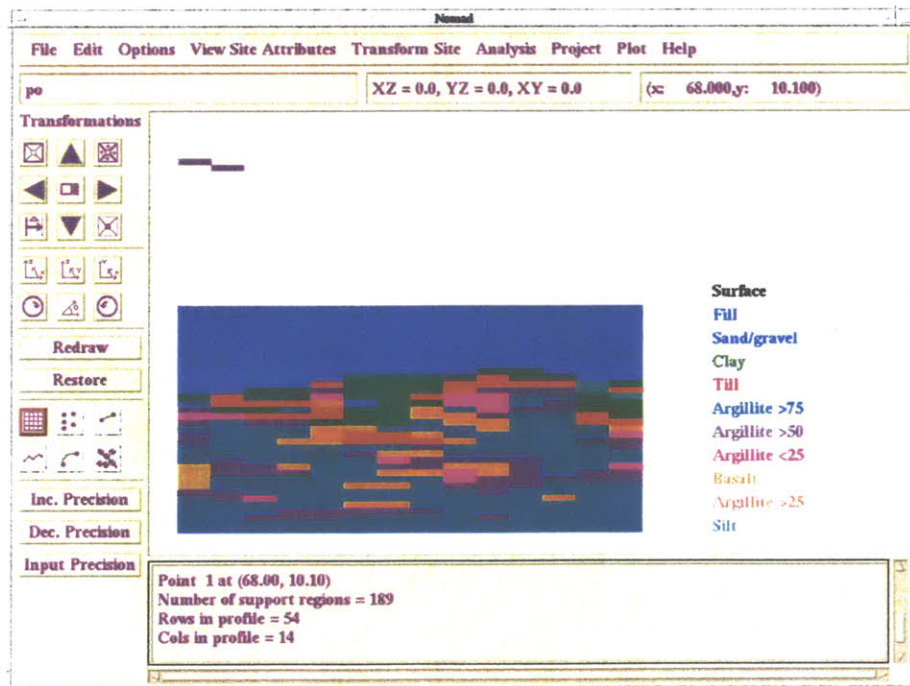


Figure 5.6b: Profile resulting from a medium grid,  $(x-y-z)=(5-5-5)$  (ft).



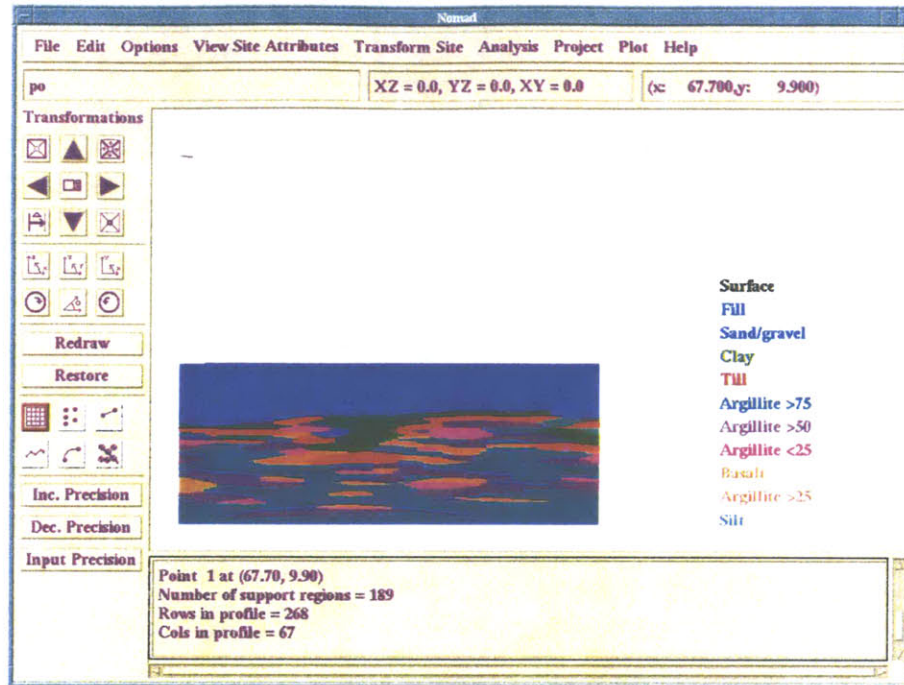


Figure 5.6c: Profile resulting from a fine grid,  $(x-y-z)=(1-1-1)$  (ft)

Should there be not isolated zones, but only continuous ground layers, correlation in any horizontal plane would be stronger than in the vertical ones, and a denser grid would be required only for the vertical direction. Since a lot of isolated lenses are expected in this area, the ground types are not uniform in the horizontal directions either, and so a homogeneous grid was chosen.

The calculated experimental semi-variograms are shown in Figure 5.7. Behavior near the origin is linear, so the model should be chosen among the spherical or the exponential one (as explained in Chapter 3.3.3). Since sample semi-variograms are quite steep near the origin (correlation is not strong), the exponential model is chosen.

The best fitting exponential semi-variogram model has parameters:

Horizontal Sill = 0.20, Horizontal Range = 15, Vertical Sill = 0.26, Vertical Range = 15, Isotropic Sill = 0.22, Isotropic Range = 15, Nugget value = 0.023.

The corresponding semi-variograms are also shown at Figure 5.7.

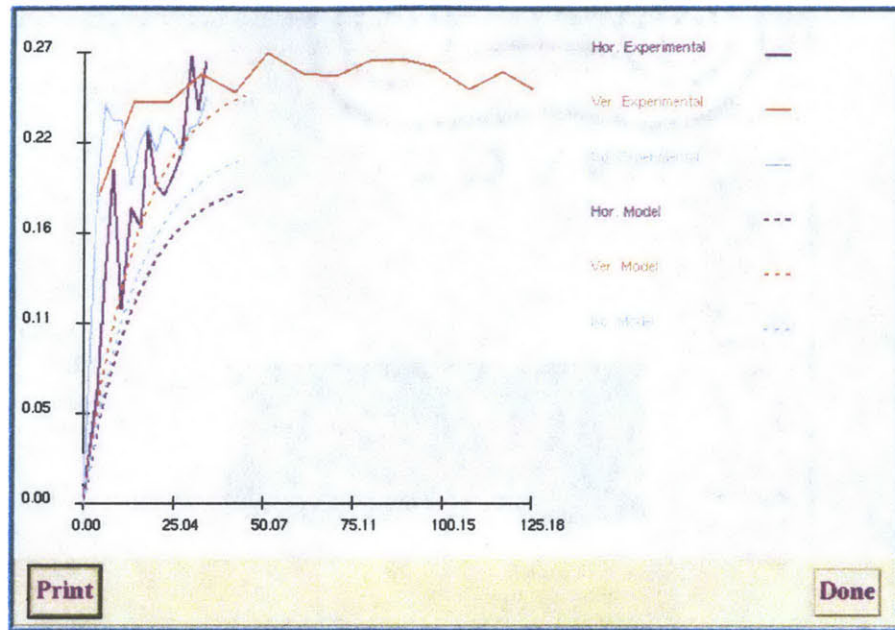


*Figure 5.7 - Porter Sq.: Experimental semi-variograms and exponential semi-variogram models*

Nevertheless, spherical semi-variogram models were also examined. The fitted semi-variogram models for this case are shown in Figure 5.8. The parameters of the best fitting spherical model are:

Horizontal Sill = 0.22, Horizontal Range = 15, Vertical Sill = 0.26, Vertical Range = 15, Isotropic Sill = 0.22, Isotropic Range = 15, Nugget value = 0.023.

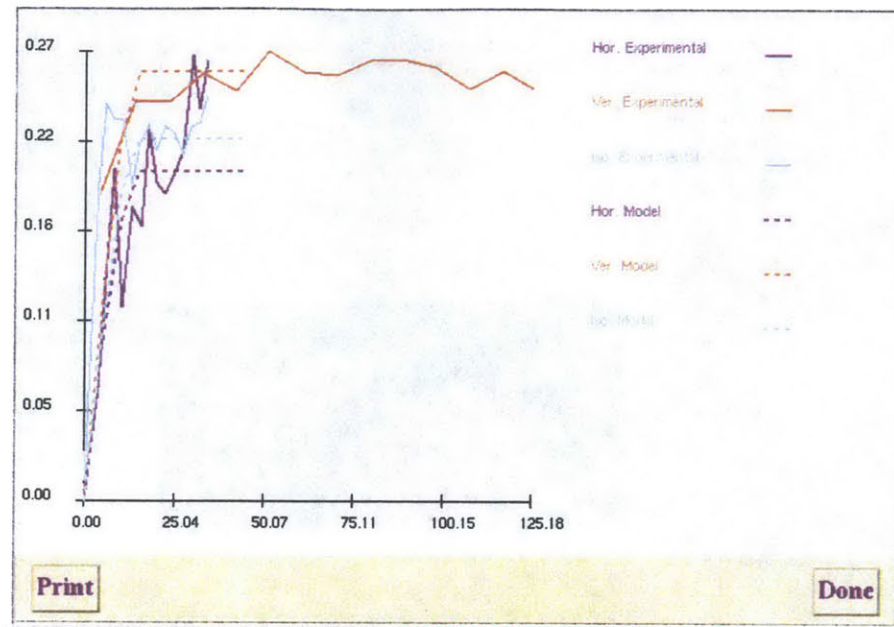


*Figure 5.8 - Porter Sq.: Experimental semi-variograms and spherical semi-variogram models*

The kriging result obtained is shown in Figure 5.9 for the exponential model and in Figure 5.10 for the spherical one. Both reflect the alignment along the site (Figure 5.2). Comparison with the simple geological profile drawn with Nomad (Figure 5.5) shows that the prediction is very close to the hand drawn profile, which, in this special case, is considered accurate, since a lot of information exists and tunneling has been performed. Even the small isolated lenses have been formed.

Figures 5.11a and 5.11b illustrate the issue of the probability threshold. In Figure 5.9 the threshold is 0%. Figures 5.11b and 5.11c show profiles with corresponding probability thresholds 30% and 50%. The blank areas in these Figures indicate where available data were not sufficient to provide a safe prediction for the corresponding threshold. In other words, areas that appear blank correspond to ground types predicted to occur with probability less than the threshold. Therefore, additional investigation should be planned for these areas.



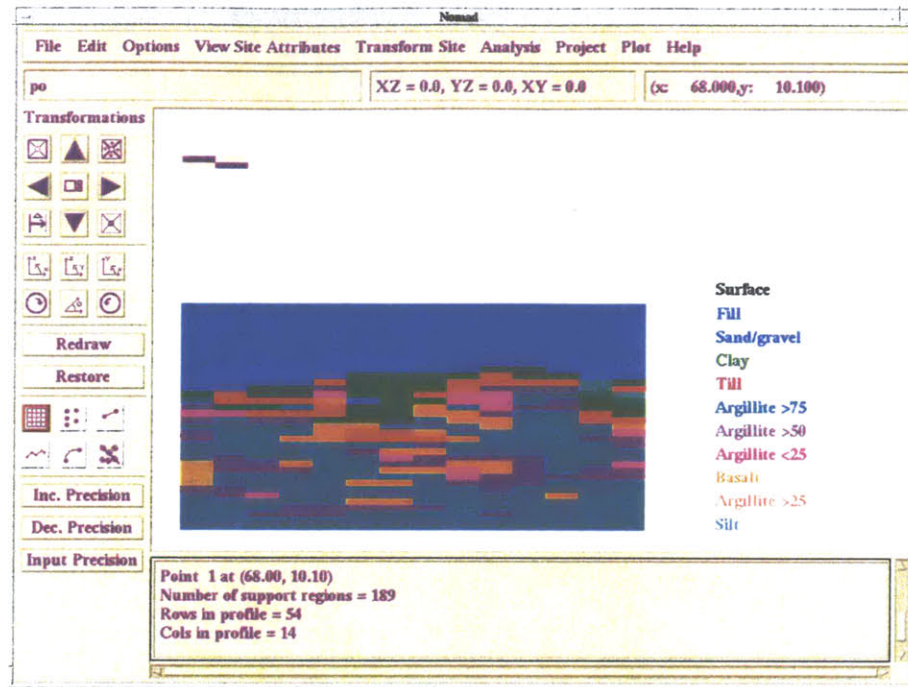


Figure 5.9: Geostatistical profile from kriging analysis based on an exponential model-Probability threshold 0%

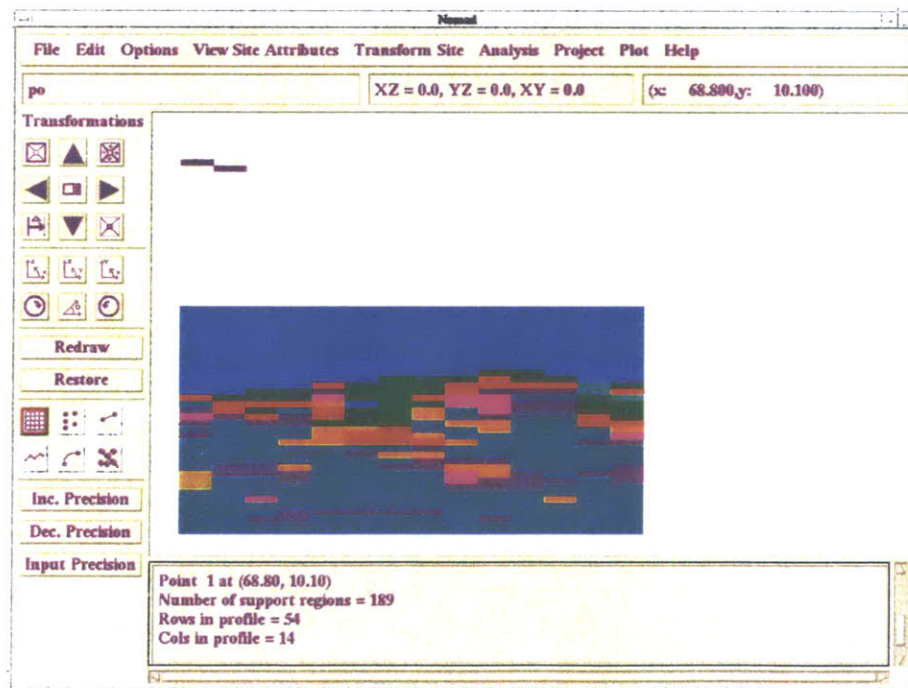
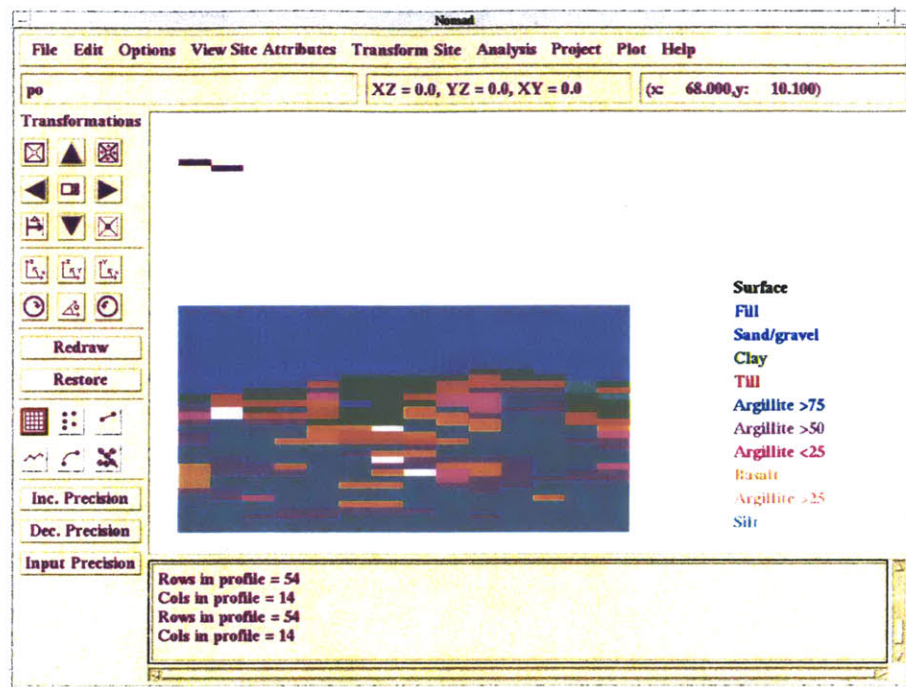
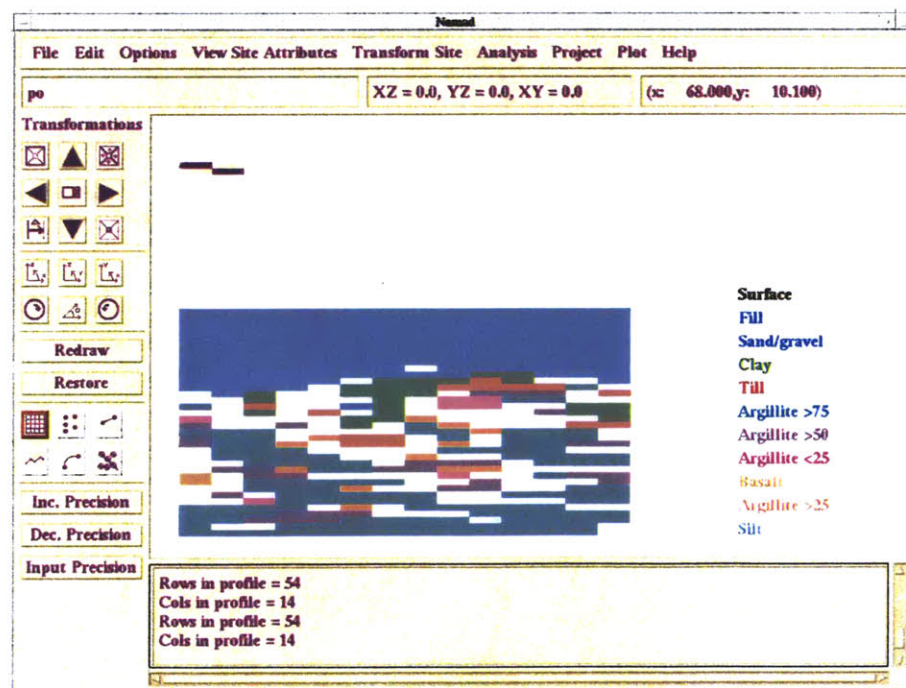


Figure 5.10: Geostatistical profile from kriging analysis based on a spherical model-Probability threshold 0%



Figures 5.11a: Kriged (geostatistical) profile with probability threshold 30%.



Figures 5.11b: Kriged (geostatistical) profile with probability threshold 50%.



A final note should be made about the selection of the range value. Initially range values of 6, 3, and 2 had been selected for the horizontal, vertical and isotropic models respectively, in order to match the experimental semi-variograms (Figure 5.12).

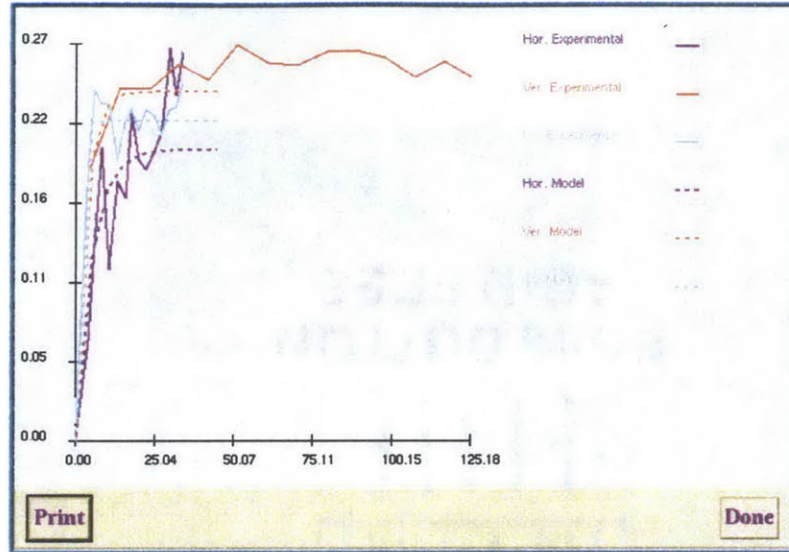


Figure 5.12: Semi-variogram models fitting the experimental data with small ranges.

Because the range values were small, blank areas were appearing in the regions where borehole distances are greater than the mean distance value, even in the 0% threshold case (Figure 5.13). As a result, a higher range (15) was selected.

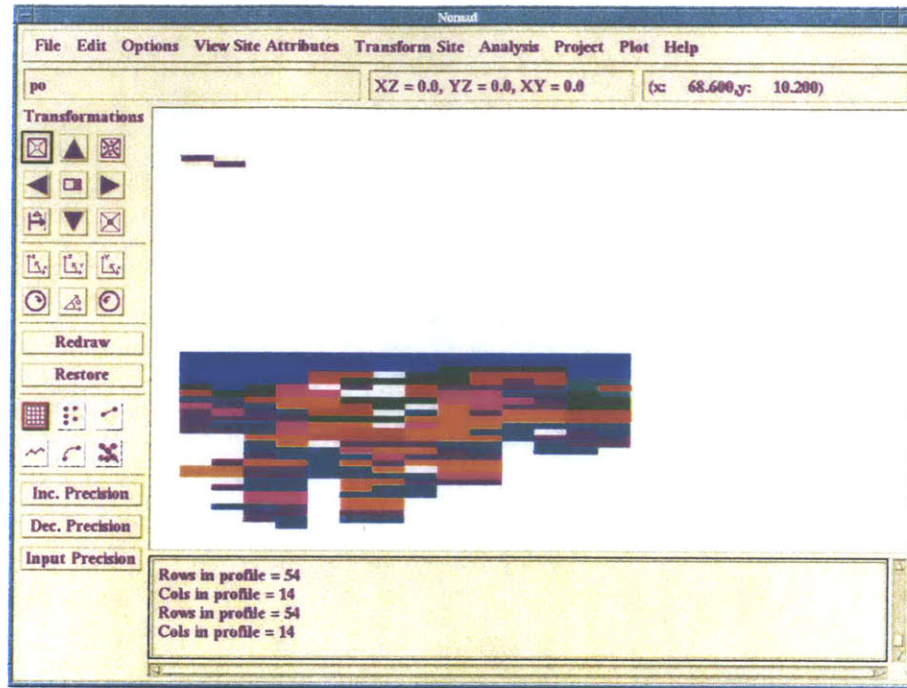


Figure 5.13: Kriged (geostatistical) profile with small range values-threshold 0%.

*Note:* In Appendix III one can find the profiles for the fine and coarse grids, the exponential and the spherical case, and for thresholds 0%, 30% and 50%.

## 5.5 Educational part

The Red Line extension case is part of a 1.383 (Underground Construction) homework problem. A report was written to introduce students to Nomad and help them use the program (in the Athena environment) to create the Porter Sq. to Davis Sq. geological profile. This can be found at Appendix I and can be used as a short introduction to the program environment and basic functionalities. For further details one should refer to Kinnicutt's Ph.D. thesis [27].



## **Chapter 6: Data changing with time: The Wellesley Maintenance Depot Site**

### **6.1 Introduction**

This case intends to study the applicability of NOMAD-KRIBS to geoenvironmental problems. Geoenvironmental problems usually involve the presence and movement of pollutants, and so, apart from having a 3D spatial nature, they involve changes over time. Such changes are of great interest to illustrate how pollutants advance and to predict their future distribution.

The program, up to now, has been used for cases not involving changes with time, so its functionality for time dependent problems will be examined and it will, possibly, be adapted to other new demands.

The study of the Wellesley case will consist of two parts:

- a) The first part will include the geological representation of the site. This will be achieved using Nomad and will reveal important information on the highly permeable paths in the subsurface. Geostatistical profiles will also be created with KRIBS. The latter will reveal the uncertainties in the geological characterization of the site.
- b) In the second part the available data of pollutant concentrations over time will be used to investigate whether NOMAD-KRIBS can be successfully used with hydrogeological and environmental data. As mentioned above, this information has dynamic characteristics, which are of great interest in order to illustrate how pollutants advance.

## 6.2 History of the site

The Wellesley Maintenance Depot site is located at the intersection of Route 9 and Route 128 in the Wellesley area, near Boston. The site has been used for about 50 years (since 1952) by the Massachusetts Highway Department (MHD) for vehicle maintenance, painting, washing, sign painting, fuel distribution, materials testing and hazardous waste storage. Numerous chemicals, such as petroleum hydrocarbons, acids, and solvents have been used or stored at the Depot. The site laboratory reportedly generated between 100 and 200 gallons per year of waste TCE 1,1,1-trichloroethane, methyl, ethyl, ketone, acetone, ether, isopropyl alcohol, and toluene. As a result the groundwater at the site was highly polluted.

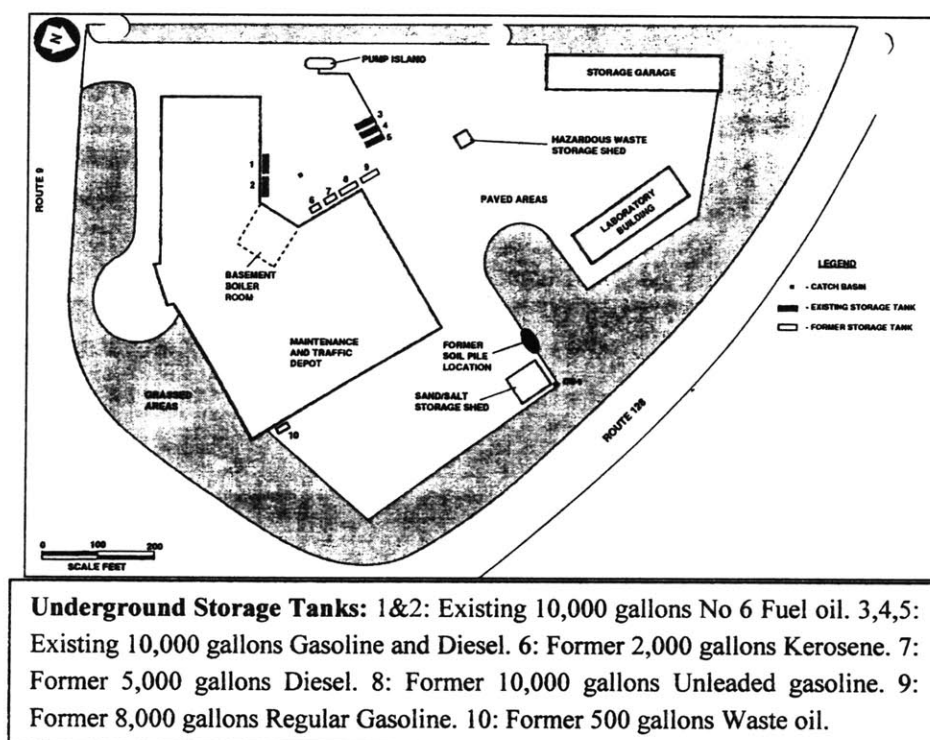


*Figure 6.1: General view of the site with some indication of stored materials (from MHD reports [32]).*

When the site changed use and an office building was planned to be built there, a general clean-up had to be done and the environmental problems emerged. In addition, it was found that some of the on-site pollutants were discharging into the local storm drain system. As a result, an extensive study of the groundwater conditions was conducted by the Massachusetts Highway Department, and data have been collected on various

pollutants at different times. Extensive information about those studies and a portion of the collected data can be found in the MHD reports [32].

### **6.3: Geologic representation of the site.**

A number of borehole logs were available, which can be divided into 2 categories: ABB boreholes and boreholes from GZA. Many of them include a screened part, so they also act as permanent wells. The detailed borehole logs can be found at Appendix IV.

#### **6.3.1: Geology and geological profiles**

The local geology can be summarized as follows:

- The fill extends to depths 5ft-8ft. It is granular and consists primarily of dense to very dense coarse to fine sand, with traces of silt and gravel.
- Below, from 7ft to 14ft there are alluvial deposits consisting of dense to very dense, coarse to fine sand, with little gravel and cobbles.
- Glaciolacustrine deposits of medium dense to very dense grey laminated silt with traces of fine sand are generally found from 13.5ft to 50ft. Lenses of silty material often appear in the upper layers as well.
- Glacial till deposits of very dense silty sand and traces of gravel extend from 50ft to 70ft.
- Bedrock was only found in two very deep boreholes (GZA-4, at depth 77ft, GZA-13, at depth 67ft). The rock is Sandstone.
- The groundwater level generally varies from 5ft to 7ft below the ground surface.

Given the collected geological data, profiles have been created using Nomad. The ground types are listed below. It should be noted that more detailed subdivisions of the ground types existed in the borehole logs, but some of them have been merged for practical reasons. These are noted in parenthesis.



*Ground types:* Widely graded sand, Sand, Gravely sand (and coarse sand), Silty sand (and fine sand), Gravel, Sandy gravel, Silt (and sandy silt), Clayey silt (silt and clay), Peat.

Figure 6.2 shows the planar view of the borehole locations. In order to obtain a better understanding of the 3-D spatial variation of ground types, profiles were drawn along three cross sections enclosing the main area of the site. These three cross sections are marked on Figure 6.2. Figures 6.3, 6.5 and 6.7 show the geologic profiles along them. Figures 6.4, 6.6 and 6.8 show the corresponding colored profiles. One may also consider the geostatistical profiles shown in section 6.3.2.

For reference, the first cross section AA consists of the boreholes ABB-B10, ABB-B11, ABB-B8, ABB-B9, ABB-B4, ABB-B5, and ABB-MW7. The second, BB, consists of boreholes ABB-SB3, ABB-SB4, GZA-8, GZA-9, ABB-15, GZA-10 and ABB-16. Finally, CC consists of ABB-16, GZA-11, ABB-12, GZA-7, GZA-12, ABB-MW10, GZA-1, GZA-2, GZA-6, and GZA-3.

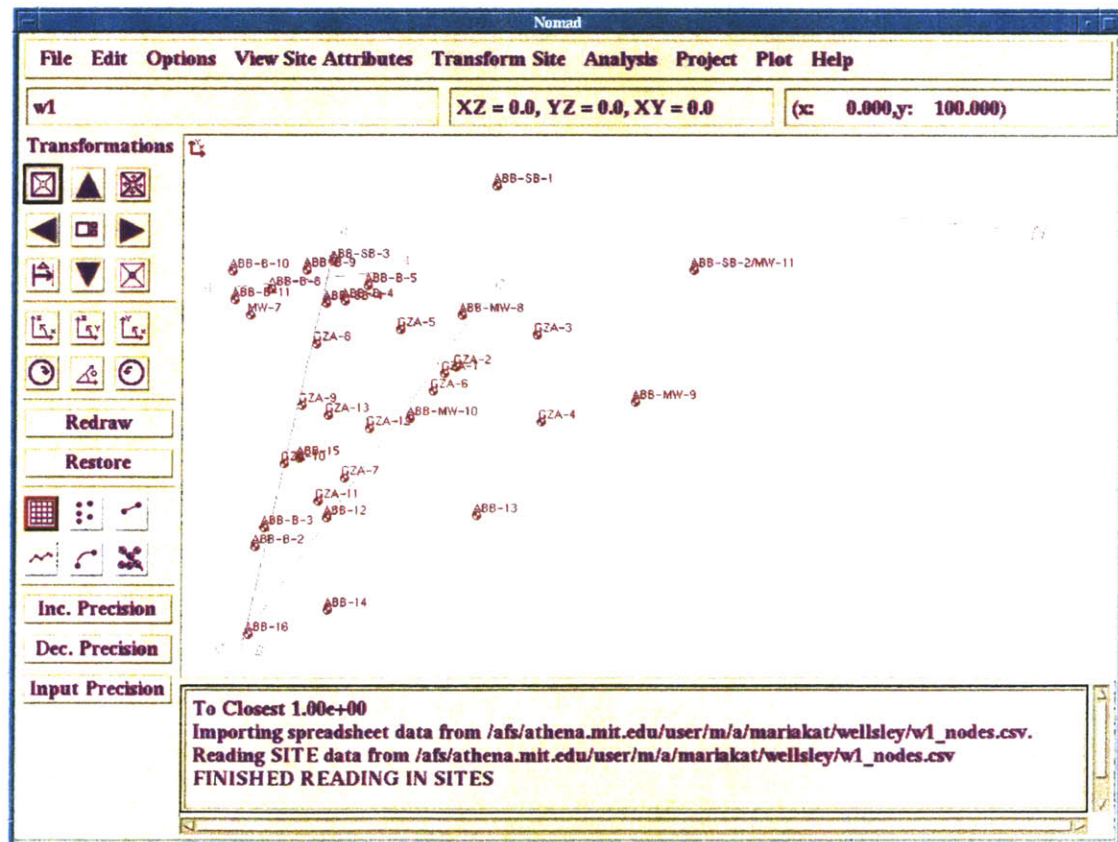


Figure 6.2: Plan view of the site

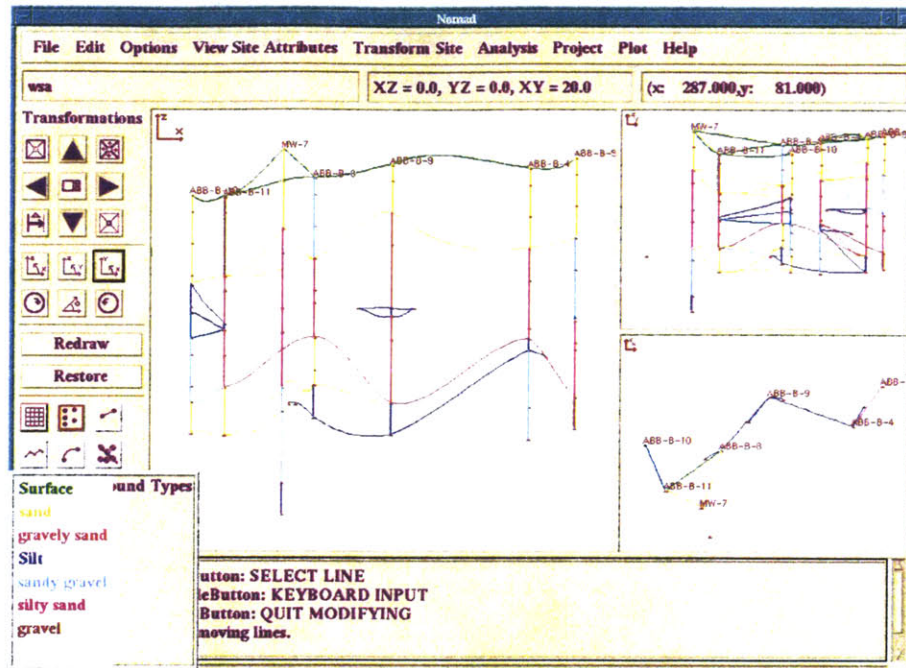


Figure 6.3: Profile along A-A

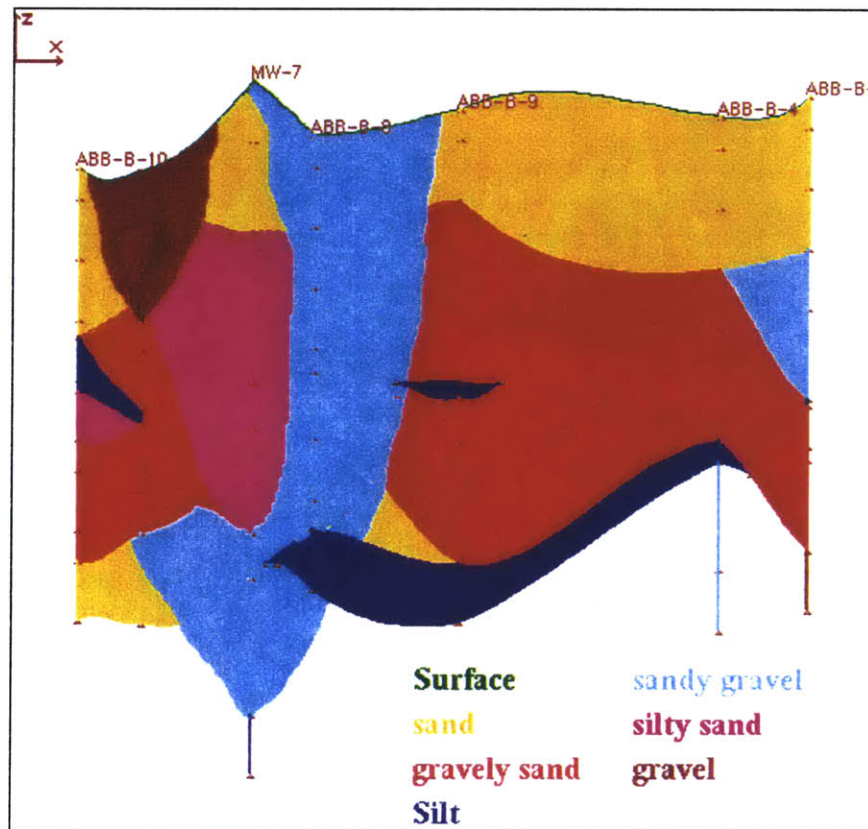


Figure 6.4: Colored profile along A-A



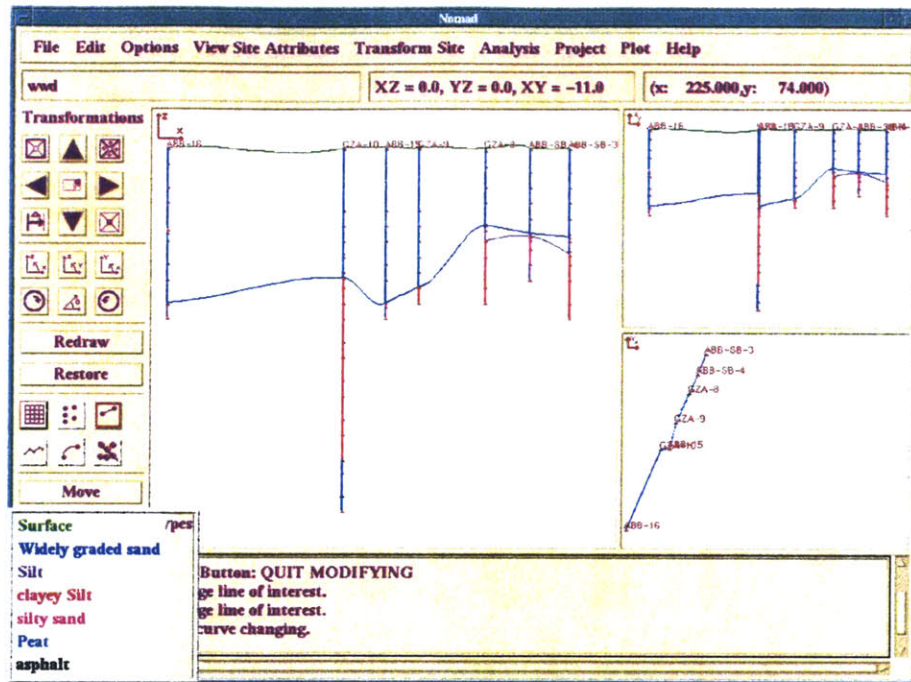


Figure 6.5: Profile along B-B

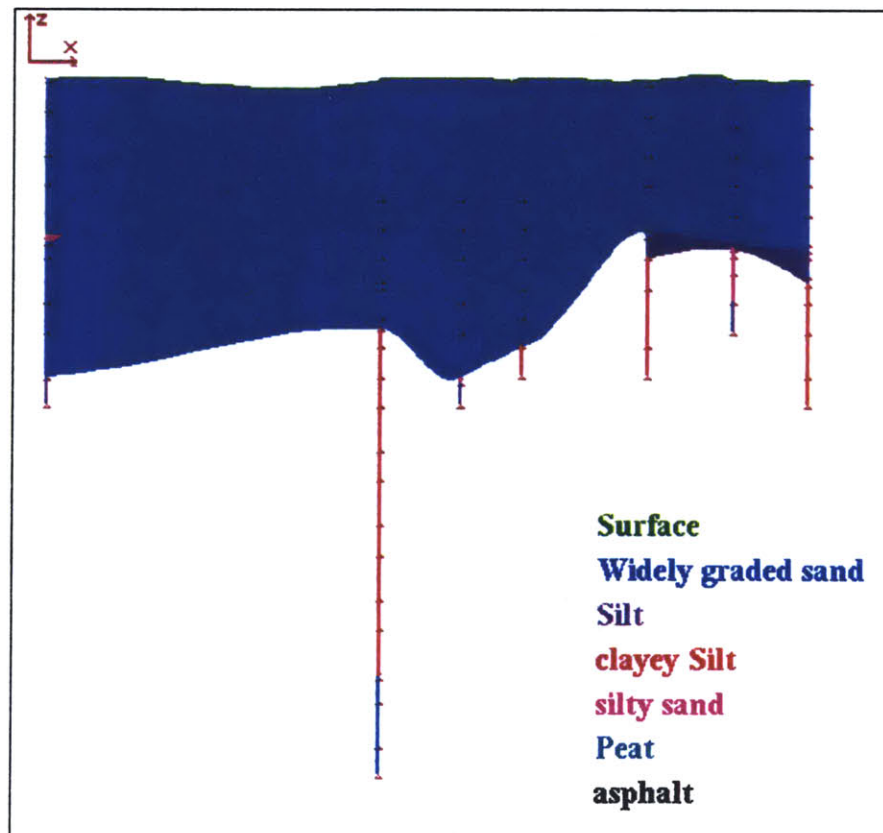


Figure 6.6: Colored profile along B-B

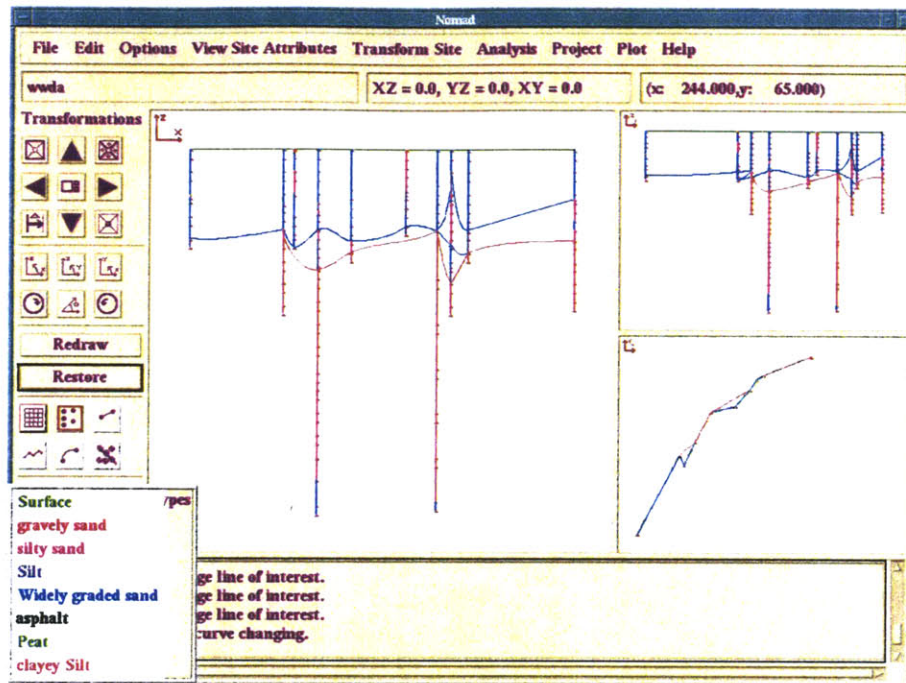


Figure 6.7: Profile along C-C

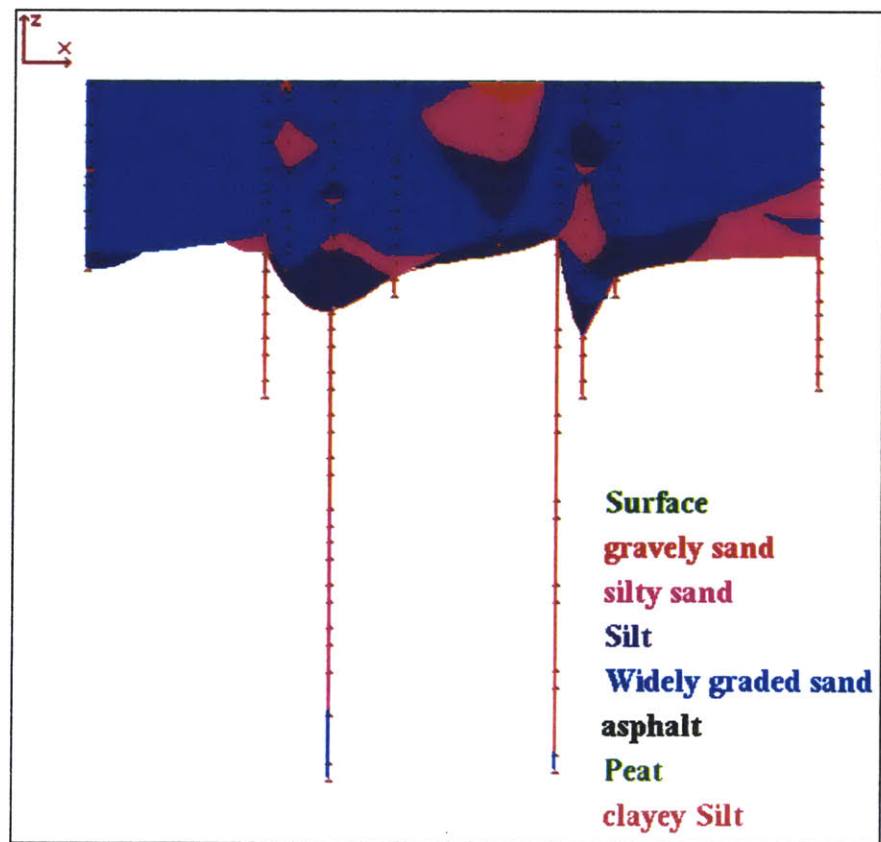


Figure 6.8: Colored profile along C-C

### 6.3.2: Geostatistical profiles

Geostatistical profiles have been generated with KRIBS. Below, the details of the analysis are given. Profiles are drawn for thresholds 0%, 35% and 50%.

#### *Cross-section A-A:*

Grid:  $(x,y,z)=(10,10,5)$  (ft). The best fitting exponential semi-variogram model to the experimental data has parameters:

Horizontal Sill = 0.30, Horizontal Range = 70, Vertical Sill = 0.30, Vertical Range = 70, Isotropic Sill = 0.33, Isotropic Range = 70, Nugget value = 0.023.

The corresponding semi-variograms are also shown in Figure 6.9. Figures 6.10, 6.11, 6.12 show the kriged profiles for thresholds 0%, 35% and 50% respectively.

#### *Cross-section B-B:*

Grid:  $(x,y,z)=(10,10,5)$  (ft). The best fitting exponential semi-variogram model to the experimental data has parameters:

Horizontal Sill = 0.25, Horizontal Range = 70, Vertical Sill = 0.30, Vertical Range = 70, Isotropic Sill = 0.25, Isotropic Range = 70, Nugget value = 0.023.

The corresponding semi-variograms are also shown in Figure 6.13. Figures 6.14, 6.15, 6.16 show the kriged profiles for thresholds 0%, 35% and 50% respectively.

#### *Cross-section C-C:*

Grid:  $(x,y,z)=(10,10,5)$  (ft). The best fitting exponential semi-variogram model to the experimental data has parameters:

Horizontal Sill = 0.19, Horizontal Range = 100, Vertical Sill = 0.35, Vertical Range = 70, Isotropic Sill = 0.25, Isotropic Range = 70, Nugget value = 0.023.

The corresponding semi-variograms are also shown in Figure 6.17. Figures 6.18, 6.19, 6.20 show the kriged profiles for thresholds 0%, 35% and 50% respectively.

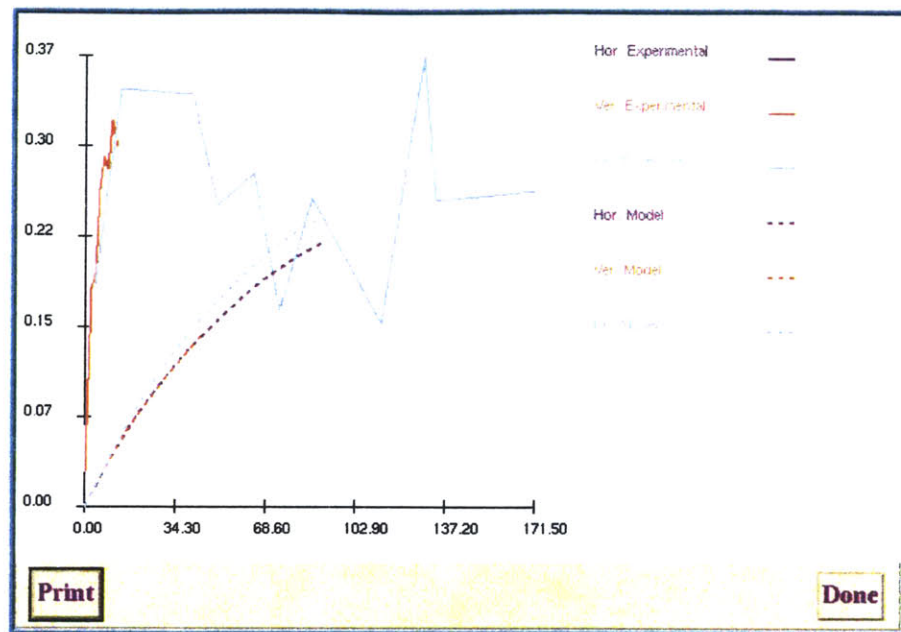


Figure 6.9: Experimental semi-variograms and semi-variogram models

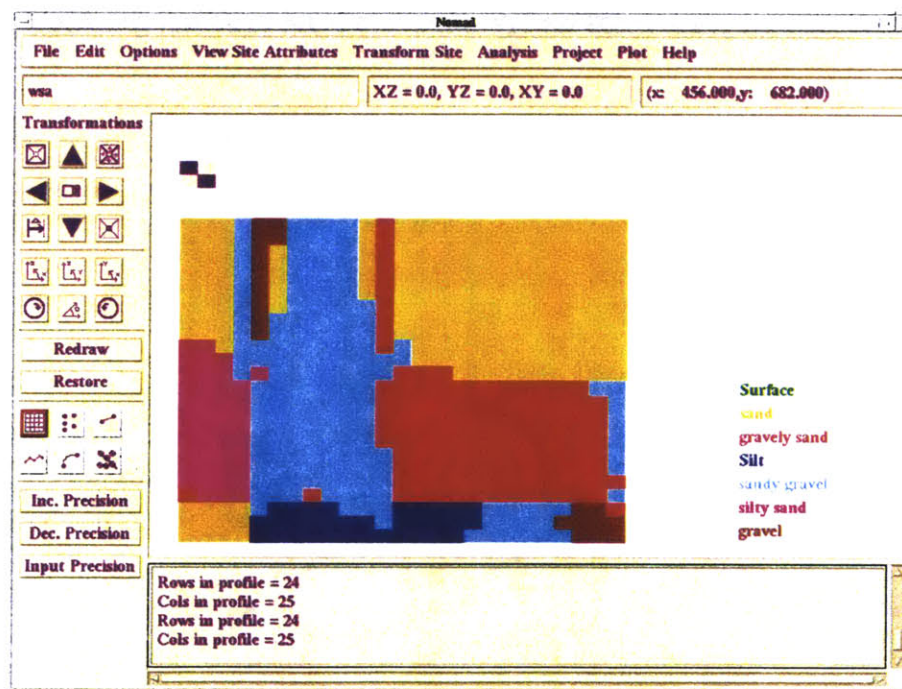


Figure 6.10: Geostatistical profile along A-A – probability threshold 0%



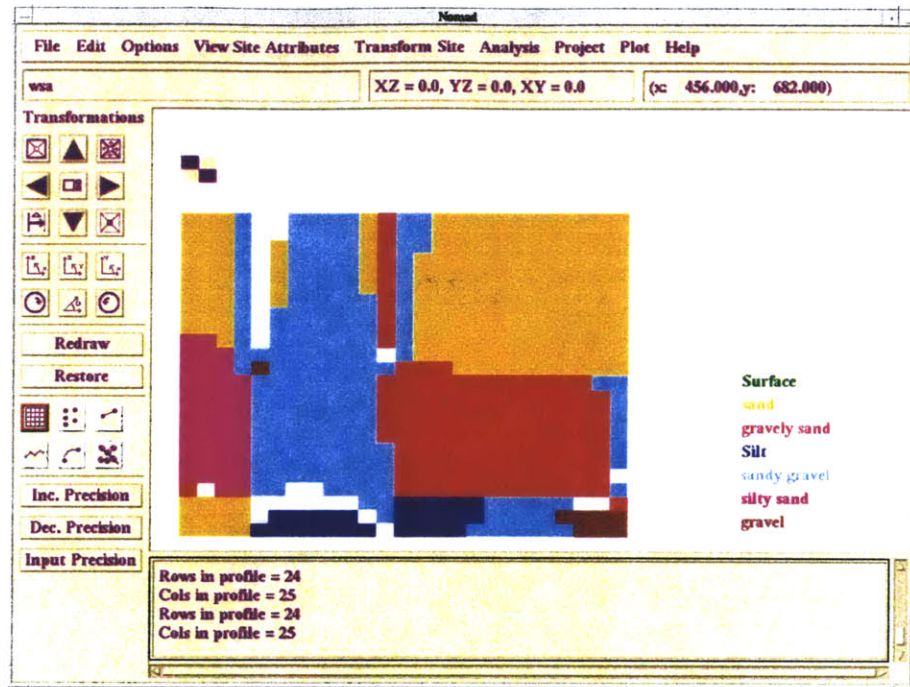


Figure 6.11: Geostatistical profile along A-A – probability threshold 35%

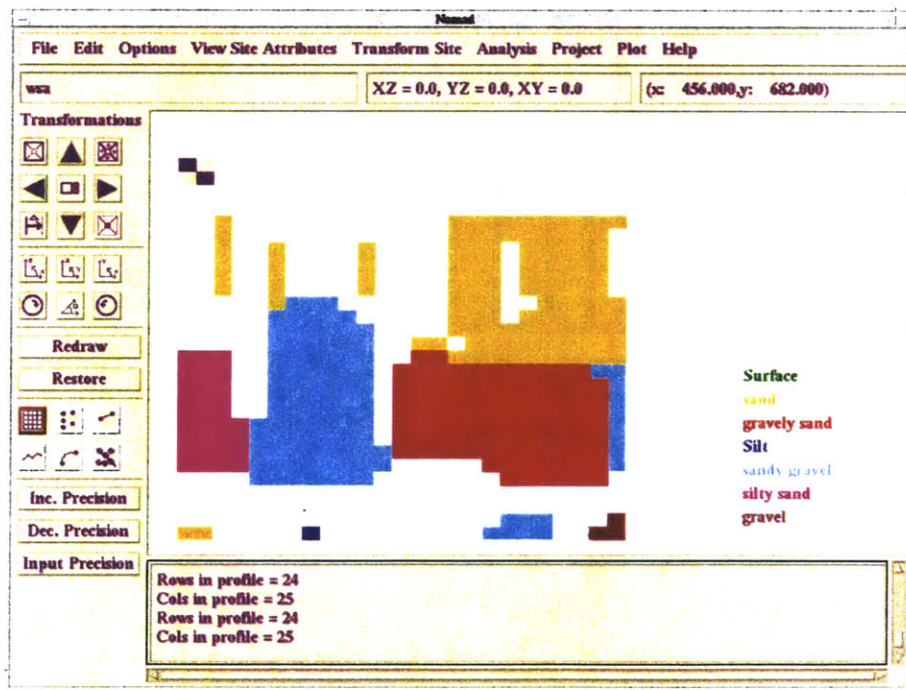


Figure 6.12: Geostatistical profile along A-A – probability threshold 50%

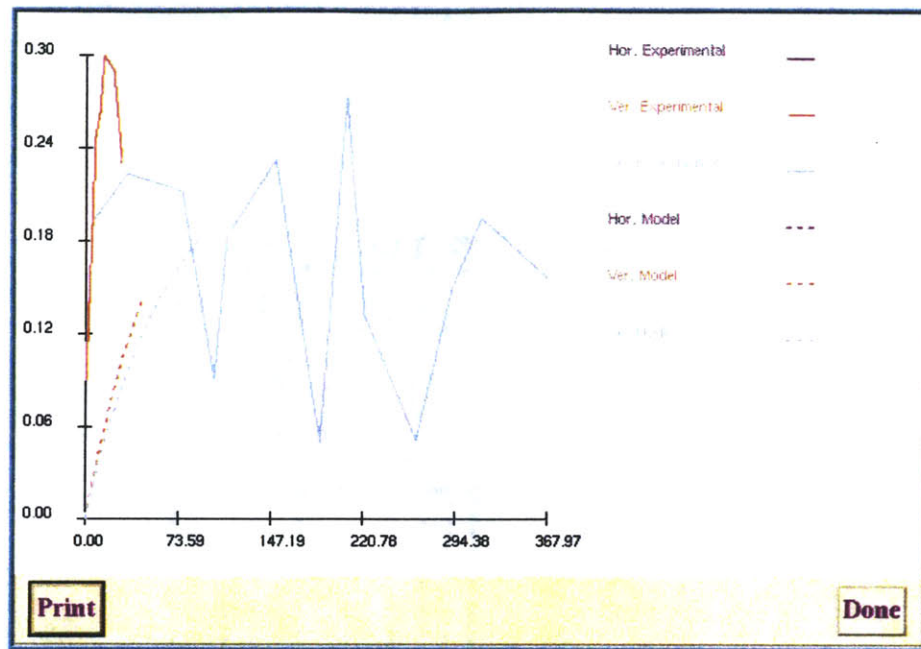


Figure 6.13: Experimental semi-variograms and semi-variogram models for profile B-B

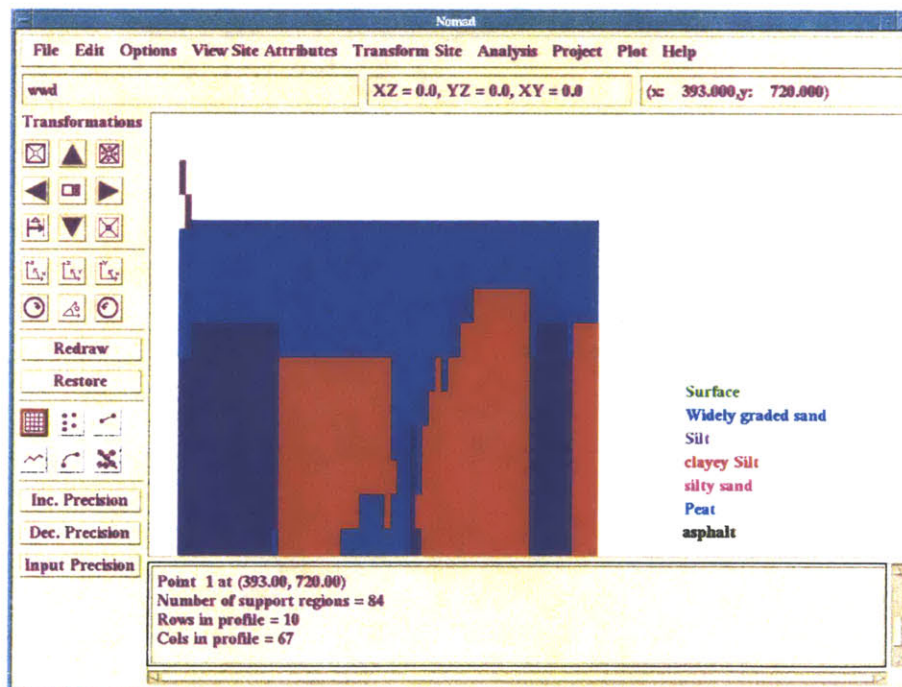


Figure 6.14: Geostatistical profile along B-B – probability threshold 0%

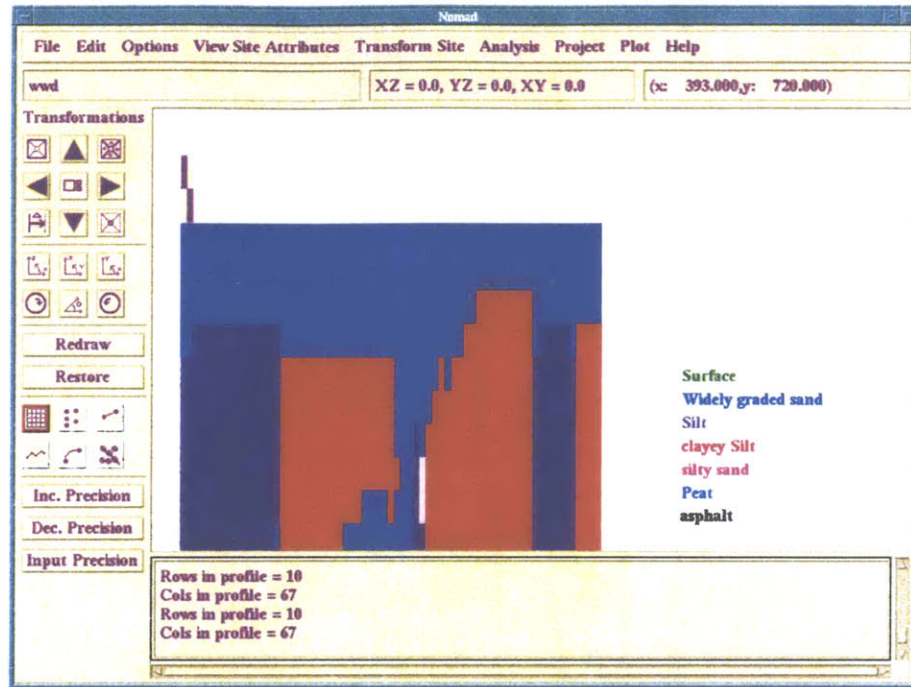


Figure 6.15: Geostatistical profile along B-B – probability threshold 35%

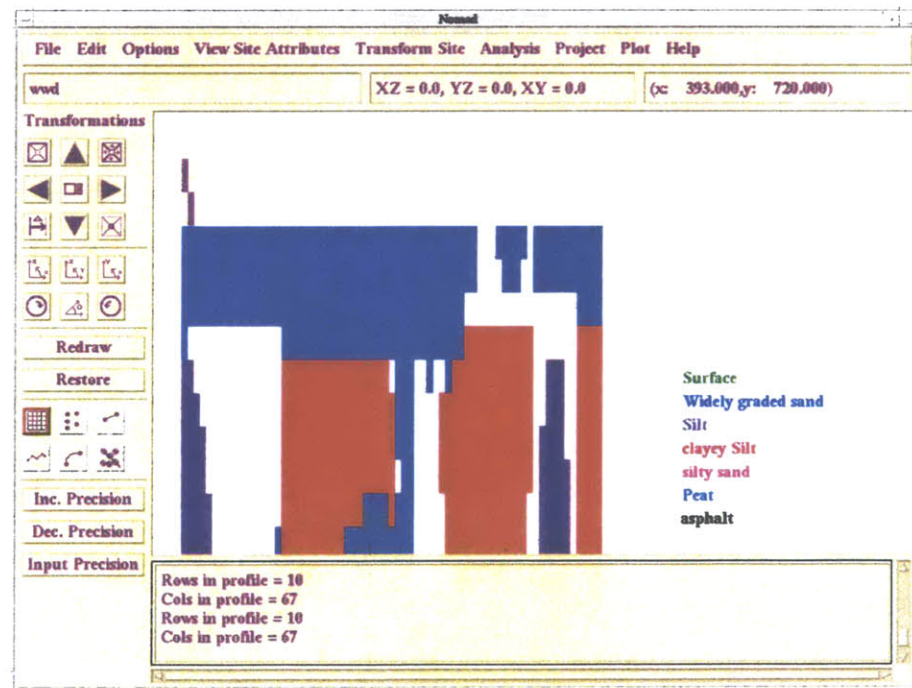


Figure 6.16: Geostatistical profile along B-B – probability threshold 50%



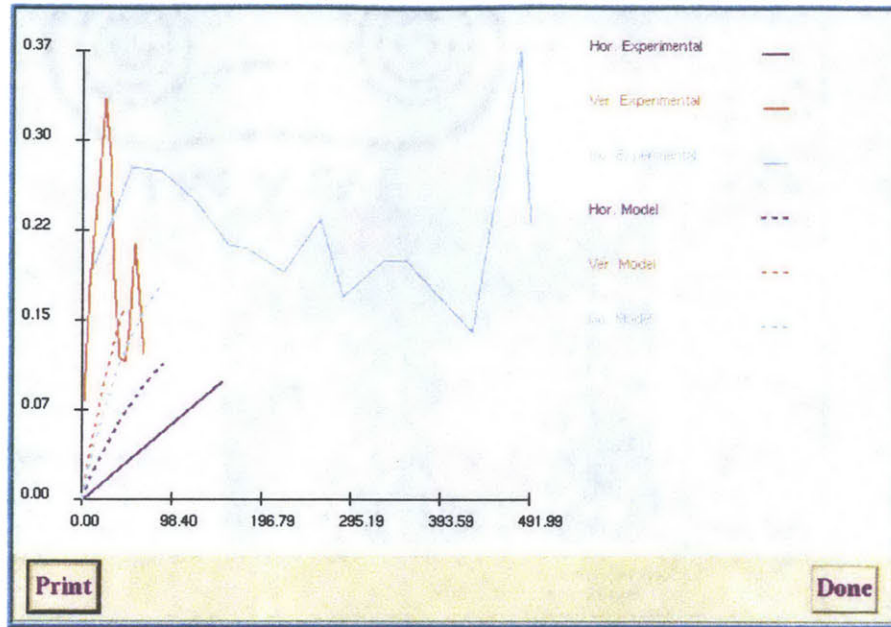


Figure 6.17: Experimental semi-variograms and semi-variogram models for profile C-C

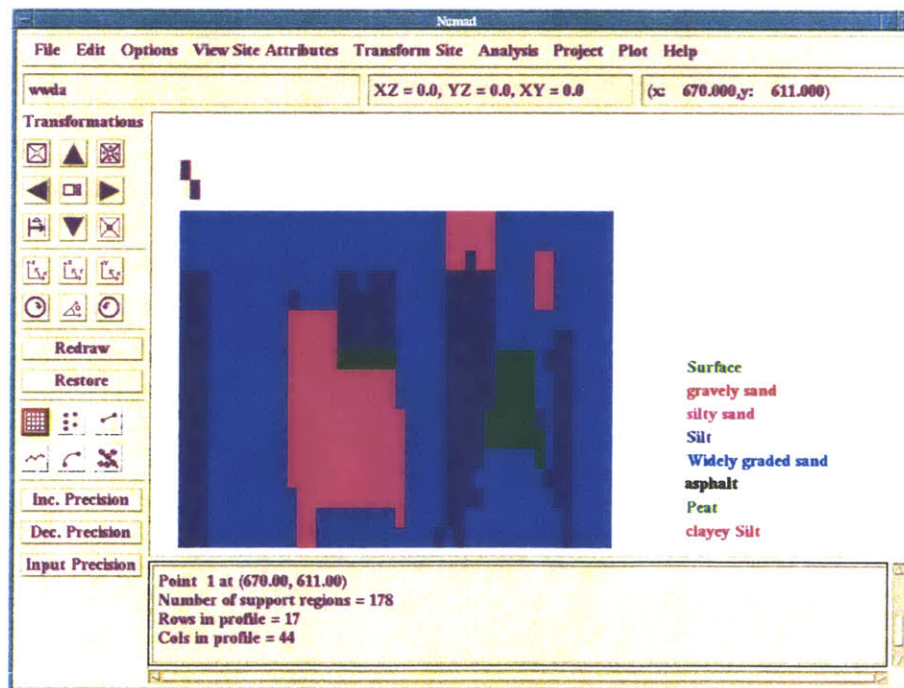


Figure 6.18: Geostatistical profile along C-C – probability threshold 0%



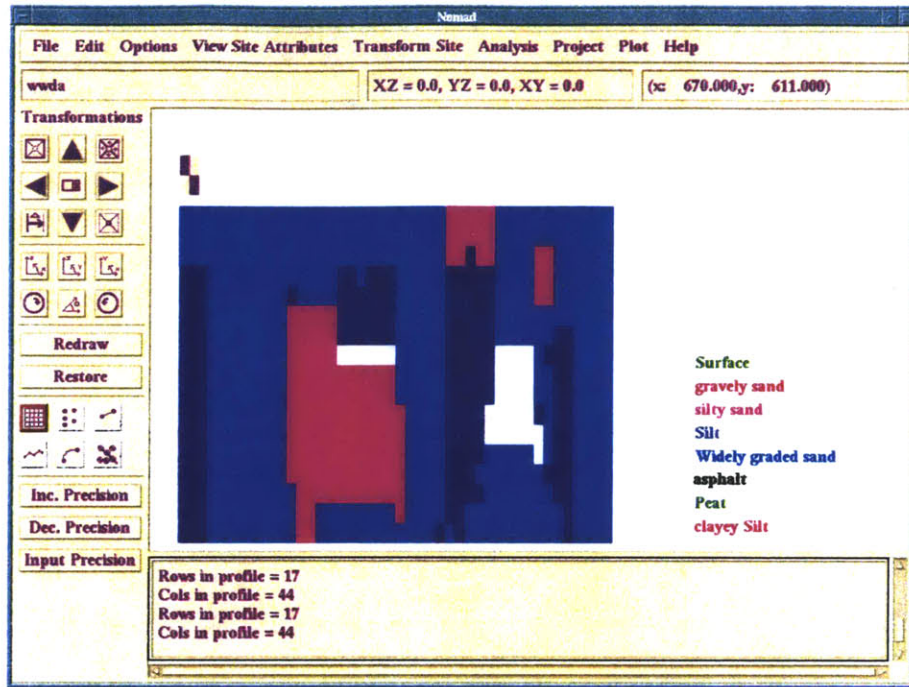


Figure 6.19: Geostatistical profile along C-C – probability threshold 35%

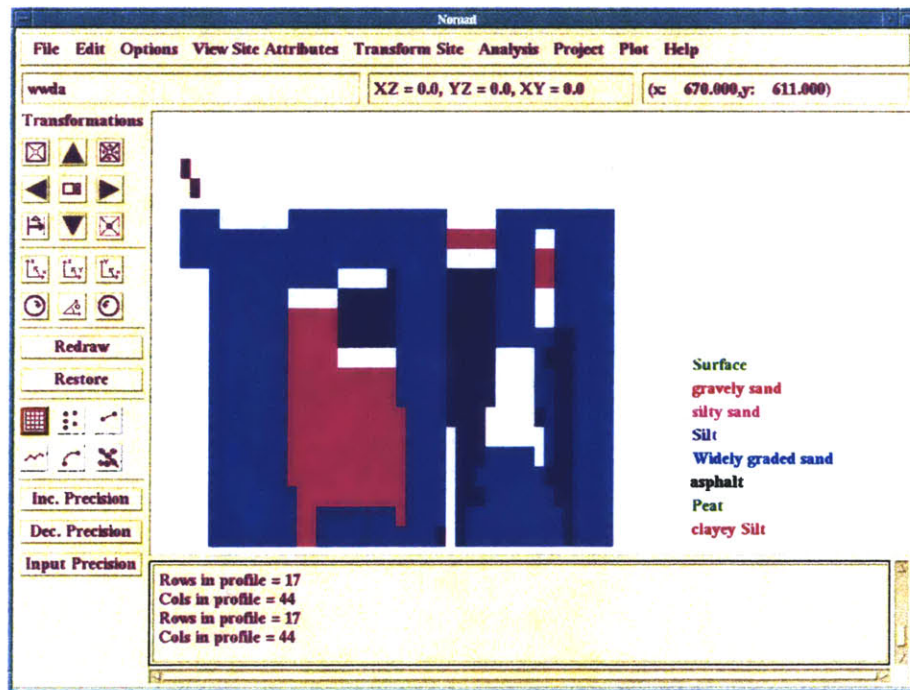


Figure 6.20: Geostatistical profile along C-C – probability threshold 50%

*Note:* The relatively high distance between the boreholes forces the range value to be also high, and this affects the kriged results. Some lenses are lost and regions are assumed to have one ground type throughout the area. An example of this can be seen when comparing Figure 6.4 (geological profile along A-A) with Figure 6.10 (geostatistical profile along A-A). The silt lenses below ABB-B-9 and ABB-B-10 are lost. Also the region below ABB-B-10 is assumed to have silty sand only instead of silty sand and gravely sand.

### **6.3.3: Interpretation of the geology with respect to expected permeabilities:**

As can be seen, from South to North at the Western part of the site (upper left in Figure 6.2, where the cross section A-A line is marked) layers of sand, gravel, gravely sand or sandy gravel dominate. In addition there are some lenses of silty material. Kriging results (especially with high thresholds like 35% or 50%) indicate that apart from the main layers (sand or gravel), there is a lot of uncertainty in this region. Therefore, one should expect isolated zones of different grain size materials in the general sandy mass, in other words, lenses of more gravely, or more silty texture.

In the perpendicular direction, (cross section B-B in Figure 6.2) a layer of widely graded sand overlies what it seems to be a fairly deep clayey silt stratum. Cross section C-C though shows that in nearby locations following a small change in direction the profile is not so clear and a lot of silty lenses exist in the upper part of the subsurface. Kriging results show that there is practically no uncertainty for the existence and extent of the widely graded sand; In contrast, the location of the silty lenses involves a lot of uncertainty.

In both cases the upper strata seem to be the highly permeable ones, but in the SN direction permeability seems more uniform and maybe higher (gravely sand) in comparison to the widely graded sand which can have very closely located points of different permeabilities. In both cases lenses of less permeable material (silt or even very fine sand) should be expected to result in local disturbance of the flow pattern and in differences of the pollutant concentrations.

## 6.4 Hydrogeological data

Among the pollutants to be studied are 1,1,1-trichloroethane, lead, benzene, arsenic, or toluene. These are among the top 25 most frequently detected groundwater contaminants at hazardous waste sites, according to the Agency for Toxic Substances and Disease Registry (Figure 6.21). The pollutant (or pollutants) used in each of the cases below has been selected to best illustrate the advance of the plume with time. In other words, we selected the pollutant which exhibits a significant change with time and for which sufficient data exist.

Rank	Compound	Common Sources
1	Trichloroethylene	Dry cleaning; metal degreasing
2	Lead	Gasoline (prior to 1975); mining; construction material (pipes); manufacturing
3	Tetrachloroethylene	Dry cleaning; metal degreasing
4	Benzene	Gasoline; manufacturing
5	Toluene	Gasoline; manufacturing
6	Chromium	Metal plating
7	Methylene chloride	Degreasing; solvents; paint removal
8	Zinc	Manufacturing; mining
9	1,1,1-Trichloroethane	Metal and plastic cleaning
10	Arsenic	Mining; manufacturing
11	Chloroform	Solvents
12	1,1-Dichloroethane	Degreasing; solvents
13	1,2-Dichloroethene, trans-	Transformation product of 1,1,1-trichloroethane
14	Cadmium	Mining; plating
15	Manganese	Manufacturing; mining; occurs in nature as oxide
16	Copper	Manufacturing; mining
17	1,1-Dichloroethene	Manufacturing
18	Vinyl chloride	Plastic and record manufacturing
19	Barium	Manufacturing; energy production
20	1,2-Dichloroethane	Metal degreasing; paint removal
21	Ethylbenzene	Styrene and asphalt manufacturing; gasoline
22	Nickel	Manufacturing; mining
23	Di(2-ethylhexyl)phthalate	Plastics manufacturing
24	Xylenes	Solvents; gasoline
25	Phenol	Wood treating; medicines

NOTE: This ranking was generated by the Agency for Toxic Substances and Disease Registry using ground water data from the National Priorities List of sites to be cleaned up under CERCLA. The ranking is based on the number of sites at which the substance was detected in ground water.

*Figure 6.21: The 25 most frequently detected groundwater contaminants at hazardous waste sites, according to the Agency for Toxic Substances and Disease Registry (from Alternatives for ground water cleanup [33]).*

The study includes two time periods; during early years, 1993-1996, not much change is observed in the pollution concentrations and it seems that cleaning-up processes had not started yet. During later years, 1997-2000 one observes significant concentration changes over a month's period.

Pollutant concentrations will be illustrated in the NOMAD environment with their values along the well logs. Similar concentrations have similar color schemes; in general green colors correspond to low concentrations, purple-red-pink are representative of medium to high concentrations, and yellow indicate very high ones. Blue colors correspond to areas above water table or where no data exists. In every case one should consult the legend of the corresponding figure. In this legend, each color is identified by the name of the pollutant and its concentration in  $\mu\text{g/l}$  (ppb); Arsenic150 stands for Arsenic concentration of 150 ppb. A sample representation is shown in Figure 6.22:

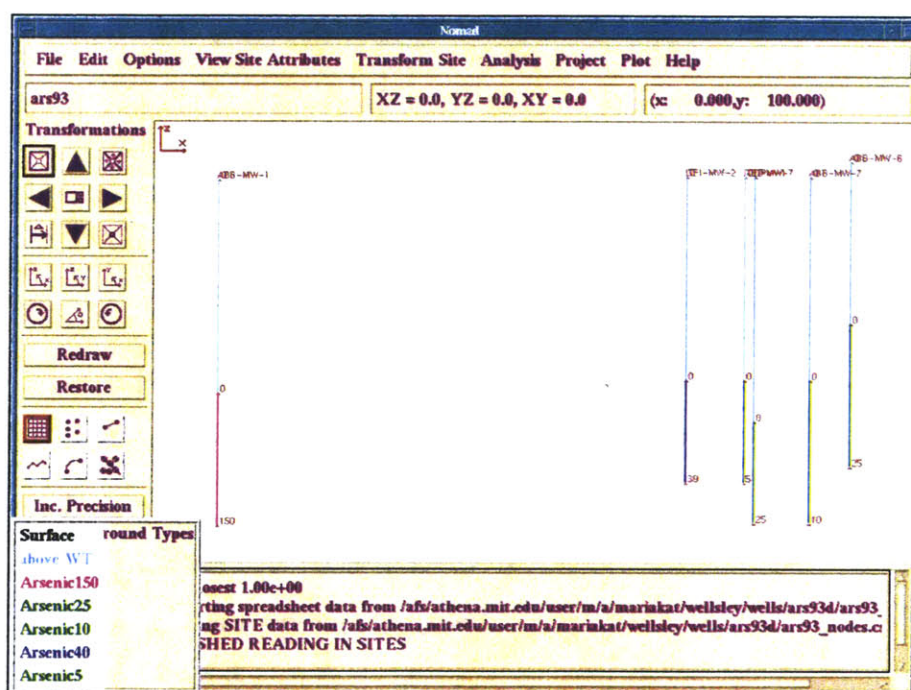


Figure 6.22: Sample representation of concentrations using NOMAD.

*The values close to the well logs indicate the concentration value at each corresponding point. In general green colors correspond to low concentrations, purple to red to pink colors are representative of medium to high concentrations, and yellow colors indicate very high concentrations. Blue colors correspond to logs above water table or where no data exist. In every case one should consult the legend of the corresponding figure. Concentration values are in  $\mu\text{g/l}$  (ppb). Arsenic150 stands for arsenic concentration of 150ppb.*



### 6.4.1: Early years: 1993-1996

Data were available for Acetone, Arsenic, Benzene, and Toluene. The Figures below show their concentration distribution for the years 1993 and 1996.

As can be seen, there is almost no change in measured concentrations.

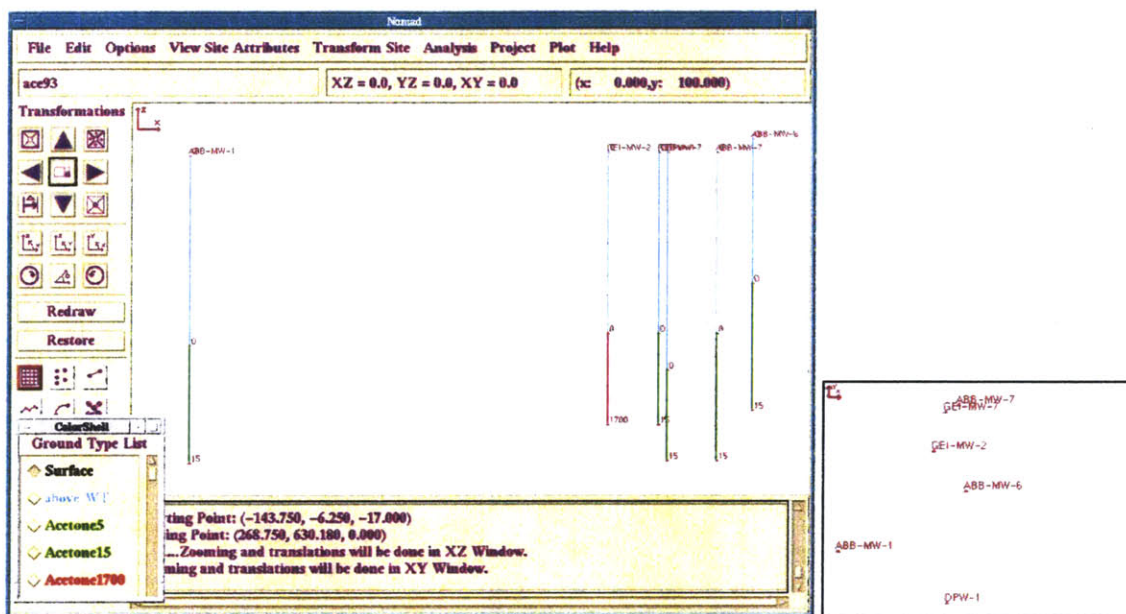


Figure 6.23: Acetone, 1993. Concentrations in  $\mu\text{g/l}$  (ppb).

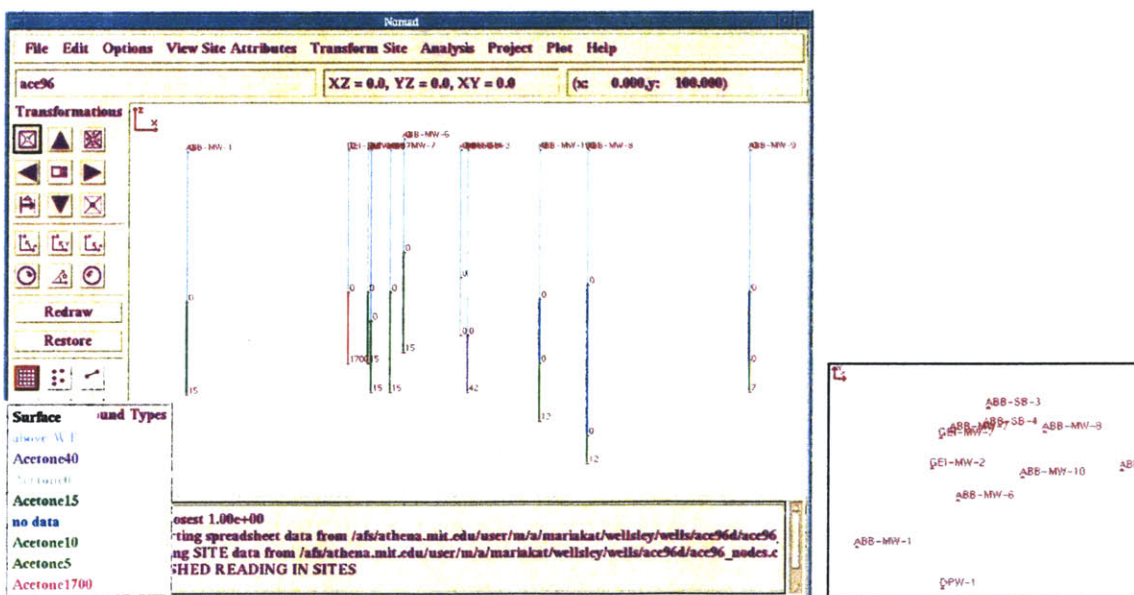


Figure 6.24: Acetone, 1996. Concentrations in  $\mu\text{g/l}$  (ppb)

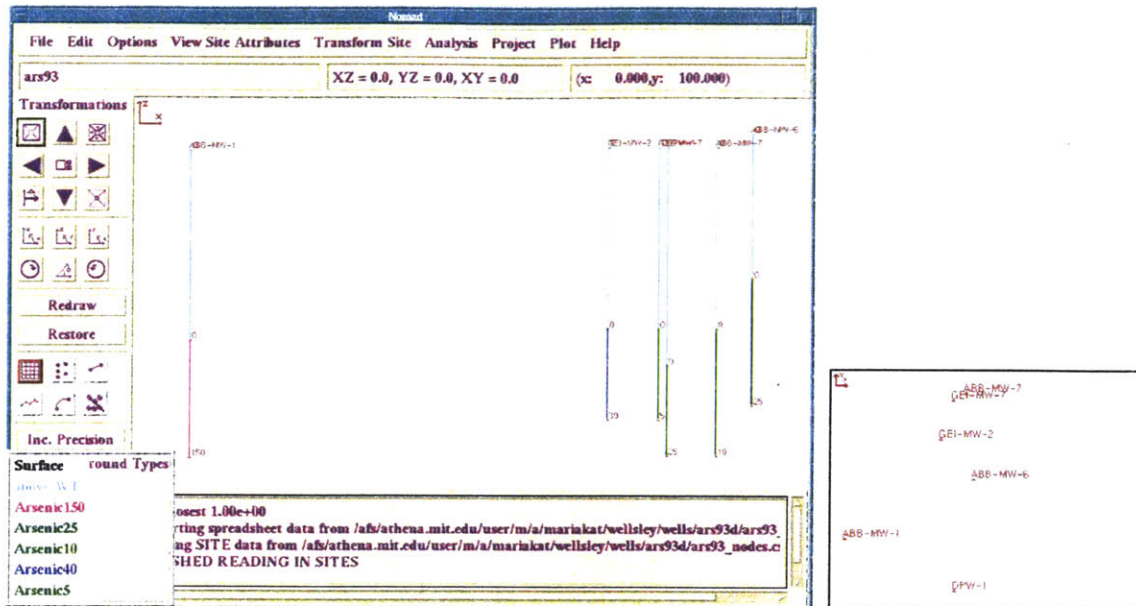


Figure 6.25: Arsenic, 1993. Concentrations in  $\mu\text{g/l}$  (ppb). Arsenic5 stands for arsenic concentration of 5ppb.

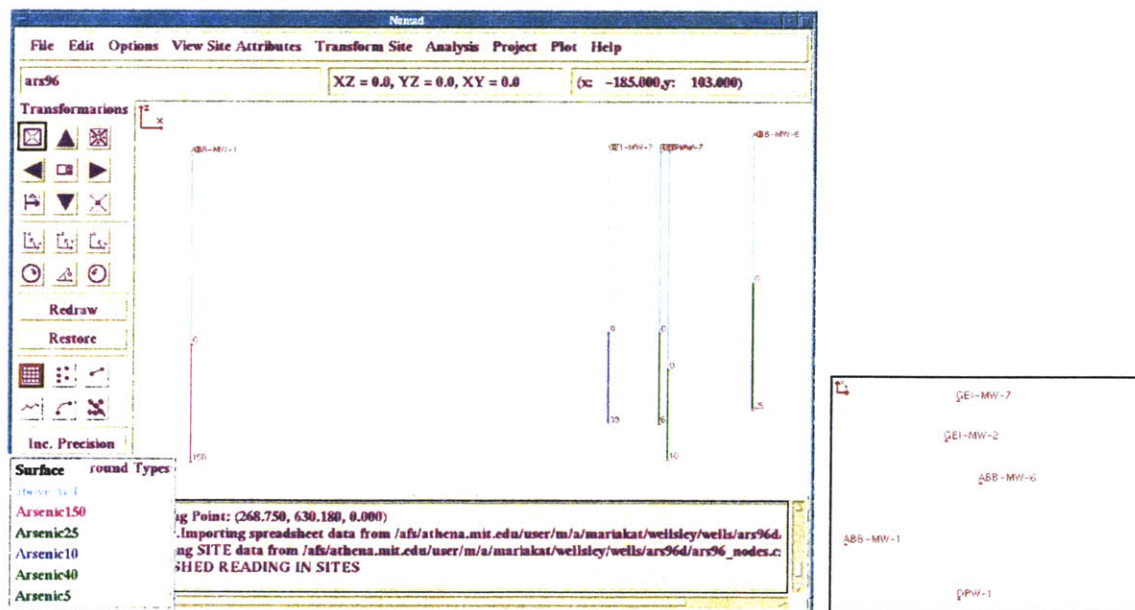


Figure 6.26: Arsenic, 1996. Concentrations in  $\mu\text{g/l}$  (ppb). Arsenic5 stands for arsenic concentration of 5ppb.

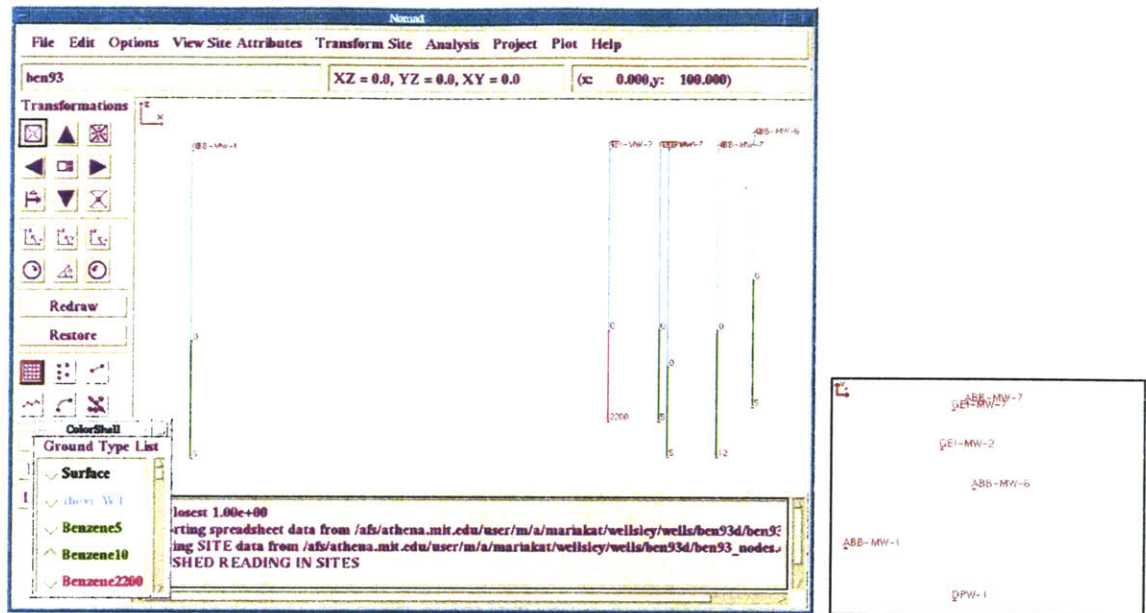


Figure 6.27: Benzene, 1993. Concentrations in  $\mu\text{g/l}$  (ppb). Benzene5 stands for benzene concentration of 5ppb.

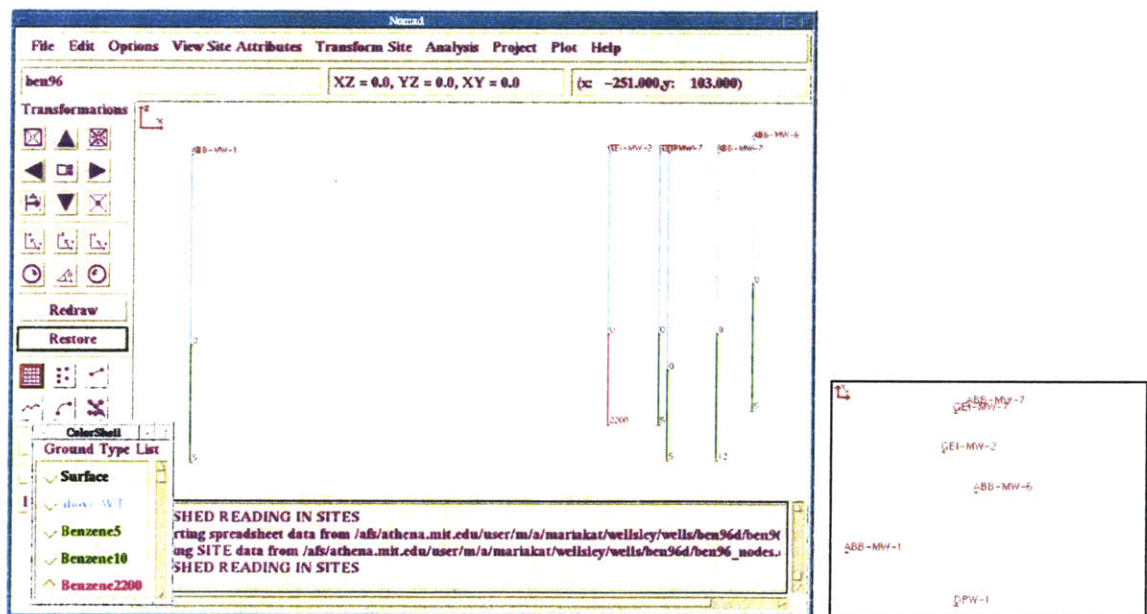


Figure 6.28: Benzene, 1996. Concentrations in  $\mu\text{g/l}$  (ppb). Benzene5 stands for benzene concentration of 5ppb.



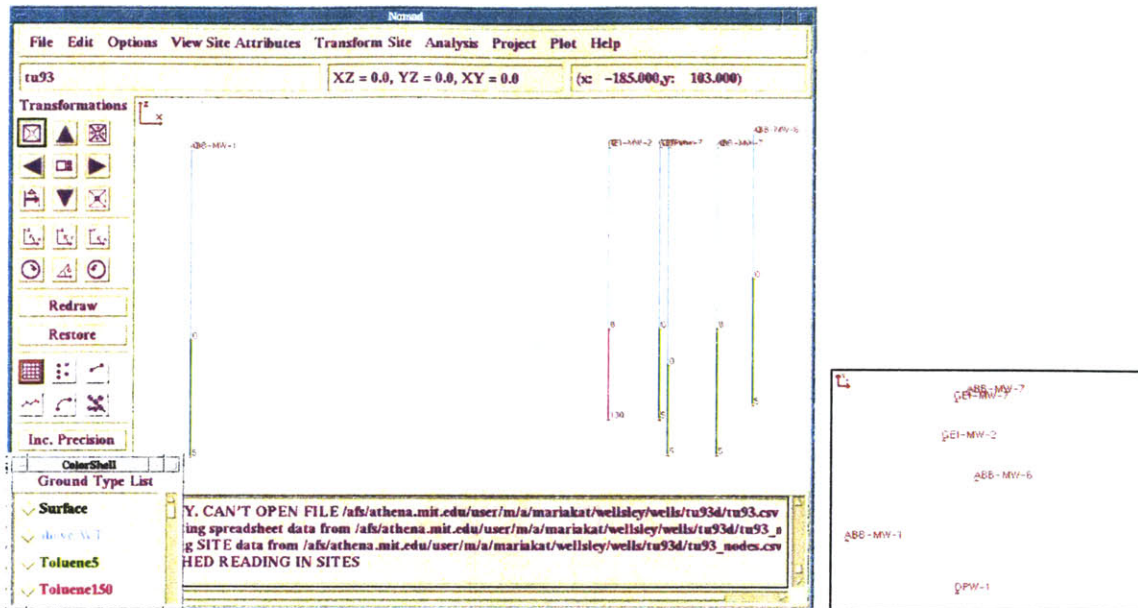


Figure 6.29: Toluene, 1993. Concentrations in  $\mu\text{g/l}$  (ppb). Toluene5 stands for toluene concentration of 5ppb.

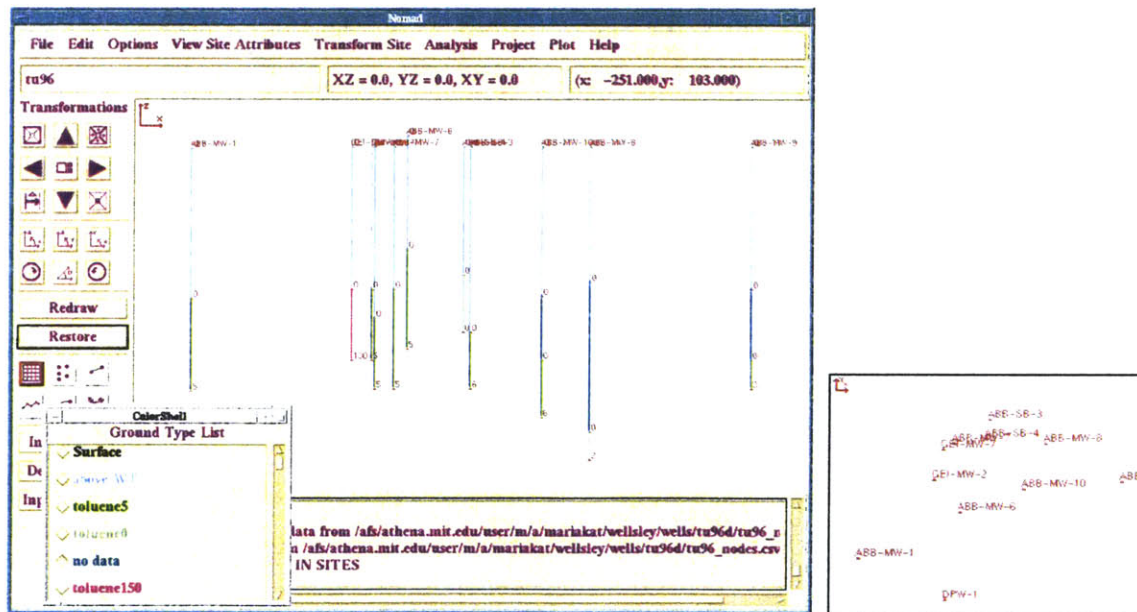


Figure 6.30: Toluene, 1996. Concentrations in  $\mu\text{g/l}$  (ppb). Toluene5 stands for toluene concentration of 5ppb.



#### 6.4.2: Later years: 1997-2000

In this section Trichloroethane (TCE) will be studied, since the most extended data existed for this pollutant and concentrations were changing significantly with time.

Prior to cleaning, the TCE source appeared to be a single release area directly below a former maintenance facility degreaser at the southeast corner of the main building (Figure 6.1). There is evidence that it moved gradually in an easterly direction towards Route 128. The “prior to cleaning” concentration at the source area was 100000  $\mu\text{g/l}$ , and it was decreasing away due to natural attenuation processes, including dilution and breakdown into degradation byproducts. The plume had even advanced beneath Route 128. Figure 6.31 shows the TCE plume in April 1997.

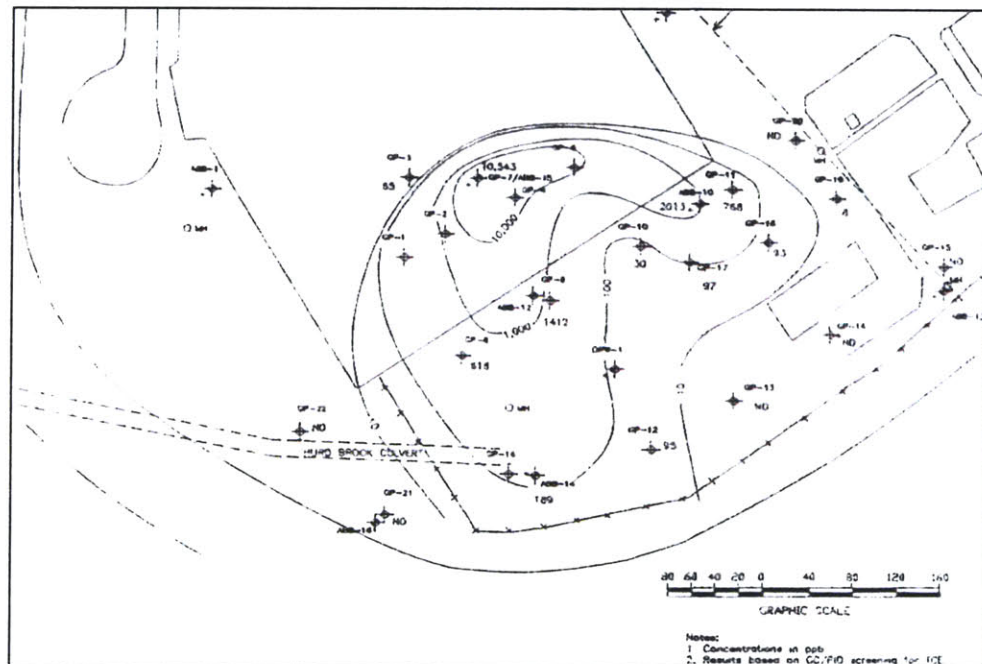


Figure 6.31: TCE plume prior to cleaning (April 1997). Concentrations are in  $\mu\text{g/l}$  (ppb) (from MHD reports [32]).

Based on information from a deep well (ABB-17), the groundwater plume had remained near the water table while travelling along the site. Actually, the low permeability silt layer above bedrock had prevented the deep migration of TCE.

During the years 1997-2000 the general clean up of the site took place. Variation in concentrations is significant in very short time periods (months) as it will be seen later in this chapter.

Data for Trichloroethane (TCE) were available for the time instances 1997 April (prior to cleaning), 1998 February, 1998 April, 1998 May, 1998 July, 1998 September, 1999 August and 2000 January.

The main treatment to address the TCE source area was started on March 1998 and ended on September 1998. The procedure included soil vapor extraction and air sparging to remediate respectively soil and groundwater contamination due to TCE. In more detail, a soil vapor extraction system was installed to remove contaminants from the soils in the vadose zone (the vadose zone is the zone above the water table where soil is not saturated), by extracting gas from the subsurface. On the other hand, the sparging procedure includes the installation of sparging wells, through which air is injected into the groundwater. As a result, contaminants are removed from the groundwater and from the soil below the water table by being transported in a vapor phase upward into the vadose zone. From there, they are recovered with soil vapor extraction. More information about these procedures can be found in Appendix V.

Figure 6.32 shows a plan view with the borehole/wells locations and Figure 6.33 tabulates the concentrations in the borehole locations over time. The latter is also illustrated in Figures 6.34 and 6.35, with 6.35 excluding the very high values of well ABB-15.

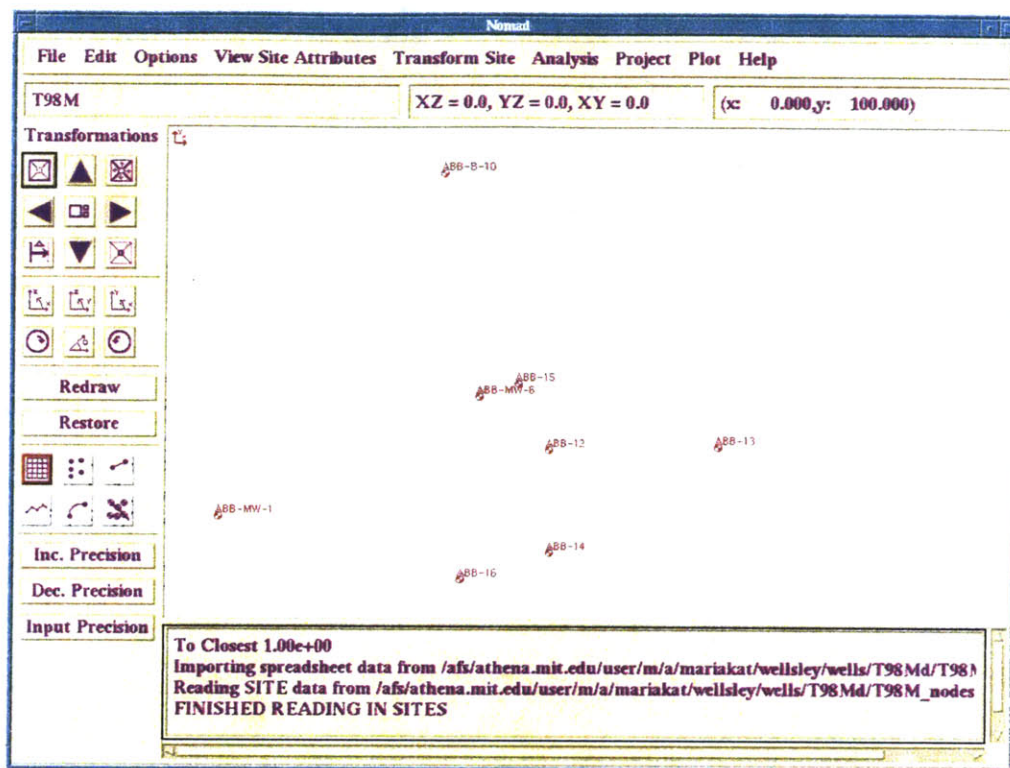


Figure 6.32: Plan view of the wells monitoring Trichloroethane concentrations during years 1997-2000. Concentrations are in  $\mu\text{g/l}$  (ppb).

	97	98F	98A	98M	98J	98S	99	T00
ABB-MW-1	5	0	0	1	1	1	1	5
ABB-MW-6	5	2	1.4	1	1	1	10	5
ABB-B-10	830	90	84	78	100	170	46	6
ABB-12	10000	14000	10000	7300	1200	2900	790	2400
ABB-13	5	0	0	1	1	1	1	5
ABB-14	560	1700	3300	3500	4100	2300	300	130
ABB-15	96000	150000	100000	100000	63000	78000	85000	29000
ABB-16	10	10	10	5	0	1	10	5

Figure 6.33: Tabulated concentrations for Trichloroethane over time. Concentrations are in  $\mu\text{g/l}$  (ppb).

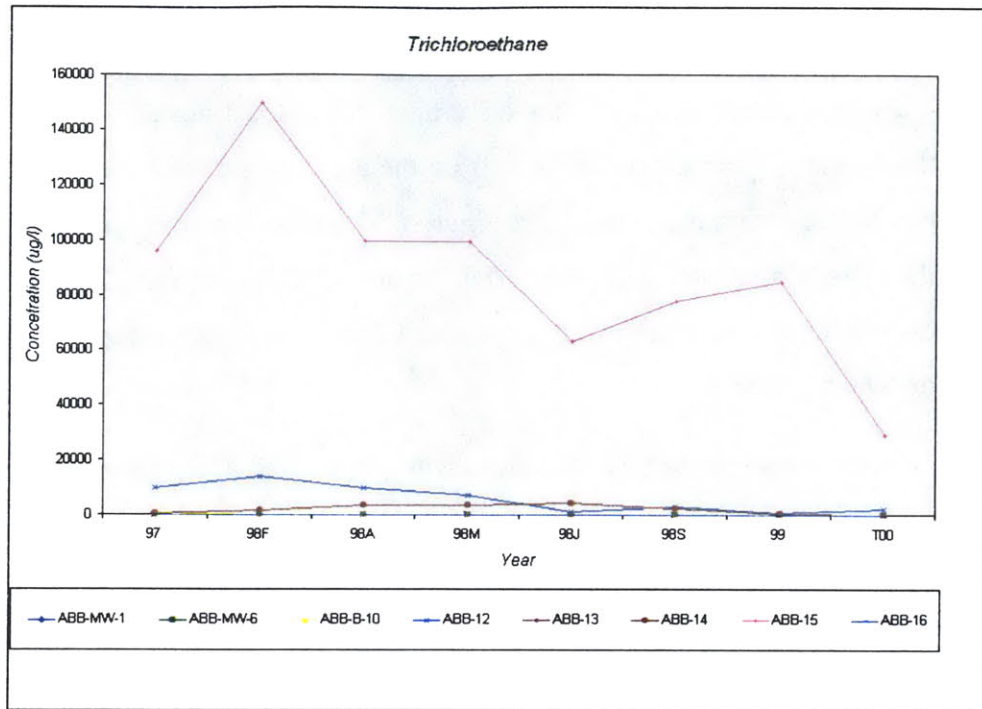


Figure 6.34: Concentrations for Trichloroethane over time at well locations.

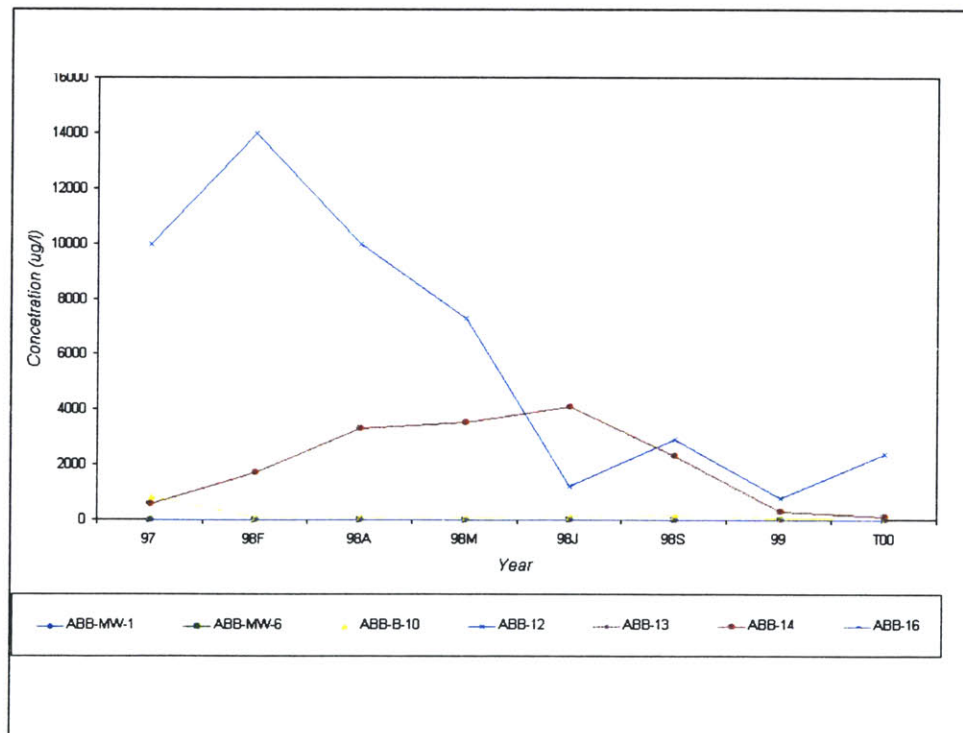


Figure 6.35: Concentrations for Trichloroethane over time at well locations, excluding the very high ones at ABB-15.

From the above figures it can be seen that:

- a) Very high values of concentration are observed in locations ABB-15 and ABB-12 but they quickly decrease as distance from the area around their location increases. This can be seen from the contours in Figure 6.31 and also from Figures 6.34-6.35, where the lines corresponding to wells ABB-15 and ABB-12 are much higher than the other ones. This spatial distribution was expected since TCE was released to the subsurface under a small area.
- b) Concentrations generally decrease with time, but a significant decrease in one location seems to slightly increase concentrations in neighboring points (Plot in Figure 6.35). This may be explained by the method of site clean up (pushing air into the groundwater - formation of gas pockets and lateral spreading due to low permeability silty layers (Refer to Appendix V)). It can also be noted that such local increases are observed east of the source area (ABB-15, Figures 6.31, 6.32), which coincides with the general tendency of the plume to migrate easterly.

These data are presented using NOMAD in Figures 6.36-6.43 on the next pages.



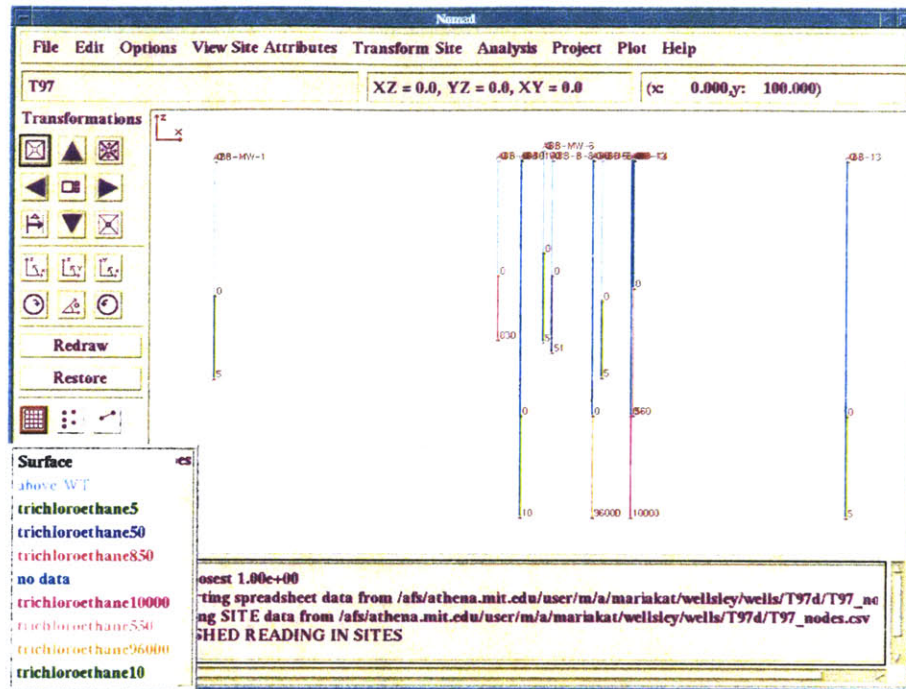


Figure 6.36: Trichloroethane, 1997. Concentrations are in  $\mu\text{g/l}$  (ppb). Trichloroethane5 stands for trichloroethane concentration of 5ppb.

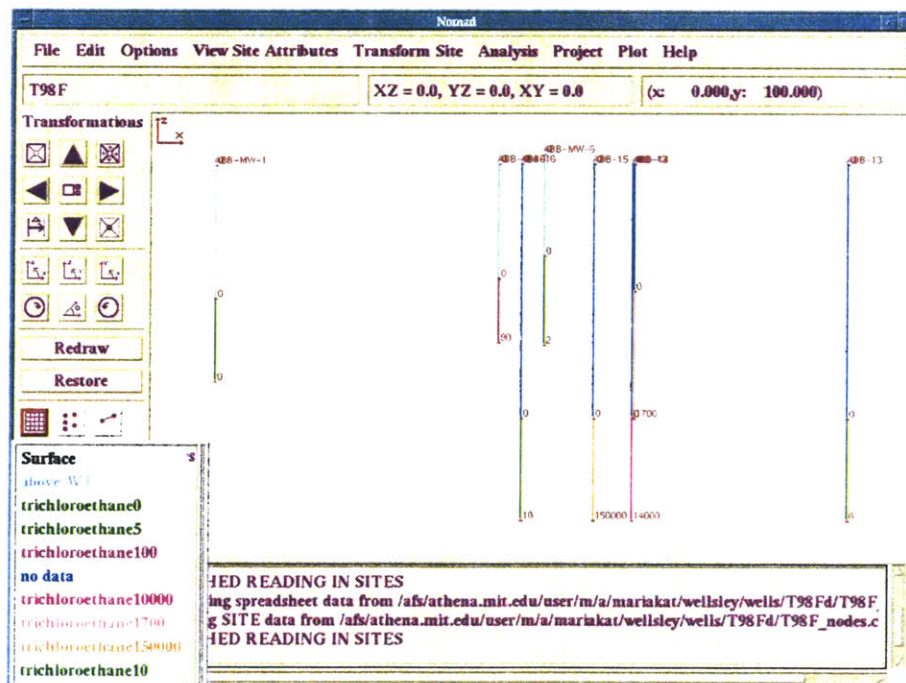


Figure 6.37: Trichloroethane, February 1998. Concentrations are in  $\mu\text{g/l}$  (ppb). Trichloroethane5 stands for trichloroethane concentration of 5ppb.

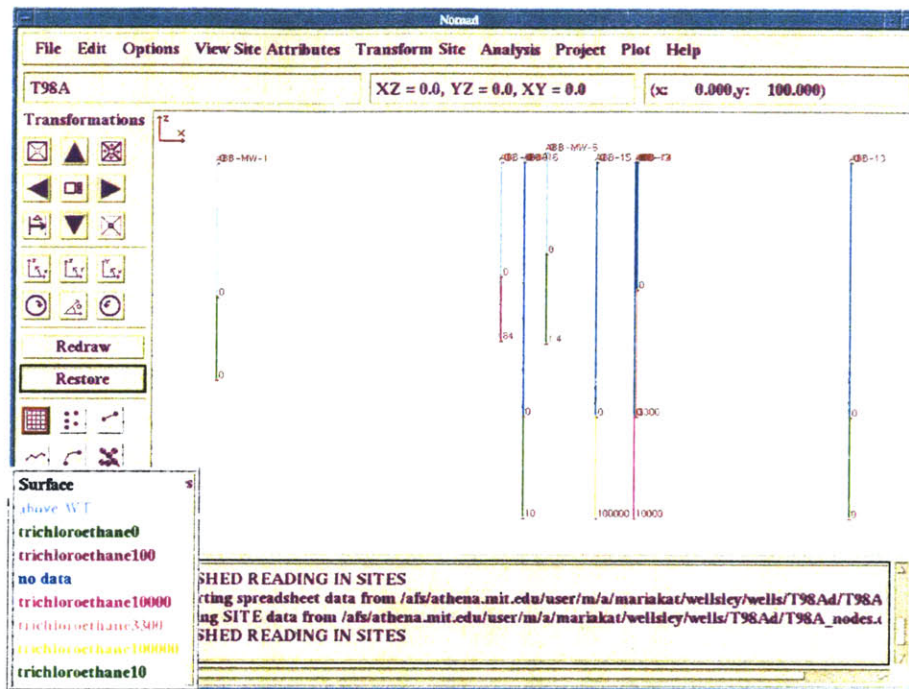


Figure 6.38: Trichloroethane, April 1998. Concentrations are in µg/l (ppb).  
Trichloroethane5 stands for trichloroethane concentration of 5ppb.

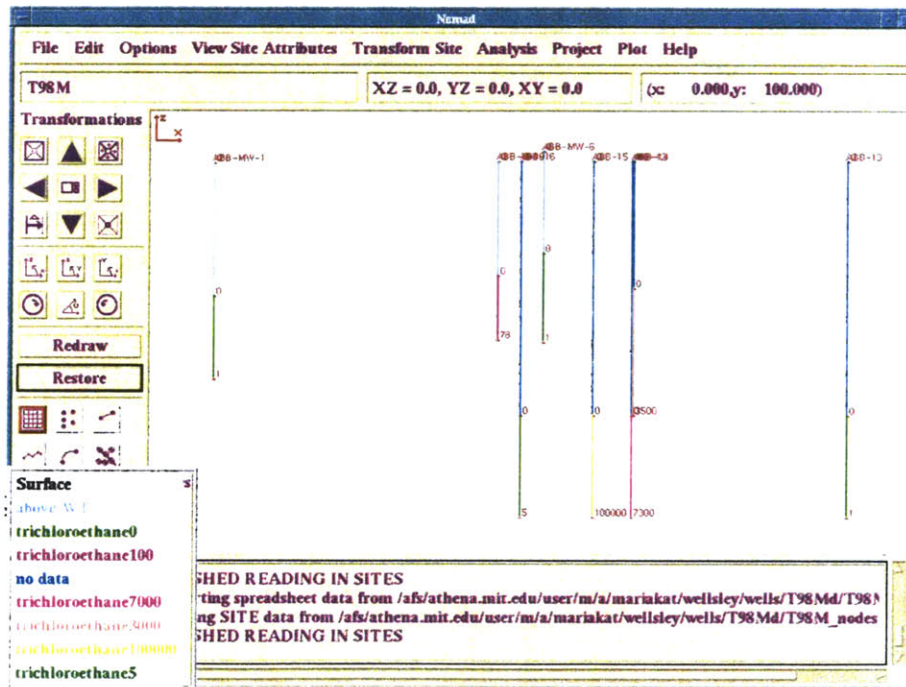


Figure 6.39: Trichloroethane, May 1998. Concentrations are in µg/l (ppb).  
Trichloroethane5 stands for trichloroethane concentration of 5ppb.

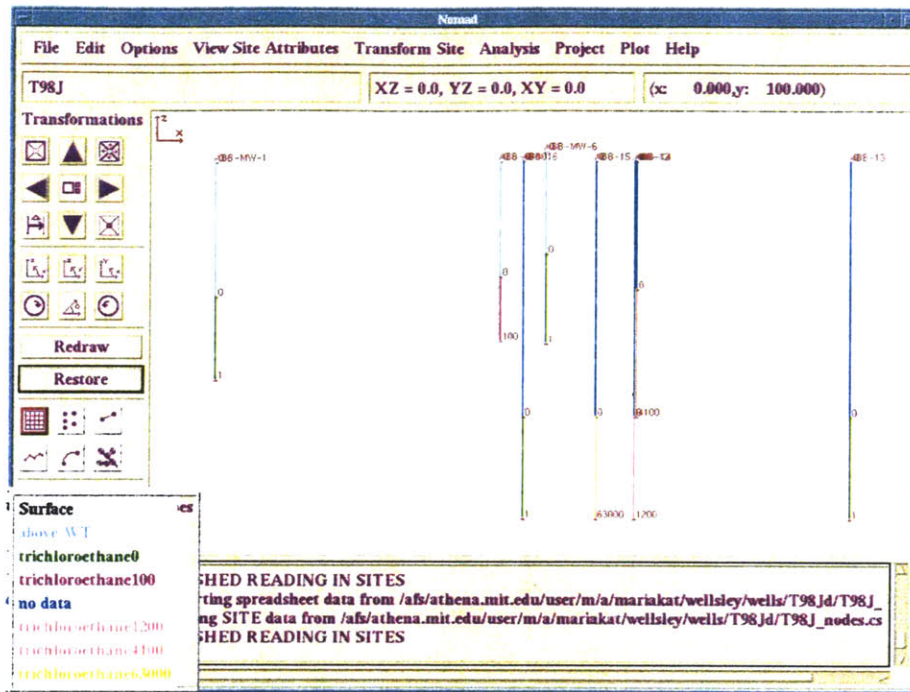


Figure 6.40: Trichloroethane, July 1998. Concentrations are in µg/l (ppb).  
Trichloroethane5 stands for trichloroethane concentration of 5ppb.

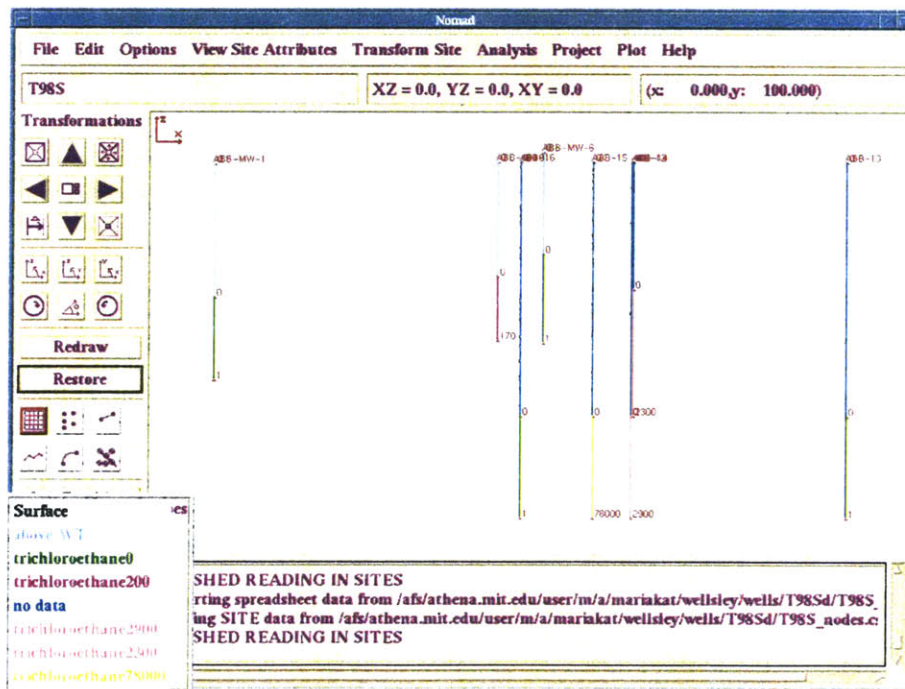


Figure 6.41: Trichloroethane, September 1998. Concentrations are in µg/l (ppb).  
Trichloroethane5 stands for trichloroethane concentration of 5ppb.



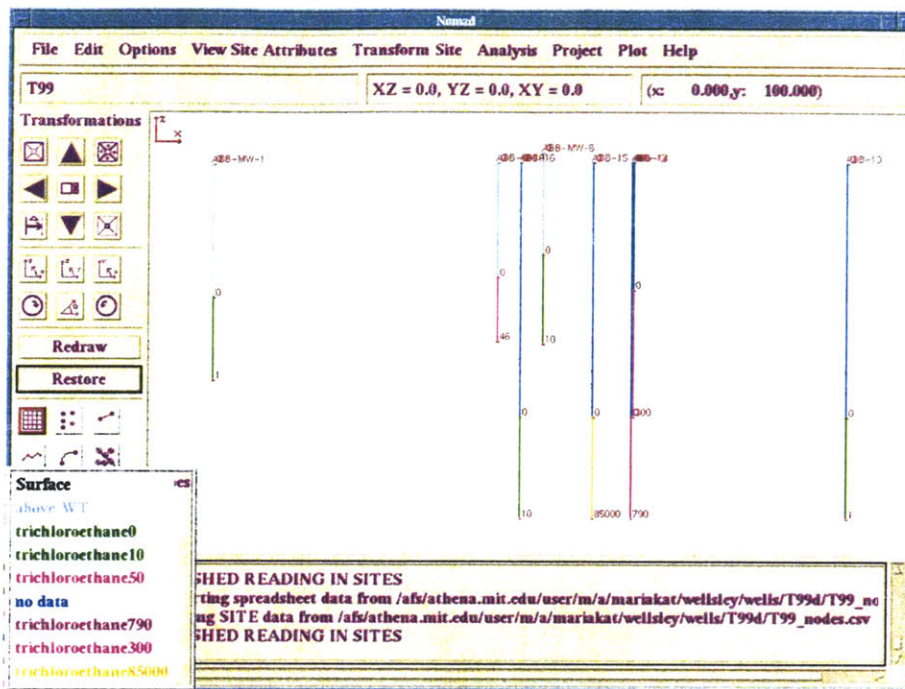


Figure 6.42: Trichloroethane, 1999. Concentrations are in  $\mu\text{g/l}$  (ppb). Trichloroethane5 stands for trichloroethane concentration of 5ppb.

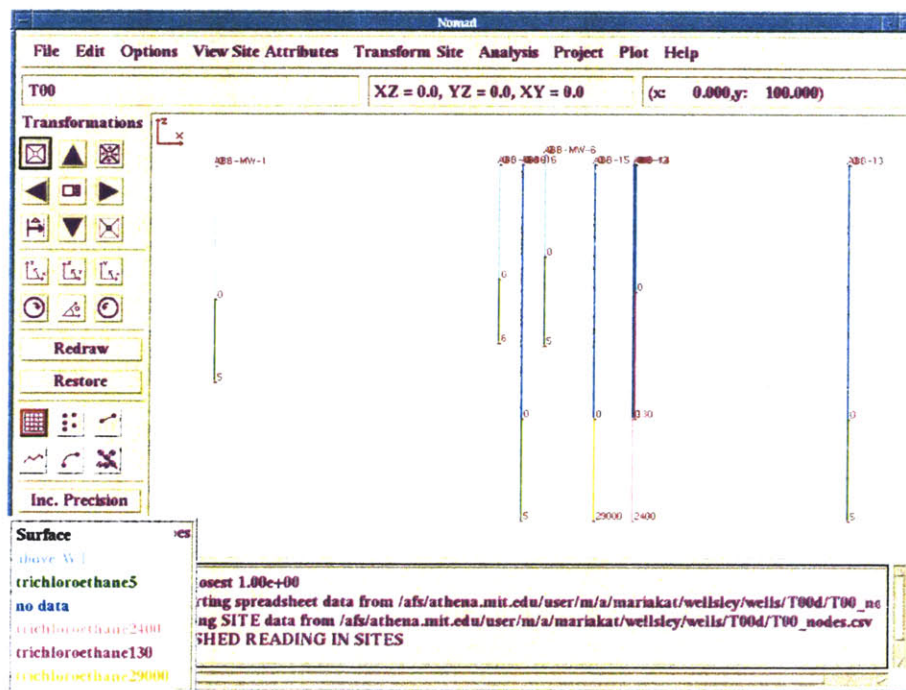


Figure 6.43: Trichloroethane, 2000. Concentrations are in  $\mu\text{g/l}$  (ppb). Trichloroethane5 stands for trichloroethane concentration of 5ppb.

### 6.4.3: Review of NOMAD representation

NOMAD offers a potential way of representing pollutant plumes. The representation of well logs provides a good illustration of the plume with depth, a feature that is missing in the conventional contour plotting of the pollutant concentrations. Furthermore, in cases where many wells exist, the plume can be drawn, as layers are formed in the geological profiles, and cross sections can be created. One should also note that the NOMAD representation is very illustrative when multiple concentration values are reported along the screened length. The information is preserved because it is not averaged for projection on the ground surface, something that is essential when one plots concentration contours.

Nevertheless, contour plots maintain their value as they offer a quick way to understand the overall presence and spreading of the plume. Such plots should accompany any other representation form so that the general image is not lost. Contours, thus, remain an essential illustrative way for environmental case studies (Figure 6.44).

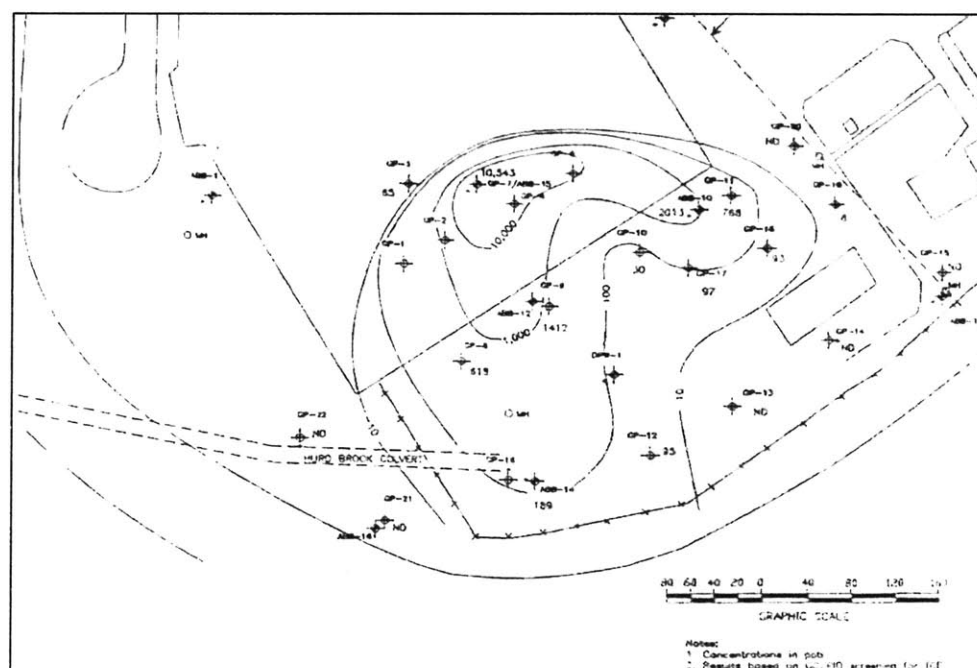


Figure 6.44: Representation of TCE concentrations using the conventional contour plot (concentrations in  $\mu\text{g/l}$  (ppb)).

As NOMAD offers, apart from the benefits mentioned above, the advantage of kriging (KRIBS is based on NOMAD for input information), a further development of NOMAD for geoenvironmental problems would be to introduce a contour function in the graphics environment, so that concentrations are projected automatically on the surface and then contours can be fitted. One should note that contour plots already exist in the program (representation of kriging analysis).

#### **6.4.4 Application of KRIBS**

It would be interesting to apply KRIBS to the hydrogeological data and obtain predictions for the concentrations of points between the existing wells.

The main constraint in performing such an analysis is the nature of the plume. As can be seen in Figure 6.44, there is a small area with very high values of concentration, which then die out very quickly. In addition, the pattern with which concentrations decrease depends highly on the examined direction. So the spatial variation characteristics of the data depend on the data point locations in space, as well as on the distance between them. The field is non-stationary, because this dependence violates the basic assumption of stationarity. Since KRIBS has been developed on variogram models that assume stationarity of the data field, one should not analyze the present hydrogeological data with it.

Here an alternative approach is suggested and theoretically developed. This is based on the usual procedure that is followed for similar plume types. Unfortunately the size of the present data set is too small to be used for the application of this approach.

Since concentration values seem to decrease logarithmically, the logarithm of the concentration  $c$ ,  $\log(c)$ , instead of the original value is taken at each data location.  $\log(c)$  values form a surface that is smoother than the original one, and changes almost linearly with distance at a given direction. So the  $\log(c)$  field is stationary. Furthermore, it can be approximated by a continuous mathematical function. The difference between these two

surfaces, the true  $\log(c)$  and the fitted one, is known only at the points where the original data exist. This is illustrated at Figure 6.45 for a simple case projected on a 2-D plane. However, these differences in each point location form a stationary field, since the mathematical function has been fitted to a stationary field and the differences are small. As a result, one can krig the differences and obtain information of how good the fitted surface is compared to the true one and so one can have an estimation of what the concentration values at any arbitrary point in the field will be.

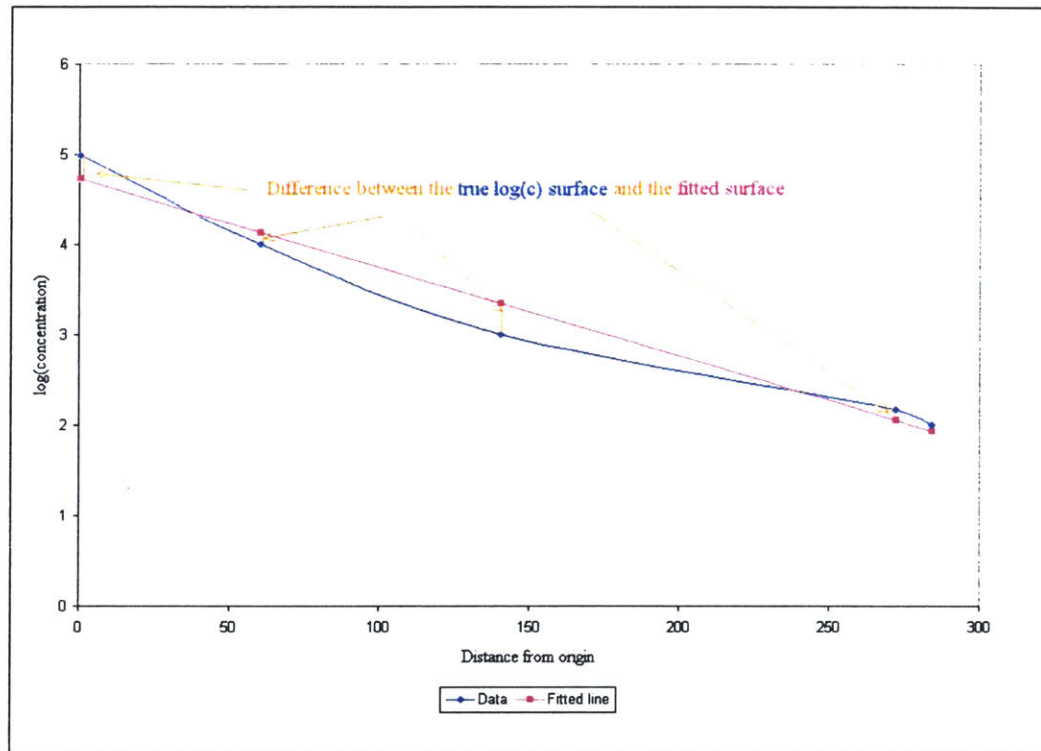


Figure 6.45: True  $\log(c)$  surface (unknown) and fitted surface.

Hard (known) data for the true  $\log(c)$  surface exist only at the points where the original data exist (diamond blue points). The differences at these locations (orange lines) are the values that are going to be kriged.

*Fitting of the log(c) surface:*

Log(c) values depend on the direction examined and on the distance along each direction. In a given direction values vary almost linearly, so a good fitting function would be:

$$\log c(r, \theta) = a - b(\theta) \cdot r \quad (1)$$

and  $b(\theta)$  is described by a Fourier series:

$$b(\theta) = b_0 + \sum_{i=1}^k (m_i \sin(2\pi i \theta) + n_i \cos(2\pi i \theta)) \quad (2)$$

Substituting:

$$\log c(r, \theta) = a - [b_0 + \sum_{i=1}^k (m_i \sin(2\pi i \theta) + n_i \cos(2\pi i \theta))] \cdot r \quad (3)$$

Equation (3) gives a continuous function for approximating the true log(c) surface at any point (r,θ).

Equation (3) contains  $(2+2k)$  unknowns, the constants  $a$ ,  $b_0$ , and the coefficients of the Fourier series  $m_i$ ,  $n_i$  ( $i=1, \dots, k$ ,  $k$  being the number of the series terms). These unknowns are best estimated with the existing point data, so that the fitted mathematical surface approximates as well as possible the true log(c) surface (the differences at the point locations between the true data values and the values obtained from the mathematical function are as small as possible). The value of  $k$  determines how many terms the Fourier series has-the more terms, the more flexible the function is to capture small differences of the true surface. However, the value of  $k$  depends on the size of data set, since the greater the number of the unknown constants is, the more constraints (equations) are required to best estimated these unknown constants.

In practice, a data set consisting of ten's or better hundred's of points would be placed in a grid, a coordinate origin would be selected and each point would be assigned (r,θ) coordinates. The log of the values would be obtained. Then, the constants  $a$ ,  $b_0$ , and  $m_i$ ,  $n_i$ ,

of equation (3) would be estimated and, subsequently the differences between the true  $\log(c)$  value at each point  $j$  of the data set and the  $\log c(r_j, \theta_j)$  value of equation (3) would be calculated. Kriging would be performed on these differences, and so one would estimate what the deviation of the model from the unknown true  $\log(c)$  surface is, at any arbitrary point in the field. Therefore, one would be able to estimate the true  $\log(c)$  values and obtain in this way a prediction of the values of the original field at any point in space.



## **Chapter 7: Conclusions and future recommendations**

This research project reestablished the functionality of the geostatistical program NOMAD-KRIBS and studied its application to geoenvironmental problems that involve changes of spatial configuration with time. A geological case study was reviewed in Chapter 5, discussing in detail the program features. Then a hydrogeological case was presented in Chapter 6, where the contamination plumes and their changes with time were successively illustrated with NOMAD. There were insufficient data to obtain kriging results, but a theoretical approach was proposed for problems of similar nature.

The main conclusions from this thesis can be summarized as follows:

- NOMAD offers a very efficient environment for presenting geological data, and studying the 3-D nature of the site subsurface. Some of the important features are that the user can interact with the input information and with the 3-D soil profile by translating it, rotating it or by creating and editing cross sections.
- KRIBS allows one to create geostatistical profiles that reproduce the general ground types, and which furthermore can predict isolated zones and lenses of different geological characteristics.
- Moreover KRIBS offers the capability of reviewing the input data, incorporating additional objective and subjective information, updating the profiles and so evaluating where additional site investigation is needed.
- Input geological or geotechnical data may include ground types, SPT/CPT or RQD data, Atterberg limits, in-situ or lab testing results. In other words, kriging can be based on any data that are believed to characterize certain soil or rock formations.
- The program (NOMAD-KRIBS) was used to represent and study hydrogeological data, which compared to geological ones includes an extra parameter, the time. The Wellesley case study showed that NOMAD can indeed illustrate data changing with time.
- An important feature that NOMAD introduces in geoenvironmental problems is the representation of well logs on the vertical plane. In this way a good illustration of the



plume with depth is provided. Such a feature is missing in the conventional contour plotting of the pollutant concentrations, and is useful when multiple concentration values are reported along the screened length.

- In addition, the fact that input information is preserved because it is not averaged for projection to the ground surface enables the user to create cross sections, and view or edit the data at any time.
- Finally, KRIBS can be further developed to offer more quantitative predictions of the plume shape and its changes with time.

### **Summary of Recommendations for Future Research**

#### ***a. Recommendations about the capabilities of the program:***

- Introduce new geostatistical concepts, especially the multipoint statistics proposed by Journel (2000)
- Extend the kriging function to 3-D space
- Build a contour representation of the input data for geological or hydrogeological information. In this way the user will be able to see the ground or plume formations projected on the ground surface.
- Introduce an algorithm for kriging non-stationary hydrogeological data, which forms a stationary field when the logs of the original values are taken (for example single release pollutant plume). A procedure for such an algorithm was proposed in section 6.4.4.

#### ***b. Recommendations about the software***

- Some parts of the kriging function are still written in FORTRAN, and this may be one of the reasons of the program's poor functionality. Rewriting the functions in C++ will ensure that the kriging function will reliably work when invoked.

## References

1. [Anand 1993] Anand V.B.: Computational Methods for the Representation of Contour Lines”, Computers in Civil Engineering, Vol. 8, 1993, pp119-128.
2. [Barnes, 1992] Barnes R.J., You K.: “Adding Bounds to Kriging”, International Association for Mathematical Geology, Vol. 24, No2, 1992, pp171-176.
3. [Bourgault, 1992] Bourgault G., Marcotte D., Legendre P.: “The Multivariate (Co)Variogram as a Spatial Weighting Function in Classification Methods”, Mathematical Geology, Vol. 24, No5, 1992, pp463-478.
4. [Carr & Mao, 1993] Carr J.R., Mao N.H.: “A General Form of Probability Kriging for Estimation of the Indicator and Uniform Transforms”, Mathematical Geology, Vol. 25, No 4, 1993, pp425-438.
5. [Carr & Myers, 1990] Carr J.R., Myers D.E.: “Efficiency of Different Equation Solvers in CoKriging”, Computers & Geosciences, Vol. 16, No5, 1990, pp705-716.
6. [Cressie, 1991] Cressie N.A.C.: “Statistics for Spatial Data”, J. Willey: New York, 1991.
7. [Culligan, 2001] Culligan P.J., Personal Communications.
8. [Domenico & Schwartz, 1997] Domenico P.A. and Schwartz F.W.: “Physical and Chemical Hydrogeology”, J. Wiley, 1997.
9. [Drake, 1967] Drake A.W.: “Fundamentals of Applied Probability Theory”, McGraw-Hill, New York, 1967.
10. [Einstein & Baecher, 1982] Einstein H.H., Baecher G.B.: “Probabilistic and Statistical Methods in Engineering Geology”, Rock Mechanics, Springer-Verlag, 1982.
11. [Freund, 1985] Freund M.J.: “CoKriging, Kriging and Trend Surface Analysis: A Comparative Study of Estimation Techniques in Geologic Mapping”, SM Thesis, Univ. Of Missouri-Rolla, 1985.
12. [Ghahreman, 1992] Ghahreman, B.: “Exploration Strategy for Underground Construction”, MIT SM Thesis, 1992.
13. [Goovaerts, 1993] Goovaerts P.: “Spatial Orthogonality of the Principal Components from Coregionalized Variables”, Mathematical Geology, Vol. 25, No 3, 1993, pp281-302.

14. [Hango, 1998] Hango, J. S., "Further Development of Subsurface Profiling and Engineering Geology Software", Master's Thesis, Massachusetts Institute of Technology.
15. [Halim, 1990] Halim I.S.: "Reliability of Geotechnical systems Considering Geological Anomaly", PhD Thesis, Dept. of Civil & Environmental Engineering, Univ. Of Illinois, Urbana, Illinois, 1990.
16. [Ingebritsen & Sanford, 1998] Ingebritsen S.E. and Sanford W.E: "Groundwater in Geologic Processes", Cambridge University Press, 1998.
17. [Isaaks & Srivastava, 1989] Isaaks, E. H. and Srivastava, R. M., "An Introduction to Applied Geostatistics", Oxford University Press, Inc., New York and Oxford.
18. [Jensen, 1996] Jensen J.L, Corbett W.M., Pickup G.E., Ringrose P.S.: "Permeability Semivariograms, Geological Structure, and Flow Performance", Mathematical Geology, Vol. 28, No4, 1996, pp419-435.
19. [Johnson] Johnson R.L.- Kinnicutt, P. G.: Personal Communications.
20. [Jones 1991] Jones N.L., Wright S.G.: "Solid Modeling for Site Representation in Geotechnical Engineering", Geotechnical Engineering Congress 1991, Geotechnical Special Publication No 27, ASCE 1991, pp1021-1031.
21. [Journal, 2000] Journal A.G.: Talk on Multipoint Statistics, MIT, April 10, 2000.
22. [Journal, 2000] Journal A.G., Mao S. G.: "Conditional 3D Simulation of Lithofacies with 2D Seismic Data", COMPUTERS & GEOSCIENCES, Aug. 1999.
23. [Journal, 1986] Journal A.G.: "Constrained Interpolation and Qualitative Information-The soft kriging approach", Mathematical Geology, Vol. 18, No3, 1986, pp269-286.
24. [Journal & Huijbergts, 1978] Journal A.G., Huijbergts C.J.: "Mining Geostatistics", Academic Press, New York, 1978.
25. [Kinnicutt, 1991] Kinnicutt, P. G.: "A User-friendly Computer-aided Soil Profiling System for Use with the Engineering Geology Educator", Master's Thesis, Massachusetts Institute of Technology, 1991.
26. [Kinnicutt et al., 1994] Kinnicutt, P. G., Einstein, H. H., Lewis, J., and Noack, C. A.: "Extended visualization and geostatistical functionality in Nomad, a 3-d subsurface modeler", Computer methods and advances in geomechanics: proceedings of the eighth international conference on computer methods and advances in geomechanics, West Virginia, May 1994.

27. [Kinnicutt, 1995] Kinnicutt, P. G.: "A Decision Support Framework for Planning Geotechnical Exploration Programs", Ph.D. Thesis, Massachusetts Institute of Technology, 1995.
28. [Kinnicutt & Einstein, 1996] Kinnicutt, P.G., Einstein H.H: "Incorporating Uncertainty, Objective and Subjective Data in Geologic Site Characterization", Proceedings, Uncertainty in the Geologic Environment: From Theory to Practice, 1996.
29. [Kinnicutt, 2000] Kinnicutt, P. G.: Personal Communications.
30. [Kitanidas, 1993] Kitanidas, P.K.: "Generalized Covariance Functions in Estimation", Mathematical Geology, Vol. 25, No5, 1993, pp525-540.
31. [Krumbein & Graybill, 1965] Krumbein W. C., Graybill F. A.: "An Introduction to Statistical Models in geology", McGraw-Hill 1965.
32. [Massachusetts Highway Department] MHD: Wellesley Maintenance Depot Site, Wellesley, Massachusetts, RTN 3-2570: Reports, drafts and investigation material, 1993-2000.
33. [National Research Council (U.S.), 1994] "Alternatives for ground water cleanup", National Research Council (U.S.), Committee on Ground Water Cleanup Alternatives, Washington, D.C., National Academy Press, 1994.
34. [Noack, 1998] Noack, C. A.: "Program and Expert System Development for Tutorial Applications in Engineering Geology", Master's Thesis, Massachusetts Institute of Technology.
35. [Nobre 1992] Nobre M.M., Sykes J.F.: "Application of Bayesian Kriging to Subsurface Characterization", Canadian Geotechnical Journal, Vol. 29, 1992, pp589-598.
36. [Pan, 1993] Pan G., Gaard D., Moss K., Heiner T.: "A Comparison between CoKriging and Ordinary Kriging: Case Study with a Polymetallic Deposit", Mathematical Geology, Vol. 25, No3, 1993, pp377-398.
37. [Posa, 1992] Posa D., Marcotte D.: "Robustness of Kriging Weights to Non-Bias Conditions", Mathematical Geology, Vol. 24, No7, 1992, pp759-773.
38. [Olea & Pawlowsky, 1996] Olea R.A., Pawlowsky V.: "Compensating for Estimation Smoothing in Kriging", Mathematical Geology, Vol. 28, No4, 1996, pp407-417.

39. [Schmitz 1990] Schmitz G.H., Kiefer E.M., Vauclin M.: "Modern Kriging and Classical Gaussian Techniques-Do They Necessarily Yield Identical Results?", *Advanced Water Resources*, Vol. 13, No2, 1990, pp90-97.
40. [Solow, 1993] Solow A.: "On the Efficiency of the Indicator Approach in Geostatistics", *Mathematical Geology*, Vol. 25, No1, 1993, pp53-57.
41. [Spikula, 1983] Spikula D.: "Statistical Estimation of Soil Properties: An Application", MIT SM Thesis 1983.
42. [Yates, 1986] Yates S.R.: "Disjunctive Kriging3. Cokriging", *Water Resources Research*, Vol. 22, No10, 1986, pp226-244.
43. [Veneziano, 2001] Veneziano D.: Personal Communications.

***APPENDIX I:***  
***Creating profiles with NOMAD***



## **Appendix I: Creating profiles with NOMAD**

The following was written aiming to introduce students to Nomad and help them use the program (in the Athena environment) to create geologic profiles for a 1.383 assignment. It can be used as a short introduction to the program environment and its basic functionalities. For further details one should refer to Kinnicutt's Ph.D. thesis [27].

### **I.1. Nomad**

NOMAD is a three-dimensional ground profiler using a combination of C, C++, XWindows and Motif on the Unix platform. It uses three dimensional block diagrams to represent nodal data, borehole profiles and layer interfaces, and displays the site from three orthogonally oriented directions. Each of the three views can be rotated, scaled and translated. Input data can contain ground types, SPT or RQD data etc. The user can interactively edit the site data by inserting, deleting and moving nodal, borehole and line data according to subjective beliefs. This does not require any changes in the input file, but can easily be done by moving the mouse. The user can also create cross sections and edit them, having the changes automatically propagated to the three-dimensional site model and to intersecting cross sections.

### **I.2. General**

Nomad can be found in the 1.38 locker. In order to access it you should type add 1.38 at the athena prompt:

```
athena% add 1.38
```

```
athena% NOMAD
```

It is advised that for each project you create, you make a different directory and store everything there.

You can make directories under you own directory (/afs/athena.mit.edu/user/....)<sup>1</sup>. You can also store data at the "data.dir" directory in the 1.38 locker.

### **I.3. Creating the input file**

Data can be created and imported in the form of a spreadsheet. This can be done using any relevant program, such as Excel or Xess. Each line in the spreadsheet will store attribute values (location, description, etc) for one node. There can be any number of

---

<sup>1</sup> This can be found by the pwd command at the athena prompt.



attributes for each node, but it is recommended to specify them in this input file rather than try to add them later when running the program. If no data exist for a certain attribute of a node, the cell can be left blank.

It is important that the data file must have all the attribute names specified in the first row of the table.

Borehole name	x	y	Description	Depth	z	Ground type	Layer
P201	0.5	10	Surface	0	138.3	Surface	0
P201	0.5	10	Fill	10	128.3	Fill	1
P201	0.5	10	Sand/gravel	25	113.3	Sand/gravel	2

*Figure I.1: Example of input spreadsheet*

Note that the first node should be a node on the surface, and that you should have a column named “Ground type”.

In order for Nomad to read the spreadsheet data, this should be exported in the comma separated value (csv) format. The export option is found under the File menu of the spreadsheet program. In the csv format data for each node is stored in a separate line, with attributes in a line being separated by a comma.

Name the exported file as **\*\*\_nodes.csv**, where **\*\*** is the name of the project, and save it in the directory you have created for the project.

Note: If you browse this directory later, you will find that there have been more than one .csv files created. That is because the program creates a .csv file for each different group of objects you insert, for example lines, layers or cross sections. You do not need to interfere with these files, since you can make all changes while running NOMAD.

#### **I.4. Program’s environment**

The program’s menu options are shown in Figure I.2 and the main window in Figure I.3.

When creating a new project do not forget to save it in the same directory as the corresponding \_nodes.csv is. From the file menu select import spreadsheet data and select the **\*\*\_nodes.csv** file.

When the data has been successfully loaded, you should be able to see the boreholes and the profile along them. (See example below). Under the “view site attributes” menu you can find information about ground types (ground type legend) and toggle on or off options like borehole numbers, nodal information, lines (after being created) etc.

File Edit Options View Site Attributes Transform Site Analysis Project Plot Help

Figure I.2: Nomad menu options.

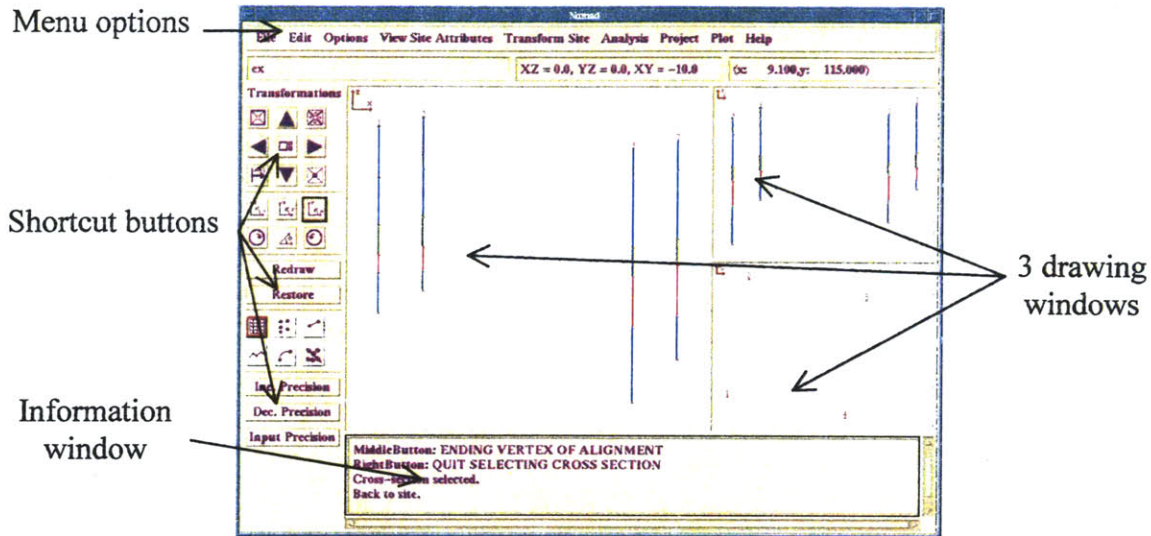
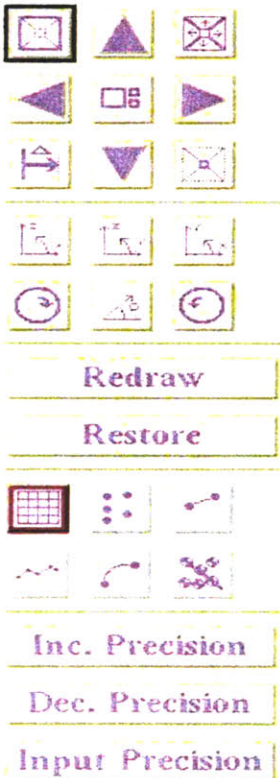


Figure I.3: Nomad main window.

#### Transformations



#### Edit the data

You can use the buttons at the left of the program window to insert, delete, edit nodes or lines (figure I.4). Follow the directions in the information window to start or quit editing. Once you have inserted lines, the program will assign the layers and you will be able to see them by toggling on the layer option (under the “View site attributes” menu).

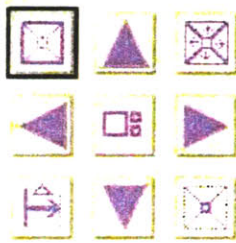
Lines can be modified into curves with the curve option under the edit menu (Figure I.6).

Keyboard input to all features can be also made with the edit menu (for example edit -> nodes (lines, etc)-> further changes).

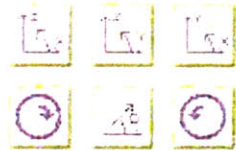
Cross sections can be created under the edit menu and then edited as above (note that right now this is the only way by which cross sections can be created). Try playing with this function to see the changes you make being automatically propagated to intersecting cross sections and to the site model. To return to the site, go again to “Edit -> Create cross-section” and choose “Return to site this time”.

Figure I.4: Shortcut buttons

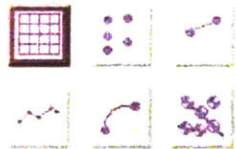
A plan view can be seen by toggling on the corresponding feature under the View site attributes menu.



*Zooming and translating buttons:* The middle button can be used to specify at which drawing window the zooming or translating should take place. Zooming in and out can be done by the upper left and lower right buttons respectively. The scaling factor is 1.2 both for enlarging and shrinking. This factor can be changed with the upper right button. Translation is done with the arrow buttons; the default factor is 10 feet and it can be modified with the lower left button.



*Rotation buttons:* Rotation takes place in all 3 windows. The default rotation degree is zero, so the user should specify the angle with the lower middle button. The lower left and right buttons change the direction of rotation, with left being clockwise. The upper three buttons specify rotation in their corresponding plane.



*Editing buttons:* The upper left button specifies the size of the grid. The middle one opens a menu for node editing, and the right one for line editing. The lower middle button corresponds to curve editing, and the lower right one to cross sections creation. (Right now the bottom three buttons do not work). It is recommended though that you use the edit menu for those last two activities.

Figure I.5: Explanation of shortcut buttons.

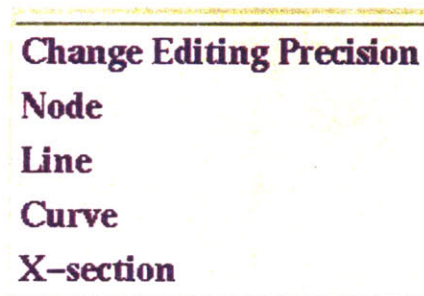


Figure I.6: The Edit menu



Figure I.7:  
Example of a  
Ground types  
legend.

Do not forget to save regularly, as the program may (and will) exit with no warning!



### Example

This example intends to illustrate the main steps followed in editing a Nomad profile. As mentioned above, after importing the spreadsheet data one can see the boreholes and the profile along them (Figure I.8).

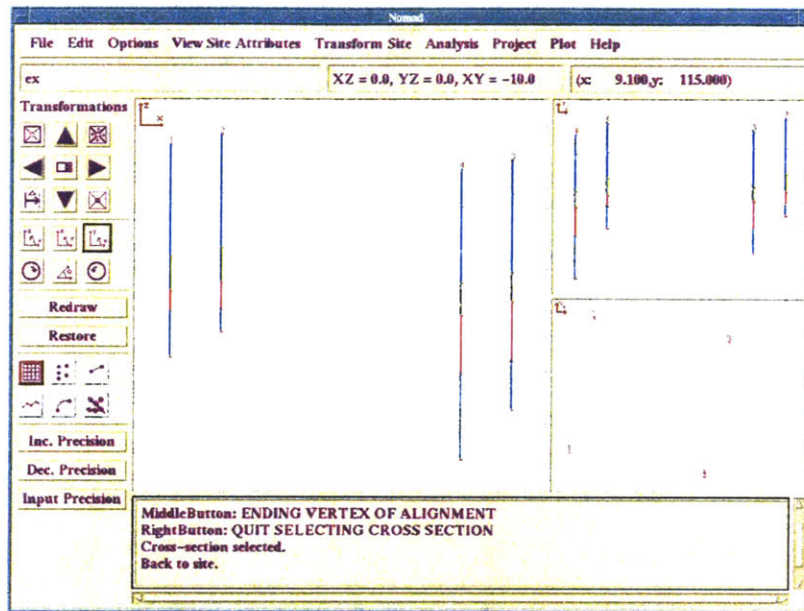


Figure I.8: Nomad window with imported borehole data.

The user can connect the nodes by inserting layer lines and form, in this way, the various ground layers.

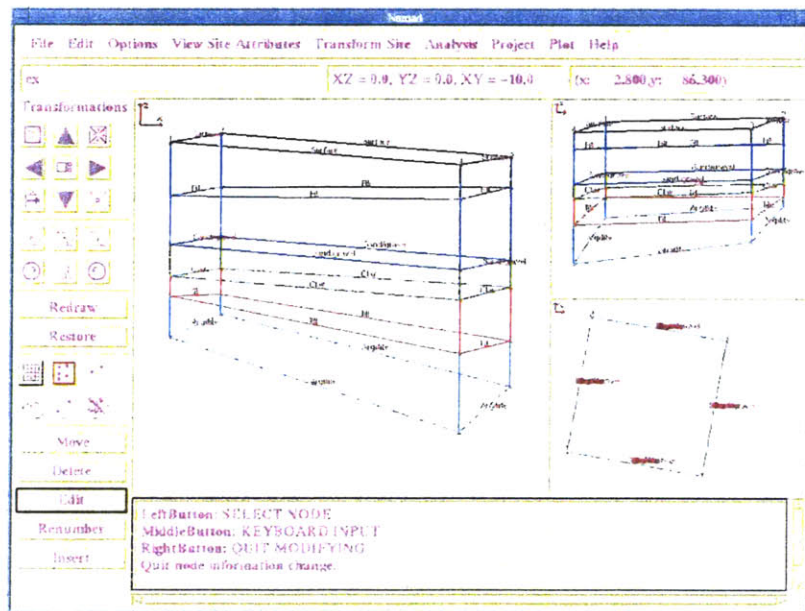
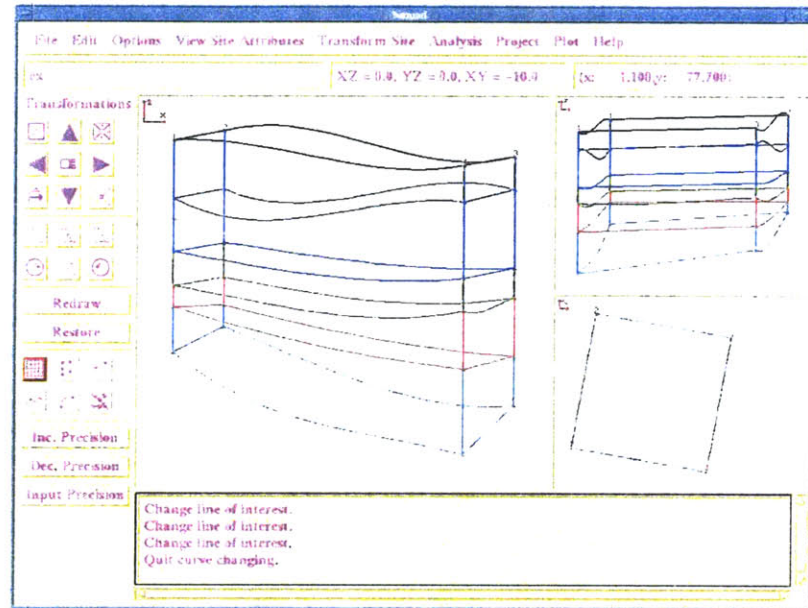


Figure I.9: Rotated profile with layers.

After rotating the 3-D profile (second family of buttons in Figure I.4, Figure I.5) and toggling on the layer option (Under site attributes menu), one gets a view like in Figure I.9.

Furthermore, the user can edit the layer lines and produce curves (see also Figure I.6). This modification reflects the users subjective understanding of the underground profile.



*Figure I.10: Model with curved lines.*

## ***APPENDIX II:***

### ***Borehole data for MBTA Porter Sq.–Davis Sq. case study***





<i>Borehole name</i>	<i>x (ft)</i>	<i>y (ft)</i>	<i>Description</i>	<i>Depth (ft)</i>	<i>Elevation (ft)</i>	<i>Ground type</i>	<i>Layer</i>
P201	0.5	10	Surface	0	138.3	Surface	0
P201	0.5	10	Fill	10	128.3	Fill	1
P201	0.5	10	Sand/gravel	25	113.3	Sand/gravel	2
P201	0.5	10	Clay	31.5	106.8	Clay	3
P201	0.5	10	Till	31.8	106.5	Till	4
P201	0.5	10	Argillite >75	40	98.3	Argillite >75	5
P201	0.5	10	Argillite >50	43.2	95.1	Argillite >50	6
P201	0.5	10	Argillite <25	45	93.3	Argillite <25	8
P201	0.5	10	Argillite >50	56.2	82.1	Argillite >50	6
P201	0.5	10	Argillite >75	57.3	81	Argillite >75	5
P201	0.5	10	Argillite >50	60	78.3	Argillite >50	6
P201	0.5	10	Basalt	125	13.3	Basalt	9
T17	5	10.5	Surface	0	136.5	Surface	0
T17	5	10.5	Fill	10	125.65	Fill	1
T17	5	10.5	Sand/gravel	36.5	99.15	Sand/gravel	2
T17	5	10.5	Argillite >75	68	67.65	Argillite >75	5
TB11	10	11	Surface	0	136.8	Surface	0
TB11	10	11	Fill	3.98	132.3	Fill	1
TB11	10	11	Sand/gravel	23.98	112.3	Sand/gravel	2
TB11	10	11	Clay	30.98	105.3	Clay	3
TB11	10	11	Till	34.48	101.8	Till	4
TB11	10	11	Argillite >75	79.5	56.78	Argillite >75	5
TB11	10	11	Argillite >50	89.5	46.78	Argillite >50	6
TB11	10	11	Argillite >75	99.5	36.78	Argillite >75	5
TB11	10	11	Argillite >50	109.5	26.78	Argillite >50	6
TB11	10	11	Argillite >75	130	6.28	Argillite >75	5
TA11	12	9.5	Surface	0	137.46	Surface	0
TA11	12	9.5	Fill	2.46	135	Fill	1
TA11	12	9.5	Sand/gravel	33.96	103.5	Sand/gravel	2
TA11	12	9.5	Clay	42.96	94.5	Clay	3
TA11	12	9.5	Till	49.06	88.4	Till	4
TA11	12	9.5	Argillite >75	48	89.49	Argillite >75	5
TA11	12	9.5	Argillite >50	53	84.49	Argillite >50	6
TA11	12	9.5	Argillite >75	89	48.49	Argillite >75	5
TA11	12	9.5	Argillite >50	95.5	41.99	Argillite >50	6
TA11	12	9.5	Argillite >75	109	28.49	Argillite >75	5
TA11	12	9.5	Argillite <25	112.5	24.99	Argillite <25	8
TA11	12	9.5	Argillite >75	119.5	17.99	Argillite >75	5
TA11	12	9.5	Argillite >50	130	7.46	Argillite >50	6
TB-12	15	10.8	Surface	0	136.98	Surface	0
TB-12	15	10.8	Fill	7.98	129	Fill	1
TB-12	15	10.8	Sand/gravel	25.98	111	Sand/gravel	2
TB-12	15	10.8	Clay	29.48	107.5	Clay	3
TB-12	15	10.8	Till	37.48	99.5	Till	4
TB-12	15	10.8	Argillite >75	44	92.98	Argillite >75	5
TB-12	15	10.8	Argillite >50	49	87.98	Argillite >50	6

<i>Borehole name</i>	<i>x (ft)</i>	<i>y (ft)</i>	<i>Description</i>	<i>Depth (ft)</i>	<i>Elevation (ft)</i>	<i>Ground type</i>	<i>Layer</i>
TB-12	15	10.8	Argillite >75	64	72.98	Argillite >75	5
TB-12	15	10.8	Argillite >25	69	67.98	Argillite >25	7
TB-12	15	10.8	Argillite >75	83.5	53.48	Argillite >75	5
TB-12	15	10.8	Argillite >25	88	48.98	Argillite >25	7
TB-12	15	10.8	Argillite >50	93	43.98	Argillite >50	6
TB-12	15	10.8	Argillite >75	121.5	15.48	Argillite >75	5
TB-12	15	10.8	Argillite >50	126.5	10.48	Argillite >50	6
TB-12	15	10.8	Argillite >75	135	1.98	Argillite >75	5
T-19P	18	10.6	Surface	0	134.53	Surface	0
T-19P	18	10.6	Fill	5	129.53	Fill	1
T-19P	18	10.6	Sand/gravel	20.25	114.28	Sand/gravel	2
T-19P	18	10.6	Till	25.5	109.03	Till	4
T-19P	18	10.6	Argillite <25	34	100.53	Argillite <25	8
T-19P	18	10.6	Argillite >25	40	94.53	Argillite >25	7
T-19P	18	10.6	Argillite <25	72	62.53	Argillite <25	8
TA-13	21	10	Surface	0	135.4	Surface	0
TA-13	21	10	Fill	2.5	132.9	Fill	1
TA-13	21	10	Sand/gravel	15.5	119.9	Sand/gravel	2
TA-13	21	10	Till	21	114.4	Till	4
TA-13	21	10	Argillite >50	26	109.4	Argillite >50	6
TA-13	21	10	Argillite >75	135	0.4	Argillite >75	5
T20-U	22	9	Surface	0	134.26	Surface	0
T20-U	22	9	Fill	3.5	130.76	Fill	1
T20-U	22	9	Sand/gravel	10	124.26	Sand/gravel	2
T20-U	22	9	Clay	34.5	99.76	Clay	3
T20-U	22	9	Till	49.3	84.96	Till	4
T20-U	22	9	Argillite >25	65	69.26	Argillite >25	7
TA-14	25	9.5	Surface	0	134.43	Surface	0
TA-14	25	9.5	Fill	2.5	131.93	Fill	1
TA-14	25	9.5	Clay	35	99.43	Clay	3
TA-14	25	9.5	Sand/gravel	38	96.43	Sand/gravel	2
TA-14	25	9.5	Clay	61.5	72.93	Clay	3
TA-14	25	9.5	Till	69	65.43	Till	4
TA-14	25	9.5	Argillite >75	118	16.43	Argillite >75	5
TA-15	28	10	Surface	0	133.28	Surface	0
TA-15	28	10	Fill	3	130.28	Fill	1
TA-15	28	10	Sand/gravel	12.5	120.78	Sand/gravel	2
TA-15	28	10	Clay	63	70.28	Clay	3
TA-15	28	10	Till	66.5	66.78	Till	4
TA-15	28	10	Argillite >75	70.5	62.78	Argillite >75	5
TA-15	28	10	Argillite >50	77.5	55.78	Argillite >50	6
TA-15	28	10	Argillite <25	78.5	54.78	Argillite <25	8
TA-15	28	10	Argillite >75	85	48.28	Argillite >75	5
TA-15	28	10	Argillite >50	88	45.28	Argillite >50	6
TA-15	28	10	Argillite >25	90.5	42.78	Argillite >25	7
TA-15	28	10	Argillite >75	99.5	33.78	Argillite >75	5

<i>Borehole name</i>	<i>x (ft)</i>	<i>y (ft)</i>	<i>Description</i>	<i>Depth (ft)</i>	<i>Elevation (ft)</i>	<i>Ground type</i>	<i>Layer</i>
TA-15	28	10	Argillite >25	102	31.28	Argillite >25	7
TA-15	28	10	Argillite >75	115	18.28	Argillite >75	5
TA-15	28	10	Argillite >25	119	14.28	Argillite >25	7
TA-15	28	10	Argillite >50	122	11.28	Argillite >50	6
TA-15	28	10	Argillite >75	135	-1.72	Argillite >75	5
TB-13	33	8	Surface	0	133.58	Surface	0
TB-13	33	8	Fill	2	131.58	Fill	1
TB-13	33	8	Silt	2.5	131.08	Silt	10
TB-13	33	8	Sand/gravel	13	120.58	Sand/gravel	2
TB-13	33	8	Clay	61	72.58	Clay	3
TB-13	33	8	Till	72	61.58	Till	4
TB-13	33	8	Argillite >25	76.5	57.08	Argillite >25	7
TB-13	33	8	Argillite >50	91.5	42.08	Argillite >50	6
TB-13	33	8	Argillite >75	126.5	7.08	Argillite >75	5
TA13	34	12	Surface	0	133.02	Surface	0
TA13	34	12	Fill	4	129.02	Fill	1
TA13	34	12	Sand/gravel	14	119.02	Sand/gravel	2
TA13	34	12	Clay	59	74.02	Clay	3
TA13	34	12	Till	62.5	70.52	Till	4
TA13	34	12	Argillite >50	73.5	59.52	Argillite >50	6
TA13	34	12	Argillite >75	120	13.02	Argillite >75	5
T-22	37	10.2	Surface	0	134.56	Surface	0
T-22	37	10.2	Fill	8	126.56	Fill	1
T-22	37	10.2	Sand/gravel	12	122.56	Sand/gravel	2
T-22	37	10.2	Clay	33.5	101.06	Clay	3
T-22	37	10.2	Till	36	98.56	Till	4
T-22	37	10.2	Argillite >25	41	93.56	Argillite >25	7
T-22	37	10.2	Argillite >75	42	92.56	Argillite >75	5
T-22	37	10.2	Argillite >25	46	88.56	Argillite >25	7
T-22	37	10.2	Argillite >75	59	75.56	Argillite >75	5
T-22	37	10.2	Argillite >25	64	70.56	Argillite >25	7
T-22	37	10.2	Argillite >75	69	65.56	Argillite >75	5
T-22	37	10.2	Argillite >50	73	61.56	Argillite >50	6
TA-17	39	10.6	Surface	0	131.93	Surface	0
TA-17	39	10.6	Fill	5.5	126.43	Fill	1
TA-17	39	10.6	Clay	24	107.93	Clay	3
TA-17	39	10.6	Till	29.5	102.43	Till	4
TA-17	39	10.6	Argillite >50	36	95.93	Argillite >50	6
TA-17	39	10.6	Argillite >75	52	79.93	Argillite >75	5
TA-17	39	10.6	Argillite <25	53	78.93	Argillite <25	8
TA-17	39	10.6	Argillite >75	115	16.93	Argillite >75	5
TB-14	41	9	Surface	0	136.54	Surface	0
TB-14	41	9	Fill	4	132.54	Fill	1
TB-14	41	9	Sand/gravel	13	123.54	Sand/gravel	2
TB-14	41	9	Clay	16	120.54	Clay	3
TB-14	41	9	Till	19	117.54	Till	4

<i>Borehole name</i>	<i>x (ft)</i>	<i>y (ft)</i>	<i>Description</i>	<i>Depth (ft)</i>	<i>Elevation (ft)</i>	<i>Ground type</i>	<i>Layer</i>
TB-14	41	9	Argillite <25	45.5	91.04	Argillite <25	8
TB-14	41	9	Argillite >25	53	83.54	Argillite >25	7
TB-14	41	9	Argillite >75	63	73.54	Argillite >75	5
TB-14	41	9	Argillite >25	69	67.54	Argillite >25	7
TB-14	41	9	Argillite >75	75	61.54	Argillite >75	5
TB-14	41	9	Argillite >50	84.5	52.04	Argillite >50	6
TB-14	41	9	Argillite >25	89	47.54	Argillite >25	7
TB-14	41	9	Argillite <25	96	40.54	Argillite <25	8
TB-14	41	9	Argillite >50	100	36.54	Argillite >50	6
T24	45	10	Surface	0	136.1	Surface	0
T24	45	10	Fill	4	132.1	Fill	1
T24	45	10	Sand/gravel	8.5	127.6	Sand/gravel	2
T24	45	10	Clay	15	121.1	Clay	3
T24	45	10	Till	18	118.1	Till	4
T24	45	10	Argillite >50	28	108.1	Argillite >50	6
T24	45	10	Argillite <25	43	93.1	Argillite <25	8
T24	45	10	Argillite >50	53	83.1	Argillite >50	6
T24	45	10	Argillite >25	58	78.1	Argillite >25	7
T24	45	10	Argillite >50	65	71.1	Argillite >50	6
TA-12	49	8.5	Surface	0	135.77	Surface	0
TA-12	49	8.5	Fill	3	132.77	Fill	1
TA-12	49	8.5	Sand/gravel	7	128.77	Sand/gravel	2
TA-12	49	8.5	Clay	16	119.77	Clay	3
TA-12	49	8.5	Till	18.5	117.27	Till	4
TA-12	49	8.5	Argillite >50	26	109.77	Argillite >50	6
TA-12	49	8.5	Argillite >75	95.5	40.27	Argillite >75	5
T-25	53	9.9	Surface	0	135	Surface	0
T-25	53	9.9	Fill	4	131	Fill	1
T-25	53	9.9	Sand/gravel	12.5	122.5	Sand/gravel	2
T-25	53	9.9	Clay	16	119	Clay	3
T-25	53	9.9	Till	21	114	Till	4
T-25	53	9.9	Argillite >50	26	109	Argillite >50	6
T-25	53	9.9	Argillite >75	36	99	Argillite >75	5
T-25	53	9.9	Argillite >50	41	94	Argillite >50	6
T-25	53	9.9	Argillite >75	46	89	Argillite >75	5
T-25	53	9.9	Argillite >25	49	86	Argillite >25	7
T-25	53	9.9	Argillite >75	54	81	Argillite >75	5
TB-15	58	11.3	Surface	0	134.91	Surface	0
TB-15	58	11.3	Fill	2	132.91	Fill	1
TB-15	58	11.3	Sand/gravel	6	128.91	Sand/gravel	2
TB-15	58	11.3	Clay	14	120.91	Clay	3
TB-15	58	11.3	Till	21	113.91	Till	4
TB-15	58	11.3	Argillite >50	60	74.91	Argillite >50	6
TB-15	58	11.3	Argillite >75	84	50.91	Argillite >75	5
TA-16	61	10	Surface	0	133.9	Surface	0
TA-16	61	10	Fill	4	129.9	Fill	1

<i>Borehole name</i>	<i>x (ft)</i>	<i>y (ft)</i>	<i>Description</i>	<i>Depth (ft)</i>	<i>Elevation (ft)</i>	<i>Ground type</i>	<i>Layer</i>
TA-16	61	10	Sand/gravel	19	114.9	Sand/gravel	2
TA-16	61	10	Silt	24	109.9	Silt	10
TA-16	61	10	Clay	45.5	88.4	Clay	3
TA-16	61	10	Till	55	78.9	Till	4
TA-16	61	10	Argillite >75	60	73.9	Argillite >75	5
TA-16	61	10	Argillite >50	68.5	65.4	Argillite >50	6
TB-16	63	8.9	Surface	0	133.9	Surface	0
TB-16	63	8.9	Fill	5	128.9	Fill	1
TB-16	63	8.9	Sand/gravel	14	119.9	Sand/gravel	2
TB-16	63	8.9	Silt	24	109.9	Silt	10
TB-16	63	8.9	Clay	45.5	88.4	Clay	3
TB-16	63	8.9	Till	55	78.9	Till	4
TB-16	63	8.9	Argillite >75	60	73.9	Argillite >75	5
TB-16	63	8.9	Argillite >50	70	63.9	Argillite >50	6
B22	65	9.3	Surface	0	134.3	Surface	0
B22	65	9.3	Fill	12	122.3	Fill	1
B22	65	9.3	Sand/gravel	14	120.3	Sand/gravel	2
B22	65	9.3	Clay	23	111.3	Clay	3
B22	65	9.3	Till	25	109.3	Till	4
B22	65	9.3	Argillite >50	30	114.3	Argillite >50	6
D101	67	10	Surface	0	133.71	Surface	0
D101	67	10	Fill	6	127.71	Fill	1
D101	67	10	Sand/gravel	24	109.71	Sand/gravel	2
D101	67	10	Silt	40.5	93.21	Silt	10
D101	67	10	Clay	49.5	84.21	Clay	3
D101	67	10	Till	49.8	83.91	Till	4
D101	67	10	Argillite >25	63	75.71	Argillite >25	7
D101	67	10	Argillite <25	65	68.71	Argillite <25	8



### ***APPENDIX III:***

#### ***Geostatistical profiles for the MBTA Porter Sq. to Davis Sq. case study***





## Appendix III: KRIBS results for Porter Sq. case study

In this appendix the results for the Porter Sq. to Davis Sq. case study are given. Results include fine and coarse grid profiles, and modeling with exponential or spherical semi-variogram models. They show thresholds 0%, 30% and 50%.

### III.1 Exponential model - Coarse grid: (x,y,z)=(50,50,5) (ft)

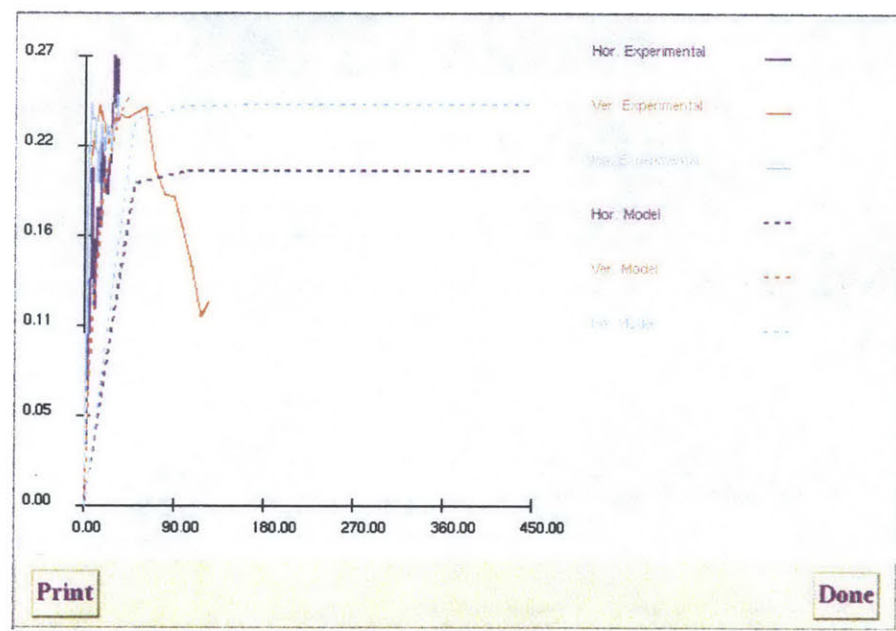


*Figure III.1: Experimental semi-variograms and exponential semi-variogram models - coarse grid*

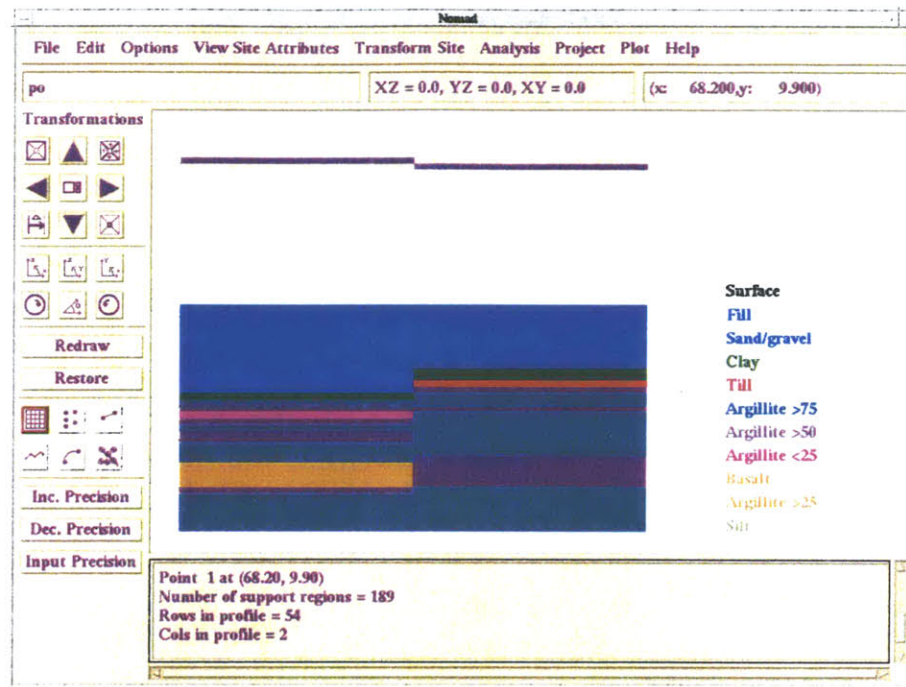


Figure III.2: Kriged (geostatistical) profile - exponential model - coarse grid – threshold 0%

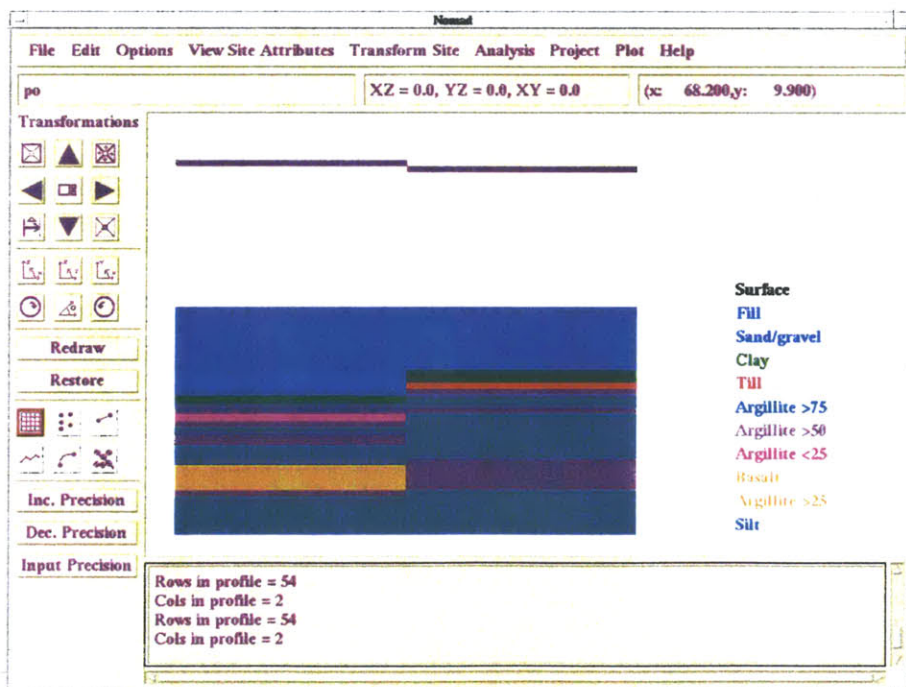


Figure III.3: Kriged (geostatistical) profile - exponential model - coarse grid – threshold 30%

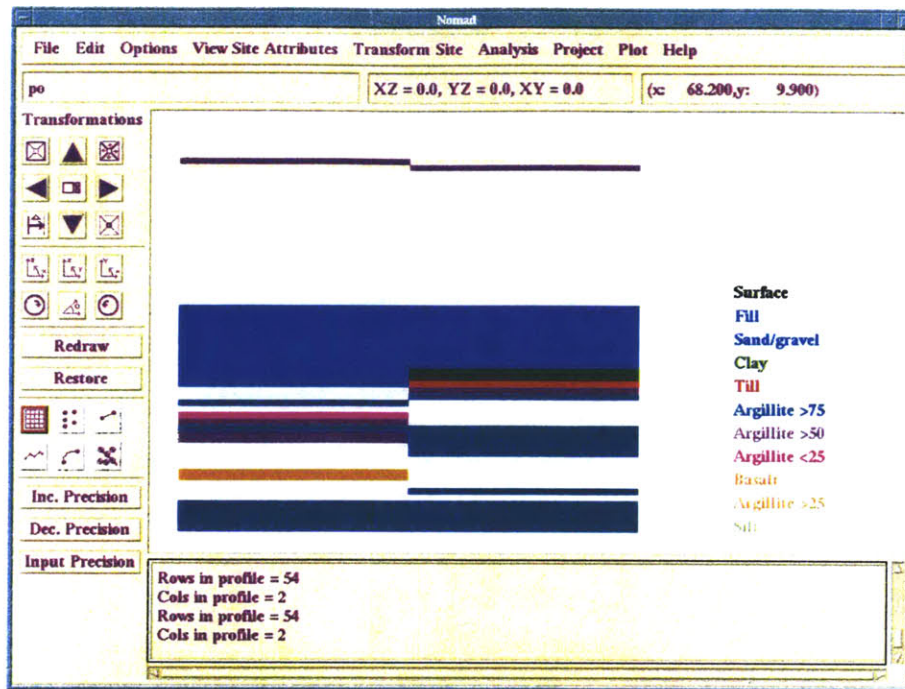


Figure III.4: Kriged (geostatistical) profile - exponential model - coarse grid – threshold 50%

### III.2 Exponential model - Medium grid: (x,y,z)=(5,5,5) (ft)

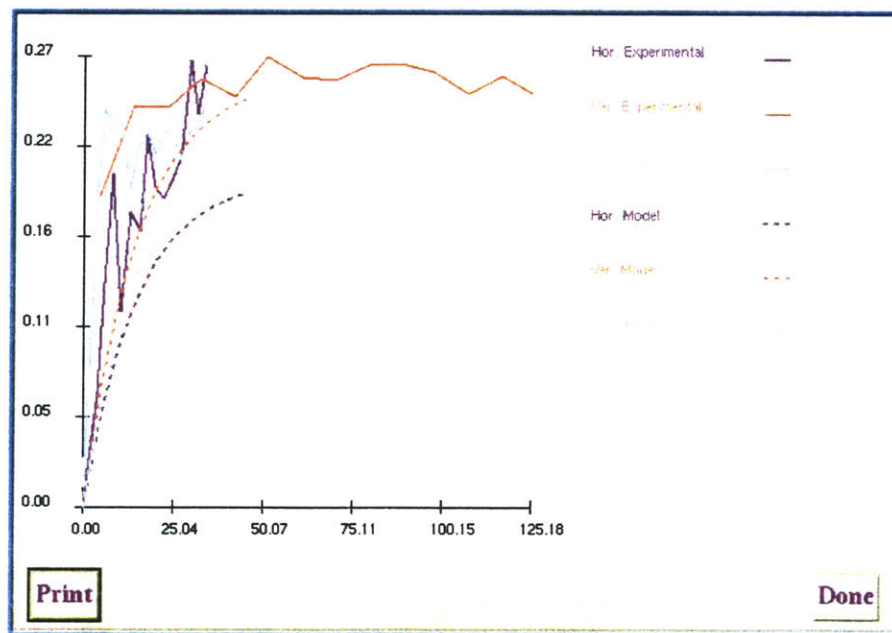


Figure III.5: Experimental semi-variograms and exponential semi-variogram models - medium grid

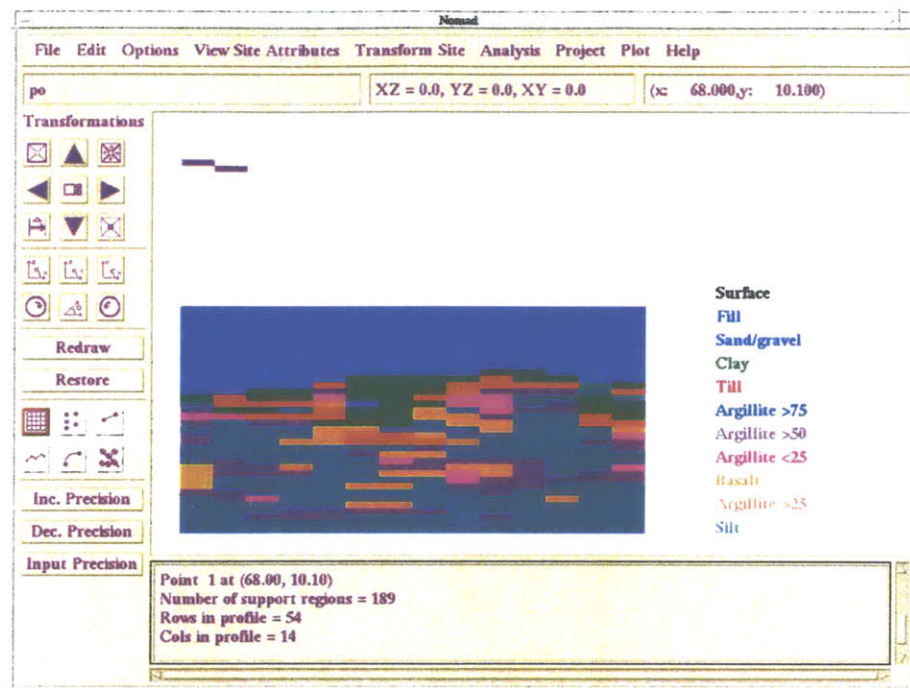


Figure III.6: Kriged (geostatistical) profile - exponential model - medium grid – threshold 0%

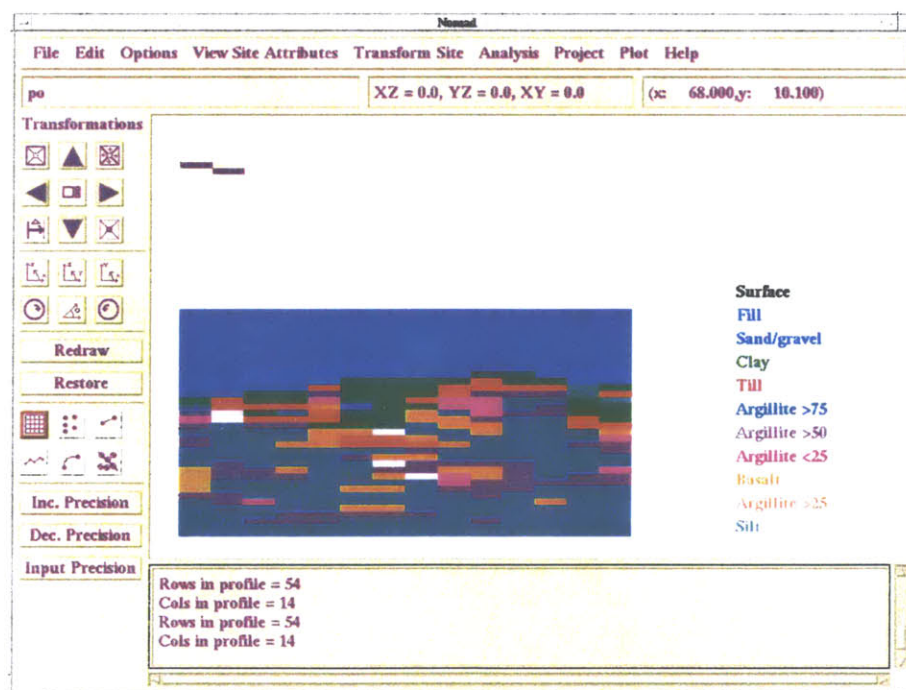


Figure III.7: Kriged (geostatistical) profile - exponential model - medium grid – threshold 30%



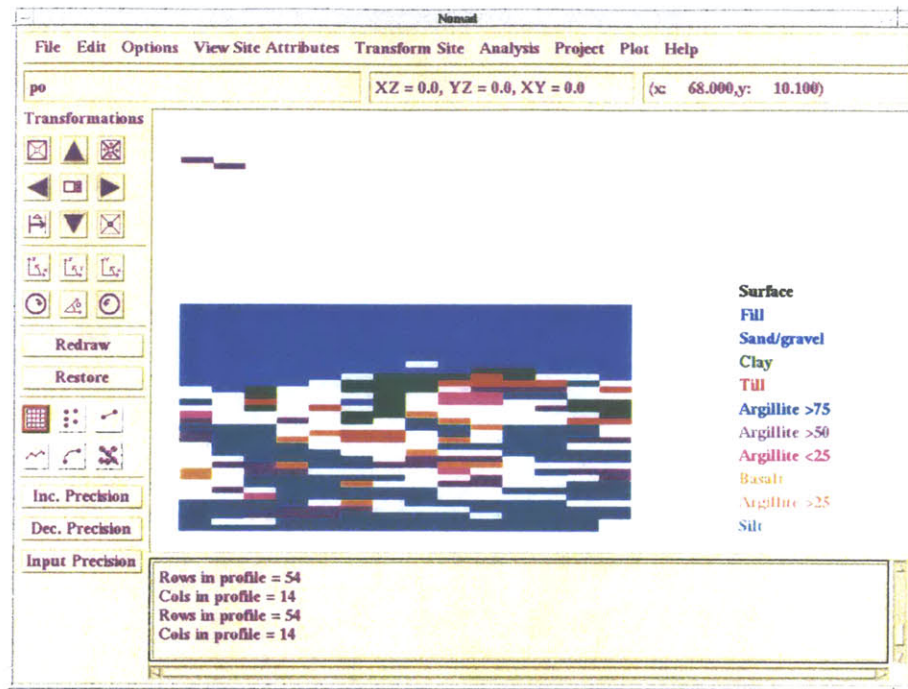


Figure III.8: Kriged (geostatistical) profile - exponential model - medium grid – threshold 50%

### III.3 Exponential model - Fine grid: (x,y,z)=(1,1,1) (ft)

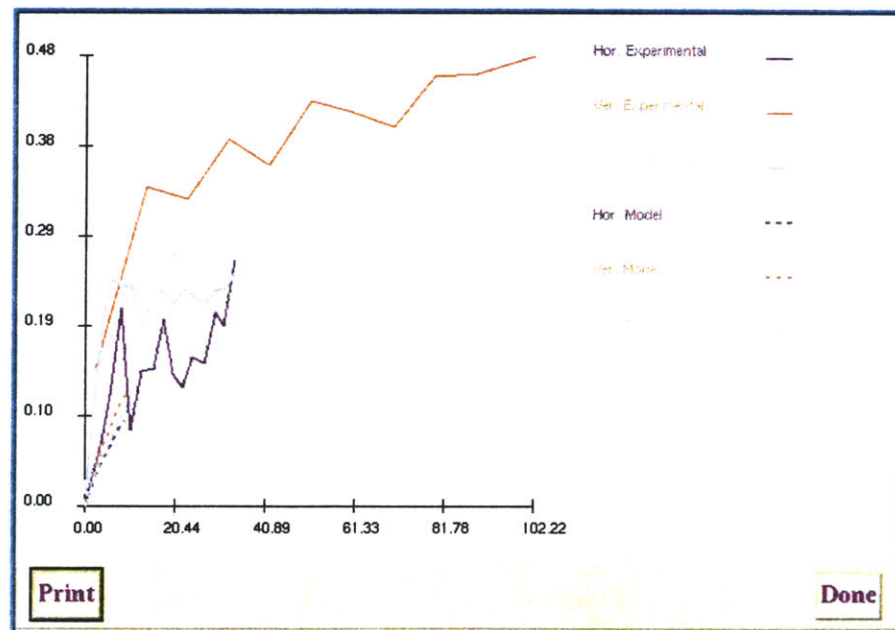


Figure III.9: Experimental semi-variograms and exponential semi-variogram models - fine grid

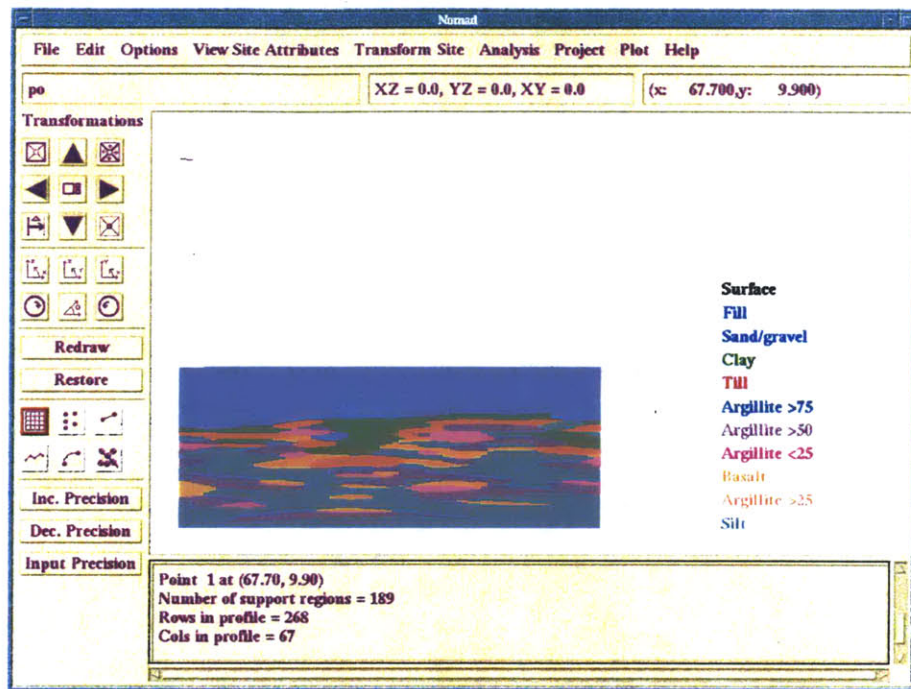


Figure III.10: Kriged (geostatistical) profile - exponential model - fine grid – threshold 0%

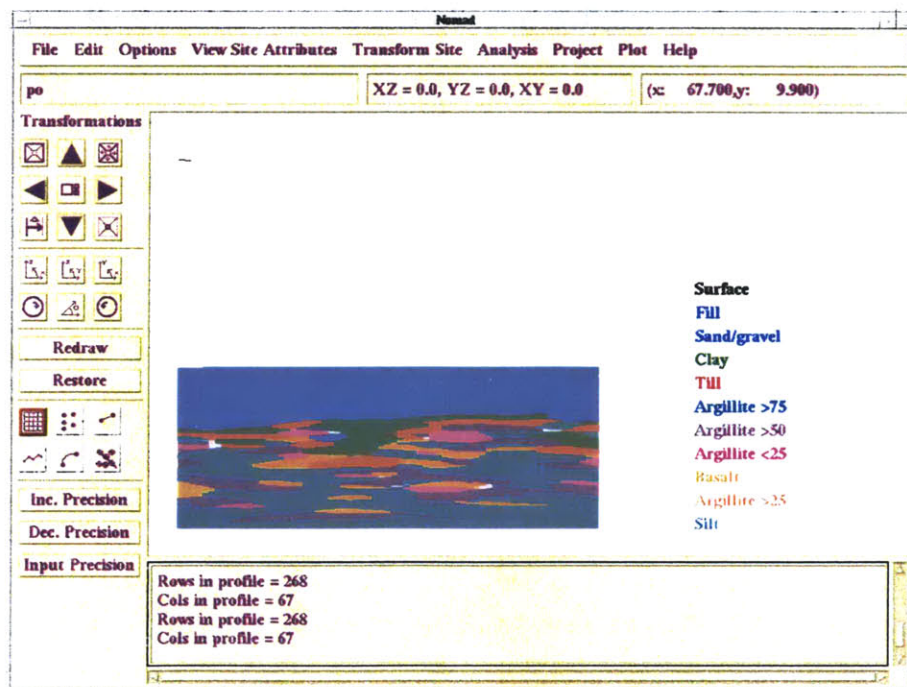


Figure III.11: Kriged (geostatistical) profile - exponential model - fine grid – threshold 30%



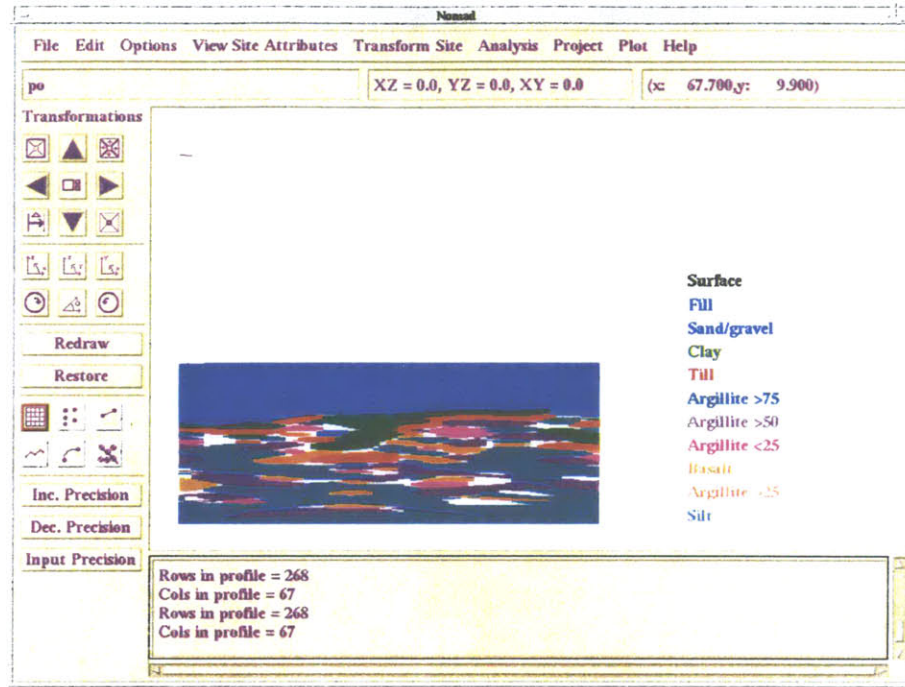


Figure III.12: Kriged (geostatistical) profile - exponential model - fine grid – threshold 40%

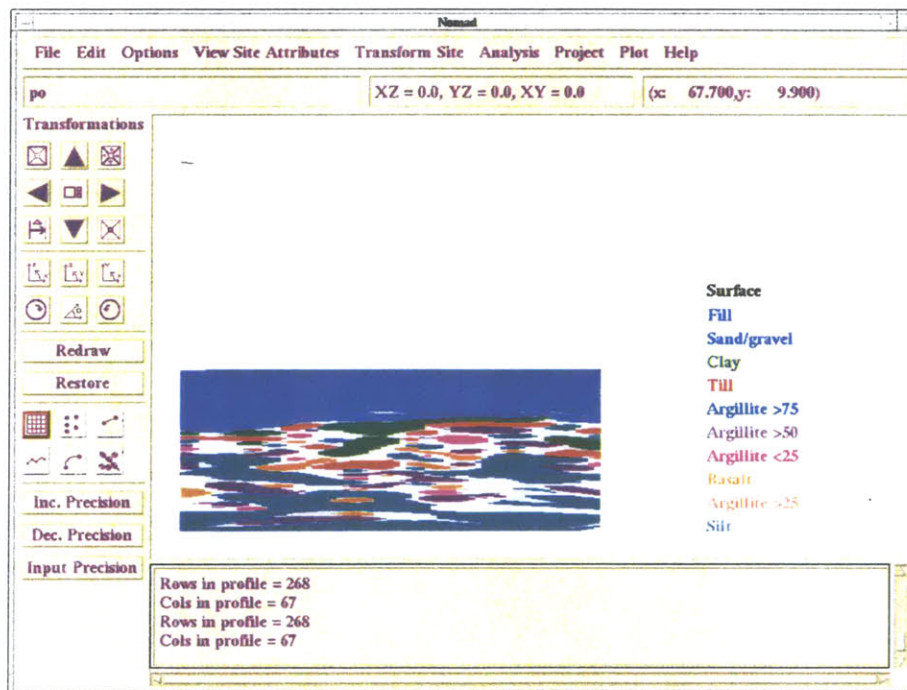


Figure III.13: Kriged (geostatistical) profile - exponential model - fine grid – threshold 50%

### III.4 Spherical model - Medium grid: (x,y,z)=(5,5,5) (ft)

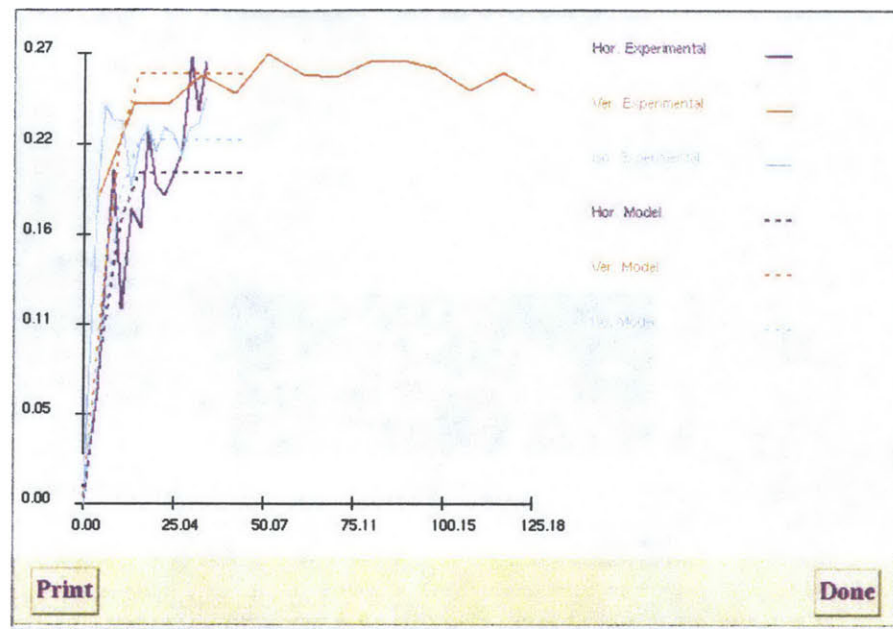


Figure III.14: Experimental semi-variograms and spherical semi-variogram models – medium grid.

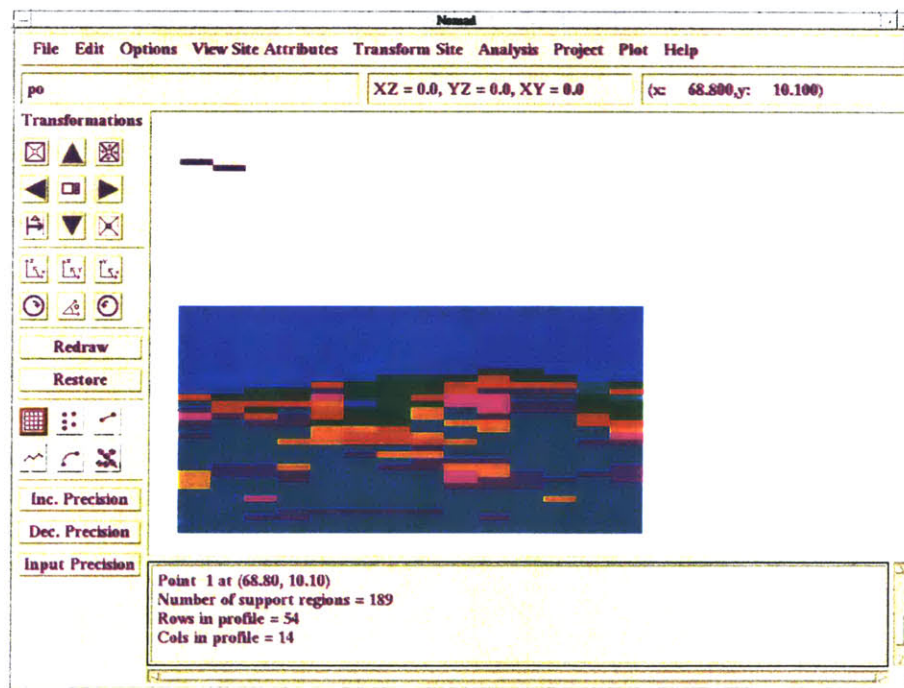


Figure III.15: Kriged (geostatistical) profile - spherical model - medium grid – threshold 0%

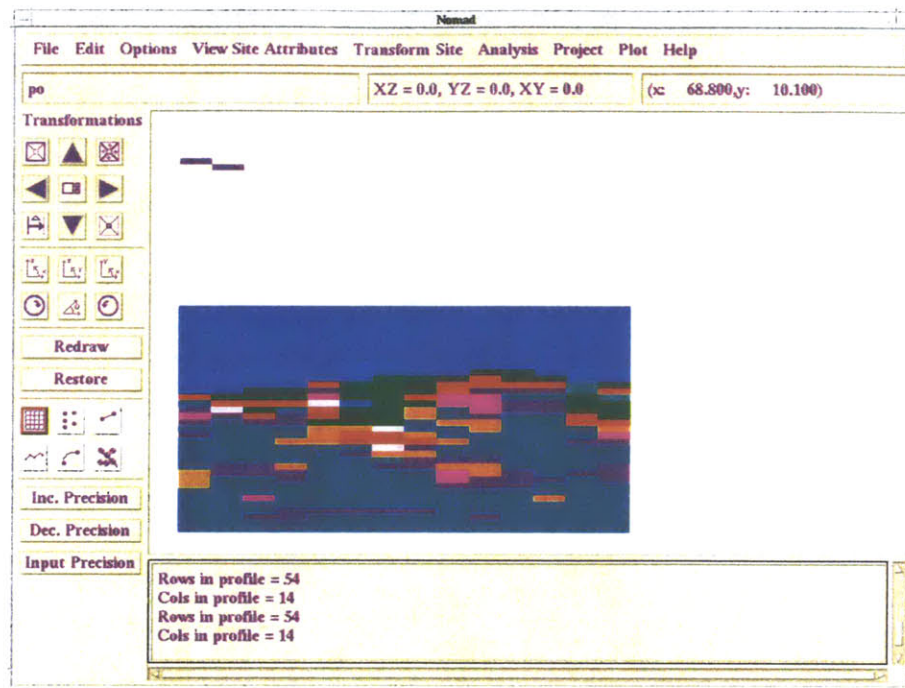


Figure III.16: Kriged (geostatistical) profile - spherical model - medium grid – threshold 30%

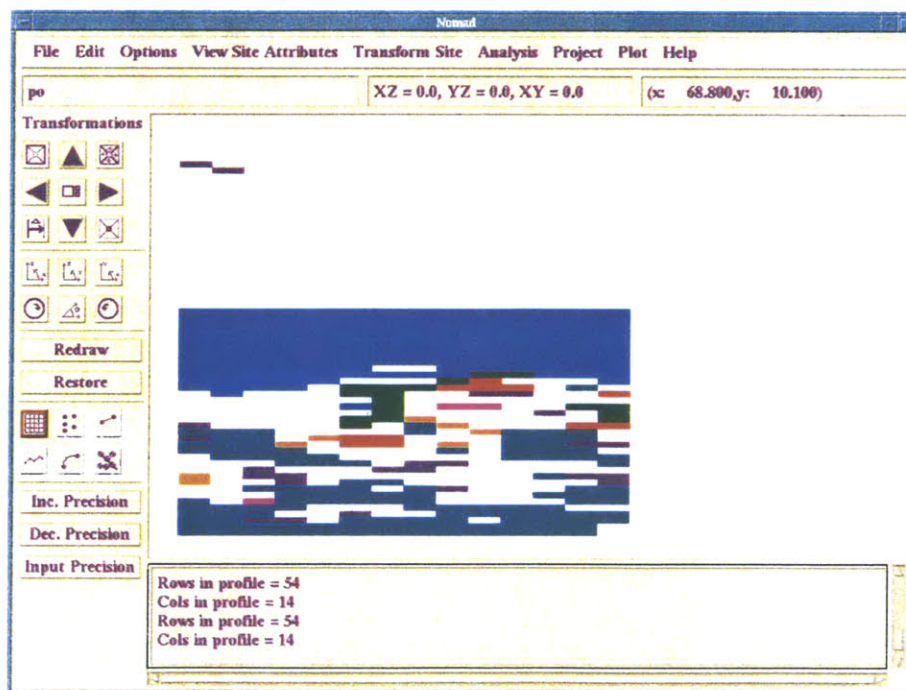


Figure III.17: Kriged (geostatistical) profile - spherical model - medium grid – threshold 50%



## ***APPENDIX IV:***

### ***Borehole and hydrogeological data for the Wellesley Maintenance Depot case study***



## Geologic Data

<i>Borehole name</i>	<i>x (ft)</i>	<i>y (ft)</i>	<i>Description</i>	<i>Depth (ft)</i>	<i>z (ft)</i>	<i>Ground type</i>	<i>SPT</i>	<i>RQD</i>	<i>Layer</i>
ABB-SB-1	680	860.8	Surface	0	100	Surface			0
ABB-SB-1	680	860.8	Widely graded sand	2	98	Widely graded sand	20		1
ABB-SB-1	680	860.8	Widely graded sand	4	96	Widely graded sand	24		1
ABB-SB-1	680	860.8	Widely graded sand	5	95	Widely graded sand			1
ABB-SB-1	680	860.8	Widely graded sand	7	92	Widely graded sand	33		1
ABB-SB-1	680	860.8	Widely graded sand	7.2	92.8	Widely graded sand	38		1
ABB-SB-1	680	860.8	Silt	7.5	92.5	Silt			2
ABB-SB-1	680	860.8	Widely graded sand	10	90	Widely graded sand			1
ABB-SB-1	680	860.8	Widely graded sand	12	88	Widely graded sand	38		1
ABB-SB-1	680	860.8	Widely graded sand	4	85	Widely graded sand			1
ABB-SB-1	680	860.8	Widely graded sand	15.2	84.8	Widely graded sand	20		1
ABB-SB-1	680	860.8	Silt	16.4	83.6	Silt	20		2
ABB-SB-1	680	860.8	Silt	20	80	Silt			2
ABB-SB-1	680	860.8	Silt	22	78	Silt	20		2
ABB-SB-1	680	860.8	Silt	25	75	Silt	7		2
ABB-SB-2/MW-11	1032	710.4	Surface	0	100	Surface			0
ABB-SB-2/MW-11	1032	710.4	Widely graded sand	3	97	Widely graded sand	22		1
ABB-SB-2/MW-11	1032	710.4	Widely graded sand	3.5	96.5	Widely graded sand	13		1
ABB-SB-2/MW-11	1032	710.4	Silt	4	96	Silt	13		2
ABB-SB-2/MW-11	1032	710.4	Silt	5	95	Silt			2
ABB-SB-2/MW-11	1032	710.4	Silt	5.5	94.5	Silt	22		2
ABB-SB-2/MW-11	1032	710.4	Widely graded sand	6.1	93.9	Widely graded sand	22		1
ABB-SB-2/MW-11	1032	710.4	Widely graded sand	10	90	Widely graded sand			1
ABB-SB-2/MW-11	1032	710.4	Widely graded sand	10.25	89.8	Widely graded sand	52		1
ABB-SB-2/MW-11	1032	710.4	Silt	12	88	Silt	52		2
ABB-SB-3	390	727.5	Surface	0	100	Surface			0
ABB-SB-3	390	727.5	Widely graded sand	3	97	Widely graded sand	42		1
ABB-SB-3	390	727.5	Widely graded sand	5	95	Widely graded sand	31		1
ABB-SB-3	390	727.5	Widely graded sand	7	93	Widely graded sand	20		1
ABB-SB-3	390	727.5	Widely graded sand	9	91	Widely graded sand	33		1
ABB-SB-3	390	727.5	Widely graded sand	11	89	Widely graded sand	13		1
ABB-SB-3	390	727.5	Widely graded sand	11.5	88.5	Widely graded sand	5		1
ABB-SB-3	390	727.5	Silt	11.9	88.1	Silt	5		2
ABB-SB-3	390	727.5	Silt	13	87	Silt			2
ABB-SB-3	390	727.5	Widely graded sand	13.2	86.8	Widely graded sand	10		1
ABB-SB-3	390	727.5	Silt	13.8	86.2	Silt	10		2
ABB-SB-3	390	727.5	clayey Silt	15	85	clayey Silt			4
ABB-SB-3	390	727.5	clayey Silt	17	83	clayey Silt	25		4
ABB-SB-3	390	727.5	clayey Silt	20	80	clayey Silt			4
ABB-SB-3	390	727.5	clayey Silt	22	78	clayey Silt	11		4
ABB-SB-4	376.9	651.6	Surface	0	100	Surface			0
ABB-SB-4	376.9	651.6	Widely graded sand	3	97	Widely graded sand	37		1



<i>Borehole name</i>	<i>x (ft)</i>	<i>y (ft)</i>	<i>Description</i>	<i>Depth (ft)</i>	<i>z (ft)</i>	<i>Ground type</i>	<i>SPT</i>	<i>RQD</i>	<i>Layer</i>
ABB-SB-4	376.9	651.6	Widely graded sand	5	95	Widely graded sand	81		1
ABB-SB-4	376.9	651.6	Widely graded sand	7	93	Widely graded sand	58		1
ABB-SB-4	376.9	651.6	Widely graded sand	9	91	Widely graded sand			1
ABB-SB-4	376.9	651.6	Widely graded sand	11	89	Widely graded sand	23		1
ABB-SB-4	376.9	651.6	Silt	11.4	88.6	Silt	34		2
ABB-SB-4	376.9	651.6	Silty sand	11.8	88.2	Silty sand	34		5
ABB-SB-4	376.9	651.6	Silty sand	13	87	Silty sand			5
ABB-SB-4	376.9	651.6	Silty sand	15	85	Silty sand	57		5
ABB-SB-4	376.9	651.6	Silt	17	83	Silt	17		2
ABB-MW-8	619.2	631.2	Surface	0	100	Surface			0
ABB-MW-8	619.2	631.2	Widely graded sand	3	97	Widely graded sand	60		1
ABB-MW-8	619.2	631.2	Widely graded sand	5	95	Widely graded sand	53		1
ABB-MW-8	619.2	631.2	Widely graded sand	7	93	Widely graded sand	70		1
ABB-MW-8	619.2	631.2	Widely graded sand	9	91	Widely graded sand			1
ABB-MW-8	619.2	631.2	Widely graded sand	9.5	90.5	Widely graded sand	20		1
ABB-MW-8	619.2	631.2	Silt	10	90	Silt	20		2
ABB-MW-8	619.2	631.2	Silt	11	89	Silt			2
ABB-MW-8	619.2	631.2	clayey Silt	11.6	88.4	clayey Silt	53		4
ABB-MW-8	619.2	631.2	Widely graded sand	12.6	87.4	Widely graded sand	53		1
ABB-MW-8	619.2	631.2	Silt	15	85	Silt			2
ABB-MW-8	619.2	631.2	Silt	17	83	Silt	24		2
ABB-MW-8	619.2	631.2	Silt	20	80	Silt			2
ABB-MW-8	619.2	631.2	Silt	22	78	Silt	9		2
ABB-MW-8	619.2	631.2	Silt	23	77	Silt			2
ABB-MW-8	619.2	631.2	Silt	25	75	Silt	9		2
ABB-MW-9	928.8	475.2	Surface	0	100	Surface			0
ABB-MW-9	928.8	475.2	Widely graded sand	2	98	Widely graded sand	14		1
ABB-MW-9	928.8	475.2	Widely graded sand	4	96	Widely graded sand	53		1
ABB-MW-9	928.8	475.2	Widely graded sand	4.7	95.3	Widely graded sand	22		1
ABB-MW-9	928.8	475.2	Silt	5	95	Silt	22		2
ABB-MW-9	928.8	475.2	Silt	6	94	Silt			2
ABB-MW-9	928.8	475.2	Silt	6.4	93.6	Silt	8		2
ABB-MW-9	928.8	475.2	Silt	7.1	92.9	Silt	8		2
ABB-MW-9	928.8	475.2	Widely graded sand	10	90	Widely graded sand	52		1
ABB-MW-9	928.8	475.2	Silt	12	88	Silt			2
ABB-MW-9	928.8	475.2	Silt	15	85	Silt	15		2
ABB-MW-10	528	446.4	Surface	0	100	Surface			0
ABB-MW-10	528	446.4	gravely sand	2	98	gravely sand	27		6
ABB-MW-10	528	446.4	Silty sand	4	96	Silty sand	26		5
ABB-MW-10	528	446.4	Silty sand	6	94	Silty sand	10		5
ABB-MW-10	528	446.4	Silty sand	8	92	Silty sand	150		5
ABB-MW-10	528	446.4	Silty sand	9	91	Silty sand			5
ABB-MW-10	528	446.4	Silty sand	9.4	90.6	Silty sand	15		5
ABB-MW-10	528	446.4	Silt	10.1	89.9	Silt	15		2

<i>Borehole name</i>	<i>x (ft)</i>	<i>y (ft)</i>	<i>Description</i>	<i>Depth (ft)</i>	<i>z (ft)</i>	<i>Ground type</i>	<i>SPT</i>	<i>RQD</i>	<i>Layer</i>
ABB-MW-10	528	446.4	Silt	11	89	Silt			2
ABB-MW-10	528	446.4	Silt	13	87	Silt	71		2
ABB-MW-10	528	446.4	Silt	15	85	Silt			2
ABB-MW-10	528	446.4	Widely graded sand	17	83	Widely graded sand	38		1
ABB-MW-10	528	446.4	Widely graded sand	17.3	82.7	Widely graded sand	29		1
ABB-MW-10	528	446.4	Silt	19	81	Silt	29		2
ABB-12	379.2	268.8	Surface	0	100	Surface			0
ABB-12	379.2	268.8	gravely sand	0.9	99.1	gravely sand	32		6
ABB-12	379.2	268.8	asphalt	1.3	98.7	asphalt	32		7
ABB-12	379.2	268.8	Widely graded sand	1.8	98.2	Widely graded sand	32		1
ABB-12	379.2	268.8	Widely graded sand	5	95	Widely graded sand			1
ABB-12	379.2	268.8	silty sand	7	93	silty sand	30		5
ABB-12	379.2	268.8	silty sand	10	90	silty sand			5
ABB-12	379.2	268.8	Widely graded sand	10.2	89.8	Widely graded sand	13		1
ABB-12	379.2	268.8	Silt	10.3	89.7	Silt	13		2
ABB-12	379.2	268.8	Widely graded sand	15	85	Widely graded sand			1
ABB-12	379.2	268.8	Widely graded sand	17	83	Widely graded sand	70		1
ABB-12	379.2	268.8	Widely graded sand	19	81	Widely graded sand	127		1
ABB-12	379.2	268.8	Widely graded sand	20	80	Widely graded sand			1
ABB-12	379.2	268.8	Widely graded sand	22	78	Widely graded sand	61		1
ABB-13	648	273.6	Surface	0	100	Surface			0
ABB-13	648	273.6	Widely graded sand	2	98	Widely graded sand	22		1
ABB-13	648	273.6	Widely graded sand	5	95	Widely graded sand			1
ABB-13	648	273.6	silty sand	6	94	silty sand	8		5
ABB-13	648	273.6	Silt	6.2	93.8	Silt	8		2
ABB-13	648	273.6	Widely graded sand	10	90	Widely graded sand			1
ABB-13	648	273.6	Widely graded sand	12	88	Widely graded sand	36		1
ABB-13	648	273.6	Widely graded sand	15	85	Widely graded sand			1
ABB-13	648	273.6	clayey Silt	15.3	84.7	clayey Silt	50		4
ABB-13	648	273.6	Widely graded sand	16.7	83.3	Widely graded sand	50		1
ABB-13	648	273.6	Widely graded sand	20	80	Widely graded sand			1
ABB-13	648	273.6	sand	21.3	78.7	sand	51		9
ABB-13	648	273.6	Silt	23	77	Silt	51		2
ABB-14	381.6	105.6	Surface	0	100	Surface			0
ABB-14	381.6	105.6	Widely graded sand	2	98	Widely graded sand	46		1
ABB-14	381.6	105.6	Widely graded sand	5	95	Widely graded sand			1
ABB-14	381.6	105.6	Widely graded sand	7	93	Widely graded sand	9		1
ABB-14	381.6	105.6	Widely graded sand	10	90	Widely graded sand			1
ABB-14	381.6	105.6	Widely graded sand	12	88	Widely graded sand	3		1
ABB-14	381.6	105.6	Widely graded sand	15	85	Widely graded sand			1
ABB-14	381.6	105.6	Widely graded sand	17	83	Widely graded sand	58		1
ABB-14	381.6	105.6	Widely graded sand	20	80	Widely graded sand			1
ABB-14	381.6	105.6	Silt	22	78	Silt	48		2
ABB-15	331.2	374.4	Surface	0	100	Surface			0

<i>Borehole name</i>	<i>x (ft)</i>	<i>y (ft)</i>	<i>Description</i>	<i>Depth (ft)</i>	<i>z (ft)</i>	<i>Ground type</i>	<i>SPT</i>	<i>RQD</i>	<i>Layer</i>
ABB-15	331.2	374.4	Widely graded sand	8	92	Widely graded sand			1
ABB-15	331.2	374.4	Widely graded sand	10	90	Widely graded sand			1
ABB-15	331.2	374.4	Widely graded sand	12	88	Widely graded sand			1
ABB-15	331.2	374.4	Widely graded sand	15	85	Widely graded sand	13		1
ABB-15	331.2	374.4	Widely graded sand	17	83	Widely graded sand	75		1
ABB-15	331.2	374.4	Widely graded sand	20	80	Widely graded sand			1
ABB-15	331.2	374.4	Widely graded sand	20.2	79.8	Widely graded sand	26		1
ABB-15	331.2	374.4	Silty sand	20.5	79.5	Silty sand	26		5
ABB-15	331.2	374.4	Silt	22	78	Silt	26		2
ABB-16	240	62.4	Surface	0	100	Surface			0
ABB-16	240	62.4	Widely graded sand	2	98	Widely graded sand	29		1
ABB-16	240	62.4	Widely graded sand	5	95	Widely graded sand			1
ABB-16	240	62.4	Widely graded sand	7	93	Widely graded sand	12		1
ABB-16	240	62.4	Widely graded sand	10	90	Widely graded sand			1
ABB-16	240	62.4	Widely graded sand	10.2	89.8	Widely graded sand	13		1
ABB-16	240	62.4	Peat	10.5	89.5	Peat	13		10
ABB-16	240	62.4	silty sand	11	89	silty sand	13		5
ABB-16	240	62.4	Widely graded sand	12	88	Widely graded sand	13		1
ABB-16	240	62.4	Widely graded sand	15	85	Widely graded sand			1
ABB-16	240	62.4	Widely graded sand	17	83	Widely graded sand	62		1
ABB-16	240	62.4	Widely graded sand	20	80	Widely graded sand			1
ABB-16	240	62.4	Silt	20.2	79.8	Silt	41		2
ABB-16	240	62.4	Silt	22	78	Silt	41		2
ABB-B-2	251.9	217.7	Surface	0	100	Surface			0
ABB-B-2	251.9	217.7	Silty sand	1	99.3	Silty sand			5
ABB-B-2	251.9	217.7	Silty sand	2	98.3	Silty sand	150		5
ABB-B-2	251.9	217.7	Silty sand	5	95.3	Silty sand			5
ABB-B-2	251.9	217.7	Silt	7	93.3	Silt	13		2
ABB-B-2	251.9	217.7	Silt	10	90.3	Silt			2
ABB-B-2	251.9	217.7	gravely sand	12	88.3	gravely sand	8		6
ABB-B-2	251.9	217.7	gravely sand	15	85.3	gravely sand			6
ABB-B-2	251.9	217.7	silty sand	17	83.3	silty sand	42		5
ABB-B-3	267.5	252.1	Surface	0	101	Surface			0
ABB-B-3	267.5	252.1	sand	5	95.8	sand			9
ABB-B-3	267.5	252.1	sandy gravel	7	93.8	sandy gravel	11		9
ABB-B-3	267.5	252.1	sandy gravel	10	90.8	sandy gravel			9
ABB-B-3	267.5	252.1	sand	12	88.8	sand	15		9
ABB-B-3	267.5	252.1	sand	15	85.8	sand			9
ABB-B-3	267.5	252.1	gravely sand	17	83.8	gravely sand	42		6
ABB-B-4	411.3	655.2	Surface	0	98.8	Surface			0
ABB-B-4	411.3	655.2	sand	1	97.8	sand			9
ABB-B-4	411.3	655.2	sand	3	95.8	sand	32		9
ABB-B-4	411.3	655.2	sand	5	93.8	sand			9
ABB-B-4	411.3	655.2	gravely sand	7	91.8	gravely sand	58		6

<i>Borehole name</i>	<i>x (ft)</i>	<i>y (ft)</i>	<i>Description</i>	<i>Depth (ft)</i>	<i>z (ft)</i>	<i>Ground type</i>	<i>SPT</i>	<i>RQD</i>	<i>Layer</i>
ABB-B-4	411.3	655.2	gravely sand	10	88.8	gravely sand			6
ABB-B-4	411.3	655.2	gravely sand	10.7	88.1	gravely sand	8		6
ABB-B-4	411.3	655.2	Silt	11.4	87.4	Silt	8		2
ABB-B-4	411.3	655.2	sandy gravel	15	83.8	sandy gravel			11
ABB-B-4	411.3	655.2	sandy gravel	17	81.8	sandy gravel	33		11
ABB-B-5	451.9	683.3	Surface	0	99.5	Surface			0
ABB-B-5	451.9	683.3	sand	1	98.5	sand			9
ABB-B-5	451.9	683.3	sand	3	96.5	sand	150		9
ABB-B-5	451.9	683.3	sand	5	94.5	sand			9
ABB-B-5	451.9	683.3	sandy gravel	7	92.5	sandy gravel	37		11
ABB-B-5	451.9	683.3	sandy gravel	10	89.5	sandy gravel			11
ABB-B-5	451.9	683.3	silty sand	10.2	89.3	silty sand	43		5
ABB-B-5	451.9	683.3	gravely sand	11.6	87.9	gravely sand			6
ABB-B-5	451.9	683.3	gravely sand	12	87.5	gravely sand	43		6
ABB-B-5	451.9	683.3	gravely sand	15	84.5	gravely sand			6
ABB-B-5	451.9	683.3	gravel	17	82.5	gravel	34		13
ABB-B-8	280	677.1	Surface	0	98.2	Surface			0
ABB-B-8	280	677.1	sandy gravel	1	97.2	sandy gravel			11
ABB-B-8	280	677.1	sandy gravel	3	95.2	sandy gravel	26		11
ABB-B-8	280	677.1	sandy gravel	5	93.2	sandy gravel			11
ABB-B-8	280	677.1	gravely sand	7	91.2	gravely sand	72		6
ABB-B-8	280	677.1	gravely sand	7.8	90.4	gravely sand	150		6
ABB-B-8	280	677.1	gravely sand	10	88.2	gravely sand			6
ABB-B-8	280	677.1	sand	12	86.2	sand	59		9
ABB-B-8	280	677.1	sand	13	85.2	sand			9
ABB-B-8	280	677.1	Silt	15	83.2	Silt	22		2
ABB-B-9	342.5	711.4	Surface	0	99	Surface			0
ABB-B-9	342.5	711.4	sand	1	98	sand			9
ABB-B-9	342.5	711.4	sand	3	96	sand			9
ABB-B-9	342.5	711.4	gravely sand	5	94	gravely sand	119		6
ABB-B-9	342.5	711.4	gravely sand	9	90	gravely sand			6
ABB-B-9	342.5	711.4	Silt	9.5	89.5	Silt	30		2
ABB-B-9	342.5	711.4	gravely sand	11	88	gravely sand	30		6
ABB-B-9	342.5	711.4	gravely sand	15	84	gravely sand			6
ABB-B-9	342.5	711.4	Silt	17	82	Silt	24		2
ABB-B-10	211.3	708.3	Surface	0	97.1	Surface			0
ABB-B-10	211.3	708.3	sand	1	96.1	sand			9
ABB-B-10	211.3	708.3	sand	3	94.1	sand	13		9
ABB-B-10	211.3	708.3	sand	5	92.1	sand			9
ABB-B-10	211.3	708.3	sand	5.6	91.5	sand	3		9
ABB-B-10	211.3	708.3	Silt	7	90.1	Silt			2
ABB-B-10	211.3	708.3	Silt	7.4	89.7	Silt	10		2
ABB-B-10	211.3	708.3	silty sand	9	88.1	silty sand	10		5
ABB-B-10	211.3	708.3	sandy gravel	10	87.1	sandy gravel			11

<i>Borehole name</i>	<i>x (ft)</i>	<i>y (ft)</i>	<i>Description</i>	<i>Depth (ft)</i>	<i>z (ft)</i>	<i>Ground type</i>	<i>SPT</i>	<i>RQD</i>	<i>Layer</i>
ABB-B-10	211.3	708.3	sandy gravel	12	85.1	sandy gravel	5		11
ABB-B-10	211.3	708.3	sandy gravel	13	84.1	sandy gravel	17		11
ABB-B-10	211.3	708.3	sand	15	82.1	sand	17		9
ABB-B-11	214.4	658.3	Surface	0	97	Surface			0
ABB-B-11	214.4	658.3	gravel	1	96	gravel			13
ABB-B-11	214.4	658.3	gravel	5	92	gravel			13
ABB-B-11	214.4	658.3	gravely sand	5.9	91.1	gravely sand	150		6
ABB-B-11	214.4	658.3	gravely sand	8	89	gravely sand			6
ABB-B-11	214.4	658.3	Silt	8.4	88.6	Silt	89		2
ABB-B-11	214.4	658.3	sand to gravely sand	10	87	gravely sand	89		6
ABB-B-11	214.4	658.3	gravely sand	12	85	gravely sand	42		6
ABB-B-11	214.4	658.3	sand	15	82	sand	25		9
MW-7	242.5	630.2	Surface	0	100	Surface			0
MW-7	242.5	630.2	sand (narrow graded)	2	98	sand	40		9
MW-7	242.5	630.2	sand (narrow graded)	5	95	sand			9
MW-7	242.5	630.2	Silty sand	6.5	93.5	Silty sand	60		5
MW-7	242.5	630.2	Silty sand	10	90	Silty sand			5
MW-7	242.5	630.2	Silty sand	11.5	88.5	Silty sand	26		5
MW-7	242.5	630.2	Silty sand	15	85	Silty sand			5
MW-7	242.5	630.2	sandy gravel	16.5	83.5	sandy gravel	35		11
MW-7	242.5	630.2	sandy gravel	21	79	sandy gravel			11
MW-7	242.5	630.2	Silt	23	77	Silt	13		2
GZA-1	588.6	526	Surface	0	100	Surface			0
GZA-1	588.6	526	Widely graded sand	2	98	Widely graded sand	51		1
GZA-1	588.6	526	Widely graded sand	5	95	Widely graded sand			1
GZA-1	588.6	526	Silt	7	93	Silt	20		2
GZA-1	588.6	526	Silt	10	90	Silt			2
GZA-1	588.6	526	silty sand	11.2	88.8	silty sand	37		5
GZA-1	588.6	526	Widely graded sand	12	88	Widely graded sand	37		1
GZA-1	588.6	526	silty sand	14	86	silty sand	21		5
GZA-1	588.6	526	silty sand	16	84	silty sand	13		5
GZA-1	588.6	526	silty sand	18	82	silty sand	15		5
GZA-1	588.6	526	silty sand	20	80	silty sand	11		5
GZA-1	588.6	526	silty sand	21.3	78.7	silty sand	26		5
GZA-1	588.6	526	Widely graded sand	22	78	Widely graded sand	26		1
GZA-1	588.6	526	Widely graded sand	25	75	Widely graded sand			1
GZA-1	588.6	526	Widely graded sand	26.2	73.8	Widely graded sand	22		1
GZA-1	588.6	526	Silt	27	73	Silt	22		2
GZA-1	588.6	526	Silt	30	70	Silt			2
GZA-1	588.6	526	clayey Silt	32	68	clayey Silt	21		4
GZA-1	588.6	526	clayey Silt	35	65	clayey Silt			4
GZA-1	588.6	526	clayey Silt	37	63	clayey Silt	22		4
GZA-2	610.8	538.3	Surface	0	100	Surface			0
GZA-2	610.8	538.3	asphalt	0.3	99.7	asphalt			7

<i>Borehole name</i>	<i>x (ft)</i>	<i>y (ft)</i>	<i>Description</i>	<i>Depth (ft)</i>	<i>z (ft)</i>	<i>Ground type</i>	<i>SPT</i>	<i>RQD</i>	<i>Layer</i>
GZA-2	610.8	538.3	Widely graded sand	2.3	97.7	Widely graded sand	150		1
GZA-2	610.8	538.3	Widely graded sand	5	95	Widely graded sand			1
GZA-2	610.8	538.3	Widely graded sand	7	93	Widely graded sand	93		1
GZA-2	610.8	538.3	Widely graded sand	10	90	Widely graded sand			1
GZA-2	610.8	538.3	Widely graded sand	12	88	Widely graded sand	57		1
GZA-2	610.8	538.3	Widely graded sand	14	86	Widely graded sand	91		1
GZA-2	610.8	538.3	Widely graded sand	16	84	Widely graded sand	22		1
GZA-2	610.8	538.3	Widely graded sand	18	82	Widely graded sand	9		1
GZA-2	610.8	538.3	Widely graded sand	18.5	81.5	Widely graded sand	26		1
GZA-2	610.8	538.3	Silt	20	80	Silt	26		2
GZA-2	610.8	538.3	Silt	23	77	Silt			2
GZA-2	610.8	538.3	clayey Silt	25	75	clayey Silt	20		4
GZA-3	753.5	595	Surface	0	100	Surface			0
GZA-3	753.5	595	asphalt	0.3	99.7	asphalt	78		7
GZA-3	753.5	595	Widely graded sand	2.3	97.7	Widely graded sand	78		1
GZA-3	753.5	595	Widely graded sand	5	95	Widely graded sand			1
GZA-3	753.5	595	Widely graded sand	7	93	Widely graded sand	76		1
GZA-3	753.5	595	Widely graded sand	10	90	Widely graded sand			1
GZA-3	753.5	595	Widely graded sand	11.1	88.9	Widely graded sand	82		1
GZA-3	753.5	595	silty sand	12	88	silty sand	82		5
GZA-3	753.5	595	silty sand	14	86	silty sand	77		5
GZA-3	753.5	595	silty sand	16	84	silty sand	20		5
GZA-3	753.5	595	Widely graded sand	18	82	Widely graded sand	45		1
GZA-3	753.5	595	silty sand	20	80	silty sand	12		5
GZA-3	753.5	595	silty sand	20.4	79.6	silty sand	20		5
GZA-3	753.5	595	Widely graded sand	20.5	79.5	Widely graded sand	20		1
GZA-3	753.5	595	clayey Silt	22	78	clayey Silt	20		4
GZA-3	753.5	595	clayey Silt	25	75	clayey Silt			4
GZA-3	753.5	595	silty sand	25.5	74.5	silty sand	20		5
GZA-3	753.5	595	clayey Silt	27	73	clayey Silt	20		4
GZA-3	753.5	595	clayey Silt	30	70	clayey Silt			4
GZA-3	753.5	595	clayey Silt	32	68	clayey Silt	14		4
GZA-3	753.5	595	clayey Silt	34	66	clayey Silt			4
GZA-3	753.5	595	clayey Silt	36	64	clayey Silt	12		4
GZA-4	760.9	439.9	Surface	0	100	Surface			0
GZA-4	760.9	439.9	asphalt	0.3	99.7	asphalt	40		7
GZA-4	760.9	439.9	Widely graded sand	2.3	97.7	Widely graded sand	40		1
GZA-4	760.9	439.9	Widely graded sand	5	95	Widely graded sand			1
GZA-4	760.9	439.9	Widely graded sand	6.4	93.6	Widely graded sand	150		1
GZA-4	760.9	439.9	Widely graded sand	10	90	Widely graded sand			1
GZA-4	760.9	439.9	Silt	11	89	Silt	74		2
GZA-4	760.9	439.9	clayey Silt	12	88	clayey Silt	74		4
GZA-4	760.9	439.9	Widely graded sand	14	86	Widely graded sand	67		1
GZA-4	760.9	439.9	Widely graded sand	16	84	Widely graded sand	47		1

<i>Borehole name</i>	<i>x (ft)</i>	<i>y (ft)</i>	<i>Description</i>	<i>Depth (ft)</i>	<i>z (ft)</i>	<i>Ground type</i>	<i>SPT</i>	<i>RQD</i>	<i>Layer</i>
GZA-4	760.9	439.9	Widely graded sand	16.25	83.8	Widely graded sand	42		1
GZA-4	760.9	439.9	Widely graded sand	17.75	82.3	Widely graded sand	42		1
GZA-4	760.9	439.9	clayey Silt	18	82	clayey Silt	42		4
GZA-4	760.9	439.9	clayey Silt	20	80	clayey Silt	26		4
GZA-4	760.9	439.9	clayey Silt	25	75	clayey Silt			4
GZA-4	760.9	439.9	clayey Silt	27	73	clayey Silt	24		4
GZA-4	760.9	439.9	clayey Silt	30	70	clayey Silt			4
GZA-4	760.9	439.9	Silt	32	68	Silt	15		2
GZA-4	760.9	439.9	Silt	35	65	Silt			2
GZA-4	760.9	439.9	clayey Silt	37	63	clayey Silt	13		4
GZA-4	760.9	439.9	clayey Silt	40	60	clayey Silt			4
GZA-4	760.9	439.9	clayey Silt	42	58	clayey Silt	13		4
GZA-4	760.9	439.9	clayey Silt	45	55	clayey Silt			4
GZA-4	760.9	439.9	clayey Silt	47	53	clayey Silt	18		4
GZA-4	760.9	439.9	clayey Silt	50	50	clayey Silt			4
GZA-4	760.9	439.9	clayey Silt	52	48	clayey Silt	18		4
GZA-4	760.9	439.9	clayey Silt	55	45	clayey Silt			4
GZA-4	760.9	439.9	clayey Silt	57	43	clayey Silt	19		4
GZA-4	760.9	439.9	clayey Silt	60	40	clayey Silt			4
GZA-4	760.9	439.9	clayey Silt	62	38	clayey Silt	15		4
GZA-4	760.9	439.9	clayey Silt	65	35	clayey Silt			4
GZA-4	760.9	439.9	clayey Silt	67	33	clayey Silt	23		4
GZA-4	760.9	439.9	clayey Silt	70	30	clayey Silt			4
GZA-4	760.9	439.9	gravel	70.4	29.6	gravel	150		13
GZA-4	760.9	439.9	gravel	75	25	gravel			13
GZA-4	760.9	439.9	Sandstone	77	23	Sandstone		36	14
GZA-5	509.9	604.8	Surface	0	100	Surface			0
GZA-5	509.9	604.8	Widely graded sand	2	98	Widely graded sand	37		1
GZA-5	509.9	604.8	Widely graded sand	5	95	Widely graded sand			1
GZA-5	509.9	604.8	Widely graded sand	7	93	Widely graded sand	87		1
GZA-5	509.9	604.8	Widely graded sand	10	90	Widely graded sand	74		1
GZA-5	509.9	604.8	Widely graded sand	12	88	Widely graded sand	21		1
GZA-5	509.9	604.8	clayey Silt	14	86	clayey Silt			4
GZA-5	509.9	604.8	clayey Silt	16	84	clayey Silt	22		4
GZA-5	509.9	604.8	clayey Silt	20	80	clayey Silt			4
GZA-5	509.9	604.8	clayey Silt	22	78	clayey Silt	19		4
GZA-5	509.9	604.8	clayey Silt	25	75	clayey Silt			4
GZA-5	509.9	604.8	clayey Silt	27	73	clayey Silt	16		4
GZA-6	569.9	494.8	Surface	0	100	Surface			0
GZA-6	569.9	494.8	Widely graded sand	8	92	Widely graded sand			1
GZA-6	569.9	494.8	Widely graded sand	10	90	Widely graded sand	16		1
GZA-6	569.9	494.8	Widely graded sand	12	88	Widely graded sand	25		1
GZA-6	569.9	494.8	Widely graded sand	14	86	Widely graded sand	27		1
GZA-6	569.9	494.8	Widely graded sand	16	84	Widely graded sand	75		1



<i>Borehole name</i>	<i>x (ft)</i>	<i>y (ft)</i>	<i>Description</i>	<i>Depth (ft)</i>	<i>z (ft)</i>	<i>Ground type</i>	<i>SPT</i>	<i>RQD</i>	<i>Layer</i>
GZA-6	569.9	494.8	Widely graded sand	18	82	Widely graded sand	30		1
GZA-6	569.9	494.8	Widely graded sand	18.25	81.8	Widely graded sand	21		1
GZA-6	569.9	494.8	clayey Silt	20	80	clayey Silt	21		4
GZA-6	569.9	494.8	clayey Silt	29	71	clayey Silt			4
GZA-6	569.9	494.8	clayey Silt	31	69	clayey Silt	15		4
GZA-6	569.9	494.8	clayey Silt	39	61	clayey Silt			4
GZA-6	569.9	494.8	clayey Silt	41	59	clayey Silt	24		4
GZA-6	569.9	494.8	clayey Silt	49	51	clayey Silt			4
GZA-6	569.9	494.8	clayey Silt	51	49	clayey Silt	17		4
GZA-6	569.9	494.8	clayey Silt	59	41	clayey Silt			4
GZA-6	569.9	494.8	clayey Silt	61	39	clayey Silt	23		4
GZA-6	569.9	494.8	clayey Silt	69	31	clayey Silt			4
GZA-6	569.9	494.8	clayey Silt	71	29	clayey Silt	18		4
GZA-6	569.9	494.8	clayey Silt	79	21	clayey Silt	150		4
GZA-6	569.9	494.8	Widely graded sand	81	19	Widely graded sand			1
GZA-7	411.4	339	Surface	0	100	Surface			0
GZA-7	411.4	339	Widely graded sand	2	98	Widely graded sand	59		1
GZA-7	411.4	339	Widely graded sand	5	95	Widely graded sand			1
GZA-7	411.4	339	Widely graded sand	7	93	Widely graded sand	35		1
GZA-7	411.4	339	Widely graded sand	10	90	Widely graded sand			1
GZA-7	411.4	339	Widely graded sand	12	88	Widely graded sand	21		1
GZA-7	411.4	339	Silt	14	86	Silt	19		2
GZA-7	411.4	339	silty sand	14.6	85.4	silty sand	107		5
GZA-7	411.4	339	Widely graded sand	16	84	Widely graded sand	107		1
GZA-7	411.4	339	Widely graded sand	18	82	Widely graded sand	76		1
GZA-7	411.4	339	Widely graded sand	18.2	81.8	Widely graded sand	49		1
GZA-7	411.4	339	silty sand	19.4	80.6	silty sand	49		5
GZA-7	411.4	339	Silty sand	20	80	Silty sand	49		5
GZA-7	411.4	339	Silt	22	78	Silt	65		2
GZA-7	411.4	339	Silt	24	76	Silt			2
GZA-7	411.4	339	Silt	26	74	Silt	25		2
GZA-7	411.4	339	Silt	27	73	Silt			2
GZA-7	411.4	339	clayey Silt	29	71	clayey Silt	37		4
GZA-7	411.4	339	clayey Silt	31	69	clayey Silt	29		4
GZA-7	411.4	339	clayey Silt	34	66	clayey Silt			4
GZA-7	411.4	339	clayey Silt	36	64	clayey Silt	25		4
GZA-7	411.4	339	clayey Silt	39	61	clayey Silt			4
GZA-7	411.4	339	clayey Silt	41	59	clayey Silt	14		4
GZA-7	411.4	339	clayey Silt	44	56	clayey Silt			4
GZA-7	411.4	339	clayey Silt	46	54	clayey Silt	14		4
GZA-7	411.4	339	clayey Silt	50	50	clayey Silt			4
GZA-7	411.4	339	Silty sand	52	48	Silty sand	36		5
GZA-7	411.4	339	Silty sand	54	46	Silty sand			5
GZA-7	411.4	339	Silty sand	56	44	Silty sand	71		5

<i>Borehole name</i>	<i>x (ft)</i>	<i>y (ft)</i>	<i>Description</i>	<i>Depth (ft)</i>	<i>z (ft)</i>	<i>Ground type</i>	<i>SPT</i>	<i>RQD</i>	<i>Layer</i>
GZA-7	411.4	339	Silty sand	59	41	Silty sand			5
GZA-7	411.4	339	Silty sand	61	39	Silty sand	40		5
GZA-7	411.4	339	Silty sand	64	36	Silty sand			5
GZA-7	411.4	339	Silty sand	66	34	Silty sand	177		5
GZA-7	411.4	339	Silty sand	69	31	Silty sand			5
GZA-7	411.4	339	Silty sand	69.3	30.7	Silty sand	150		5
GZA-7	411.4	339	Silty sand	74	26	Silty sand			5
GZA-7	411.4	339	Widely graded sand	74.2	25.8	Widely graded sand	150		1
GZA-7	411.4	339	Widely graded sand	80	20	Widely graded sand			1
GZA-7	411.4	339	Widely graded sand	82	18	Widely graded sand	150		1
GZA-8	359.7	580.2	Surface	0	100	Surface			0
GZA-8	359.7	580.2	asphalt	0.3	99.7	asphalt	79		7
GZA-8	359.7	580.2	Widely graded sand	2.3	97.7	Widely graded sand	79		1
GZA-8	359.7	580.2	Widely graded sand	5	95	Widely graded sand			1
GZA-8	359.7	580.2	Widely graded sand	7	93	Widely graded sand	44		1
GZA-8	359.7	580.2	Widely graded sand	10	90	Widely graded sand			1
GZA-8	359.7	580.2	Peat	10.5	89.5	Peat	40		10
GZA-8	359.7	580.2	Silt	12	88	Silt	40		2
GZA-8	359.7	580.2	clayey Silt	14	86	clayey Silt	52		4
GZA-8	359.7	580.2	clayey Silt	18	82	clayey Silt			4
GZA-8	359.7	580.2	clayey Silt	20	80	clayey Silt	14		4
GZA-9	335.1	469.4	Surface	0	100	Surface			0
GZA-9	335.1	469.4	Widely graded sand	8	92	Widely graded sand			1
GZA-9	335.1	469.4	Widely graded sand	10	90	Widely graded sand	77		1
GZA-9	335.1	469.4	Widely graded sand	12	88	Widely graded sand	57		1
GZA-9	335.1	469.4	Widely graded sand	14	86	Widely graded sand	69		1
GZA-9	335.1	469.4	Widely graded sand	16	84	Widely graded sand	69		1
GZA-9	335.1	469.4	Widely graded sand	18	82	Widely graded sand	58		1
GZA-9	335.1	469.4	clayey Silt	20	80	clayey Silt	14		4
GZA-10	303.1	366	Surface	0	100	Surface			0
GZA-10	303.1	366	Widely graded sand	8	92	Widely graded sand			1
GZA-10	303.1	366	Widely graded sand	10	90	Widely graded sand	19		1
GZA-10	303.1	366	Widely graded sand	12	88	Widely graded sand	27		1
GZA-10	303.1	366	Widely graded sand	13.6	86.4	Widely graded sand	83		1
GZA-10	303.1	366	Widely graded sand	14	86	Widely graded sand	83		1
GZA-10	303.1	366	Widely graded sand	16	84	Widely graded sand	27		1
GZA-10	303.1	366	Widely graded sand	16.8	83.2	Widely graded sand	83		1
GZA-10	303.1	366	clayey Silt	18	82	clayey Silt	83		4
GZA-10	303.1	366	clayey Silt	20	80	clayey Silt			4
GZA-10	303.1	366	clayey Silt	22	78	clayey Silt	29		4
GZA-10	303.1	366	clayey Silt	25	75	clayey Silt			4
GZA-10	303.1	366	clayey Silt	27	73	clayey Silt	28		4
GZA-10	303.1	366	clayey Silt	30	70	clayey Silt			4
GZA-10	303.1	366	clayey Silt	32	68	clayey Silt	30		4

<i>Borehole name</i>	<i>x (ft)</i>	<i>y (ft)</i>	<i>Description</i>	<i>Depth (ft)</i>	<i>z (ft)</i>	<i>Ground type</i>	<i>SPT</i>	<i>RQD</i>	<i>Layer</i>
GZA-10	303.1	366	clayey Silt	35	65	clayey Silt			4
GZA-10	303.1	366	clayey Silt	37	63	clayey Silt	20		4
GZA-10	303.1	366	clayey Silt	40	60	clayey Silt			4
GZA-10	303.1	366	clayey Silt	40.4	59.6	clayey Silt	29		4
GZA-10	303.1	366	Widely graded sand	42	58	Widely graded sand	29		1
GZA-10	303.1	366	Widely graded sand	45	55	Widely graded sand			1
GZA-10	303.1	366	Widely graded sand	47	53	Widely graded sand	150		1
GZA-11	364.6	299.6	Surface	0	100	Surface			0
GZA-11	364.6	299.6	Widely graded sand	2	98	Widely graded sand	32		1
GZA-11	364.6	299.6	Widely graded sand	5	95	Widely graded sand			1
GZA-11	364.6	299.6	Widely graded sand	7	93	Widely graded sand	17		1
GZA-11	364.6	299.6	Widely graded sand	10	90	Widely graded sand			1
GZA-11	364.6	299.6	Widely graded sand	12	88	Widely graded sand	47		1
GZA-11	364.6	299.6	Widely graded sand	12.5	87.5	Widely graded sand			1
GZA-11	364.6	299.6	Widely graded sand	13.9	86.1	Widely graded sand	17		1
GZA-11	364.6	299.6	Silt	14	86	Silt	17		2
GZA-11	364.6	299.6	Widely graded sand	16	84	Widely graded sand	86		1
GZA-11	364.6	299.6	Widely graded sand	18	82	Widely graded sand	38		1
GZA-11	364.6	299.6	silty sand	20	80	silty sand	54		5
GZA-11	364.6	299.6	clayey Silt	22	78	clayey Silt	35		4
GZA-11	364.6	299.6	clayey Silt	25	75	clayey Silt			4
GZA-11	364.6	299.6	clayey Silt	27	73	clayey Silt	19		4
GZA-11	364.6	299.6	clayey Silt	30	70	clayey Silt			4
GZA-11	364.6	299.6	clayey Silt	32	68	clayey Silt	16		4
GZA-11	364.6	299.6	clayey Silt	35	65	clayey Silt			4
GZA-11	364.6	299.6	clayey Silt	37	63	clayey Silt	21		4
GZA-12	455.7	427.6	Surface	0	100	Surface			0
GZA-12	455.7	427.6	Widely graded sand	9	91	Widely graded sand			1
GZA-12	455.7	427.6	Widely graded sand	11	89	Widely graded sand	9		1
GZA-12	455.7	427.6	Widely graded sand	13	87	Widely graded sand	7		1
GZA-12	455.7	427.6	Widely graded sand	15	85	Widely graded sand	72		1
GZA-12	455.7	427.6	Widely graded sand	17	83	Widely graded sand	77		1
GZA-12	455.7	427.6	Widely graded sand	19	81	Widely graded sand	80		1
GZA-12	455.7	427.6	Widely graded sand	20.4	79.6	Widely graded sand	150		1
GZA-12	455.7	427.6	silty sand	21	79	silty sand	150		5
GZA-12	455.7	427.6	silty sand	23	77	silty sand	62		5
GZA-12	455.7	427.6	clayey Silt	25	75	clayey Silt	45		4
GZA-13	381.9	452.2	Surface	0	100	Surface			0
GZA-13	381.9	452.2	Silt	2	98	Silt	7		2
GZA-13	381.9	452.2	Silt	5	95	Silt			2
GZA-13	381.9	452.2	Widely graded sand	7	93	Widely graded sand	8		1
GZA-13	381.9	452.2	Widely graded sand	10	90	Widely graded sand			1
GZA-13	381.9	452.2	Widely graded sand	12	88	Widely graded sand	18		1
GZA-13	381.9	452.2	Silt	14	86	Silt	28		2

<i>Borehole name</i>	<i>x (ft)</i>	<i>y (ft)</i>	<i>Description</i>	<i>Depth (ft)</i>	<i>z (ft)</i>	<i>Ground type</i>	<i>SPT</i>	<i>RQD</i>	<i>Layer</i>
GZA-13	381.9	452.2	Widely graded sand	16	84	Widely graded sand	46		1
GZA-13	381.9	452.2	Widely graded sand	17.2	82.8	Widely graded sand	40		1
GZA-13	381.9	452.2	clayey Silt	18	82	clayey Silt	40		4
GZA-13	381.9	452.2	clayey Silt	20	80	clayey Silt	28		4
GZA-13	381.9	452.2	clayey Silt	22	78	clayey Silt	28		4
GZA-13	381.9	452.2	clayey Silt	25	75	clayey Silt			4
GZA-13	381.9	452.2	clayey Silt	27	73	clayey Silt	13		4
GZA-13	381.9	452.2	clayey Silt	30	70	clayey Silt			4
GZA-13	381.9	452.2	clayey Silt	32	68	clayey Silt	14		4
GZA-13	381.9	452.2	clayey Silt	35	65	clayey Silt			4
GZA-13	381.9	452.2	clayey Silt	37	63	clayey Silt	14		4
GZA-13	381.9	452.2	clayey Silt	40	60	clayey Silt			4
GZA-13	381.9	452.2	clayey Silt	42	58	clayey Silt	18		4
GZA-13	381.9	452.2	clayey Silt	45	55	clayey Silt			4
GZA-13	381.9	452.2	clayey Silt	47	53	clayey Silt	16		4
GZA-13	381.9	452.2	clayey Silt	50	50	clayey Silt			4
GZA-13	381.9	452.2	clayey Silt	52	48	clayey Silt	31		4
GZA-13	381.9	452.2	clayey Silt	55	45	clayey Silt			4
GZA-13	381.9	452.2	Widely graded sand	55.7	44.3	Widely graded sand	150		1
GZA-13	381.9	452.2	Widely graded sand	60	40	Widely graded sand			1
GZA-13	381.9	452.2	Widely graded sand	60.9	39.1	Widely graded sand	150		1
GZA-13	381.9	452.2	Widely graded sand	65	35	Widely graded sand			1
GZA-13	381.9	452.2	Widely graded sand	65.3	34.7	Widely graded sand	150		1
GZA-13	381.9	452.2	Sandstone	67	33	Sandstone		77	4

## Hydrogeologic data: Early Years: 1993-1996

### Acetone-93

Borehole name	x (ft)	y (ft)	Depth (ft)	Elevation (ft)	Ground type	Concentration (ppb)	Layer
ABB-MW-1	-143.75	162.5	0	99.85	Surface	0	0
ABB-MW-1	-143.75	162.5	10.5	89.35	above WT	0	1
ABB-MW-1	-143.75	162.5	17	82.85	Acetone5	15	5
ABB-MW-6	268.75	353.13	0	100.78	Surface	0	0
ABB-MW-6	268.75	353.13	8	92.78	above WT	0	1
ABB-MW-6	268.75	353.13	15	85.78	Acetone5	15	5
ABB-MW-7	242.5	630.18	0	100	Surface	0	0
ABB-MW-7	242.5	630.18	10	90	above WT	0	1
ABB-MW-7	242.5	630.18	17	83	Acetone15	15	5
DPW-1	206.25	-6.25	0	100	Surface	0	0
DPW-1	206.25	-6.25	12	88	above WT	0	1
DPW-1	206.25	-6.25	17	83	Acetone5	15	5
GEI-MW-2	162.5	481.25	0	100	Surface	0	0
GEI-MW-2	162.5	481.25	10	90	above WT	0	1
GEI-MW-2	162.5	481.25	15	85	Acetone1700	1700	27
GEI-MW-7	200	606.25	0	100	Surface	0	0
GEI-MW-7	200	606.25	10	90	above WT	0	1
GEI-MW-7	200	606.25	15	85	Acetone5	15	5

### Acetone-96

Borehole name	x (ft)	y (ft)	Depth (ft)	Elevation (ft)	Ground type	Concentration (ppb)	Layer
ABB-SB-3	390	727.47	0	100	Surface	0	0
ABB-SB-3	390	727.47	13	87	above WT	0	1
ABB-SB-3	390	727.47	17	83	Acetone40	42	10
ABB-SB-4	376.92	651.57	0	100	Surface	0	0
ABB-SB-4	376.92	651.57	9	91	above WT	0	1
ABB-SB-4	376.92	651.57	13	87	Acetone0	0	2
ABB-MW-1	-143.75	162.5	0	99.85	Surface	0	0
ABB-MW-1	-143.75	162.5	10.5	89.35	above WT	0	1
ABB-MW-1	-143.75	162.5	17	82.85	Acetone15	15	5
ABB-MW-6	268.75	353.13	0	100.78	Surface	0	0
ABB-MW-6	268.75	353.13	8	92.78	above WT	0	1
ABB-MW-6	268.75	353.13	15	85.78	Acetone15	15	5
ABB-MW-7	242.5	630.18	0	100	Surface	0	0
ABB-MW-7	242.5	630.18	10	90	above WT	0	1
ABB-MW-7	242.5	630.18	17	83	Acetone15	15	5
ABB-MW-8	619.2	631.2	0	100	Surface	0	0
ABB-MW-8	619.2	631.2	9.5	90.5	above WT	0	1
ABB-MW-8	619.2	631.2	20	80	no data	0	2
ABB-MW-8	619.2	631.2	22	78	Acetone10	12	4
ABB-MW-9	928.8	475.2	0	100	Surface	0	0
ABB-MW-9	928.8	475.2	10	90	above WT	0	1
ABB-MW-9	928.8	475.2	15	85	no data	0	2

**(Acetone-96)**

<b>Borehole name</b>	<b>x (ft)</b>	<b>y (ft)</b>	<b>Depth (ft)</b>	<b>Elevation (ft)</b>	<b>Ground type</b>	<b>Concentration (ppb)</b>	<b>Layer</b>
ABB-MW-9	928.8	475.2	17	83	Acetone5	7	3
ABB-MW-10	528	446.4	0	100	Surface	0	0
ABB-MW-10	528	446.4	10.5	89.5	above WT	0	1
ABB-MW-10	528	446.4	15	85	no data	0	2
ABB-MW-10	528	446.4	19	81	Acetone10	12	4
DPW-1	206.25	-6.25	0	100	Surface	0	0
DPW-1	206.25	-6.25	12	88	above WT	0	1
DPW-1	206.25	-6.25	17	83	Acetone15	15	5
GEI-MW-2	162.5	481.25	0	100	Surface	0	0
GEI-MW-2	162.5	481.25	10	90	above WT	0	1
GEI-MW-2	162.5	481.25	15	85	Acetone1700	1700	27
GEI-MW-7	200	606.25	0	100	Surface	0	0
GEI-MW-7	200	606.25	10	90	above WT	0	1
GEI-MW-7	200	606.25	15	85	Acetone15	15	5

**Arsenic-93**

<b>Borehole name</b>	<b>x (ft)</b>	<b>y (ft)</b>	<b>Depth (ft)</b>	<b>Elevation (ft)</b>	<b>Ground type</b>	<b>Concentration (ppb)</b>	<b>Layer</b>
ABB-MW-1	-143.75	162.5	0	99.85	Surface	0	0
ABB-MW-1	-143.75	162.5	10.5	89.35	above WT	0	1
ABB-MW-1	-143.75	162.5	17	82.85	Arsenic150	150	14
ABB-MW-6	268.75	353.13	0	100.78	Surface	0	0
ABB-MW-6	268.75	353.13	8	92.78	above WT	0	1
ABB-MW-6	268.75	353.13	15	85.78	Arsenic25	25	7
ABB-MW-7	242.5	630.18	0	100	Surface	0	0
ABB-MW-7	242.5	630.18	10	90	above WT	0	1
ABB-MW-7	242.5	630.18	17	83	Arsenic10	10	4
DPW-1	206.25	-6.25	0	100	Surface	0	0
DPW-1	206.25	-6.25	12	88	above WT	0	1
DPW-1	206.25	-6.25	17	83	Arsenic25	25	7
GEI-MW-2	162.5	481.25	0	100	Surface	0	0
GEI-MW-2	162.5	481.25	10	90	above WT	0	1
GEI-MW-2	162.5	481.25	15	85	Arsenic40	39	10
GEI-MW-7	200	606.25	0	100	Surface	0	0
GEI-MW-7	200	606.25	10	90	above WT	0	1
GEI-MW-7	200	606.25	15	85	Arsenic5	5	3

### Arsenic-96

<i>Borehole name</i>	<i>x (ft)</i>	<i>y (ft)</i>	<i>Depth (ft)</i>	<i>Elevation (ft)</i>	<i>Ground type</i>	<i>Concentration (ppb)</i>	<i>Layer</i>
ABB-MW-1	-143.75	162.5	0	99.85	Surface	0	0
ABB-MW-1	-143.75	162.5	10.5	89.35	above WT	0	1
ABB-MW-1	-143.75	162.5	17	82.85	Arsenic150	150	14
ABB-MW-6	268.75	353.13	0	100.78	Surface	0	0
ABB-MW-6	268.75	353.13	8	92.78	above WT	0	1
ABB-MW-6	268.75	353.13	15	85.78	Acetone25	25	7
GEI-MW-2	162.5	481.25	0	100	Surface	0	0
GEI-MW-2	162.5	481.25	10	90	above WT	0	1
GEI-MW-2	162.5	481.25	15	85	Arsenic40	39	10
GEI-MW-7	200	606.25	0	100	Surface	0	0
GEI-MW-7	200	606.25	10	90	above WT	0	1
GEI-MW-7	200	606.25	15	85	Arsenic5	6	3
DPW-1	206.25	-6.25	0	100	Surface	0	0
DPW-1	206.25	-6.25	12	88	above WT	0	1
DPW-1	206.25	-6.25	17	83	Arsenic10	10	4

### Benzene-93

<i>Borehole name</i>	<i>x (ft)</i>	<i>y (ft)</i>	<i>Depth (ft)</i>	<i>Elevation (ft)</i>	<i>Ground type</i>	<i>Concentration (ppb)</i>	<i>Layer</i>
ABB-MW-1	-143.75	162.5	0	99.85	Surface	0	0
ABB-MW-1	-143.75	162.5	10.5	89.35	above WT	0	1
ABB-MW-1	-143.75	162.5	17	82.85	Benzene5	5	3
ABB-MW-6	268.75	353.13	0	100.78	Surface	0	0
ABB-MW-6	268.75	353.13	8	92.78	above WT	0	1
ABB-MW-6	268.75	353.13	15	85.78	Benzene5	5	3
ABB-MW-7	242.5	630.18	0	100	Surface	0	0
ABB-MW-7	242.5	630.18	10	90	above WT	0	1
ABB-MW-7	242.5	630.18	17	83	Benzene10	12	3
DPW-1	206.25	-6.25	0	100	Surface	0	0
DPW-1	206.25	-6.25	12	88	above WT	0	1
DPW-1	206.25	-6.25	17	83	Benzene5	5	3
GEI-MW-2	162.5	481.25	0	100	Surface	0	0
GEI-MW-2	162.5	481.25	10	90	above WT	0	1
GEI-MW-2	162.5	481.25	15	85	Benzene2200	2200	32
GEI-MW-7	200	606.25	0	100	Surface	0	0
GEI-MW-7	200	606.25	10	90	above WT	0	1
GEI-MW-7	200	606.25	15	85	Benzene5	5	3

***Benzene-96***

<b><i>Borehole name</i></b>	<b><i>x (ft)</i></b>	<b><i>y (ft)</i></b>	<b><i>Depth (ft)</i></b>	<b><i>Elevation (ft)</i></b>	<b><i>Ground type</i></b>	<b><i>Concentration (ppb)</i></b>	<b><i>Layer</i></b>
ABB-MW-1	-143.75	162.5	0	99.85	Surface	0	0
ABB-MW-1	-143.75	162.5	10.5	89.35	above WT	0	1
ABB-MW-1	-143.75	162.5	17	82.85	Benzene5	5	3
ABB-MW-6	268.75	353.13	0	100.78	Surface	0	0
ABB-MW-6	268.75	353.13	8	92.78	above WT	0	1
ABB-MW-6	268.75	353.13	15	85.78	Benzene5	5	3
ABB-MW-7	242.5	630.18	0	100	Surface	0	0
ABB-MW-7	242.5	630.18	10	90	above WT	0	1
ABB-MW-7	242.5	630.18	17	83	Benzene10	12	4
DPW-1	206.25	-6.25	0	100	Surface	0	0
DPW-1	206.25	-6.25	12	88	above WT	0	1
DPW-1	206.25	-6.25	17	83	Benzene5	5	3
GEI-MW-2	162.5	481.25	0	100	Surface	0	0
GEI-MW-2	162.5	481.25	10	90	above WT	0	1
GEI-MW-2	162.5	481.25	15	85	Benzene2200	2200	32
GEI-MW-7	200	606.25	0	100	Surface	0	0
GEI-MW-7	200	606.25	10	90	above WT	0	1
GEI-MW-7	200	606.25	15	85	Benzene5	5	3

***Toluene-93***

<b><i>Borehole name</i></b>	<b><i>x (ft)</i></b>	<b><i>y (ft)</i></b>	<b><i>Depth (ft)</i></b>	<b><i>Elevation (ft)</i></b>	<b><i>Ground type</i></b>	<b><i>Concentration (ppb)</i></b>	<b><i>Layer</i></b>
ABB-MW-1	-143.75	162.5	0	99.85	Surface	0	0
ABB-MW-1	-143.75	162.5	10.5	89.35	above WT	0	1
ABB-MW-1	-143.75	162.5	17	82.85	Toluene5	5	3
ABB-MW-6	268.75	353.13	0	100.78	Surface	0	0
ABB-MW-6	268.75	353.13	8	92.78	above WT	0	1
ABB-MW-6	268.75	353.13	15	85.78	Toluene5	5	3
ABB-MW-7	242.5	630.18	0	100	Surface	0	0
ABB-MW-7	242.5	630.18	10	90	above WT	0	1
ABB-MW-7	242.5	630.18	17	83	Toluene5	5	3
DPW-1	206.25	-6.25	0	100	Surface	0	0
DPW-1	206.25	-6.25	12	88	above WT	0	1
DPW-1	206.25	-6.25	17	83	Toluene5	5	3
GEI-MW-2	162.5	481.25	0	100	Surface	0	0
GEI-MW-2	162.5	481.25	10	90	above WT	0	1
GEI-MW-2	162.5	481.25	15	85	Toluene150	130	14
GEI-MW-7	200	606.25	0	100	Surface	0	0
GEI-MW-7	200	606.25	10	90	above WT	0	1
GEI-MW-7	200	606.25	15	85	Toluene5	5	3



***Toluene-96***

<b><i>Borehole name</i></b>	<b><i>x (ft)</i></b>	<b><i>y (ft)</i></b>	<b><i>Depth (ft)</i></b>	<b><i>Elevation (ft)</i></b>	<b><i>Ground type</i></b>	<b><i>Concentration (ppb)</i></b>	<b><i>Layer</i></b>
ABB-SB-3	390	727.47	0	100	Surface	0	0
ABB-SB-3	390	727.47	13	87	above WT	0	1
ABB-SB-3	390	727.47	17	83	toluene5	6	3
ABB-SB-4	376.92	651.57	0	100	Surface	0	0
ABB-SB-4	376.92	651.57	9	91	above WT	0	1
ABB-SB-4	376.92	651.57	13	87	toluene0	0	2
ABB-MW-1	-143.75	162.5	0	99.85	Surface	0	0
ABB-MW-1	-143.75	162.5	10.5	89.35	above WT	0	1
ABB-MW-1	-143.75	162.5	17	82.85	toluene5	5	3
ABB-MW-6	268.75	353.13	0	100.78	Surface	0	0
ABB-MW-6	268.75	353.13	8	92.78	above WT	0	1
ABB-MW-6	268.75	353.13	15	85.78	toluene5	5	3
ABB-MW-7	242.5	630.18	0	100	Surface	0	0
ABB-MW-7	242.5	630.18	10	90	above WT	0	1
ABB-MW-7	242.5	630.18	17	83	toluene5	5	3
ABB-MW-8	619.2	631.2	0	100	Surface	0	0
ABB-MW-8	619.2	631.2	9.5	90.5	above WT	0	1
ABB-MW-8	619.2	631.2	20	80	no data	0	2
ABB-MW-8	619.2	631.2	22	78	toluene0	2	2
ABB-MW-9	928.8	475.2	0	100	Surface	0	0
ABB-MW-9	928.8	475.2	10	90	above WT	0	1
ABB-MW-9	928.8	475.2	15	85	no data	0	2
ABB-MW-9	928.8	475.2	17	83	toluene5	3	3
ABB-MW-10	528	446.4	0	100	Surface	0	0
ABB-MW-10	528	446.4	10.5	89.5	above WT	0	1
ABB-MW-10	528	446.4	15	85	no data	0	2
ABB-MW-10	528	446.4	19	81	toluene5	6	3
DPW-1	206.25	-6.25	0	100	Surface	0	0
DPW-1	206.25	-6.25	12	88	above WT	0	1
DPW-1	206.25	-6.25	17	83	toluene5	5	3
GEI-MW-2	162.5	481.25	0	100	Surface	0	0
GEI-MW-2	162.5	481.25	10	90	above WT	0	1
GEI-MW-2	162.5	481.25	15	85	toluene150	130	14
GEI-MW-7	200	606.25	0	100	Surface	0	0
GEI-MW-7	200	606.25	10	90	above WT	0	1
GEI-MW-7	200	606.25	15	85	toluene5	5	3

## ***Hydrogeologic data: Later years: 1997-2000 (clean-up)***

### ***Trichloroethane-April 1997***

<b>Borehole name</b>	<b>x (ft)</b>	<b>y (ft)</b>	<b>Depth (ft)</b>	<b>Elevation (ft)</b>	<b>Ground type</b>	<b>Concentr. (ppb)</b>	<b>Layer</b>
ABB-MW-1	-143.75	162.5	0	99.85	Surface	0	0
ABB-MW-1	-143.75	162.5	10.5	89.35	above WT	0	1
ABB-MW-1	-143.75	162.5	17	82.85	trichloroethane5	5	3
ABB-MW-6	268.75	353.13	0	100.78	Surface	0	0
ABB-MW-6	268.75	353.13	8	92.78	above WT	0	1
ABB-MW-6	268.75	353.13	15	85.78	trichloroethane5	5	3
ABB-B-10	211.25	708.3	0	100	Surface	0	0
ABB-B-10	211.25	708.3	9	91	above WT	0	1
ABB-B-10	211.25	708.3	14	86	trichloroethane850	830	19
ABB-12	379.2	268.8	0	100	Surface	0	0
ABB-12	379.2	268.8	20	80	no data	0	2
ABB-12	379.2	268.8	22	72	trichloroethane10000	10000	38
ABB-13	648	273.6	0	100	Surface	0	0
ABB-13	648	273.6	20	80	no data	0	2
ABB-13	648	273.6	22	72	trichloroethane5	5	3
ABB-14	381.6	105.6	0	100	Surface	0	0
ABB-14	381.6	105.6	10	90	no data	0	2
ABB-14	381.6	105.6	20	80	trichloroethane550	560	17
ABB-15	331.2	374.4	0	100	Surface	0	0
ABB-15	331.2	374.4	20	80	no data	0	2
ABB-15	331.2	374.4	22	72	trichloroethane96000	96000	48
ABB-16	240	62.4	0	100	Surface	0	0
ABB-16	240	62.4	20	80	no data	0	2
ABB-16	240	62.4	22	72	trichloroethane10	10	4

### ***Trichloroethane-February 1998***

<b>Borehole name</b>	<b>x (ft)</b>	<b>y (ft)</b>	<b>Depth (ft)</b>	<b>Elevation (ft)</b>	<b>Ground type</b>	<b>Concentration</b>	<b>Layer</b>
ABB-MW-1	-143.75	162.5	0	99.85	Surface	0	0
ABB-MW-1	-143.75	162.5	10.5	89.35	above WT	0	1
ABB-MW-1	-143.75	162.5	17	82.85	trichloroethane0	0	2
ABB-MW-6	268.75	353.13	0	100.78	Surface	0	0
ABB-MW-6	268.75	353.13	8	92.78	above WT	0	1
ABB-MW-6	268.75	353.13	15	85.78	trichloroethane5	2	3
ABB-B-10	211.25	708.3	0	100	Surface	0	0
ABB-B-10	211.25	708.3	9	91	above WT	0	1
ABB-B-10	211.25	708.3	14	86	trichloroethane100	90	13
ABB-12	379.2	268.8	0	100	Surface	0	0
ABB-12	379.2	268.8	20	80	no data	0	2
ABB-12	379.2	268.8	22	72	trichloroethane10000	14000	38
ABB-13	648	273.6	0	100	Surface	0	0
ABB-13	648	273.6	20	80	no data	0	2
ABB-13	648	273.6	22	72	trichloroethane0	0	2

***(Trichloroethane-February 1998)***

<b>Borehole name</b>	<b>x (ft)</b>	<b>y (ft)</b>	<b>Depth (ft)</b>	<b>Elevation (ft)</b>	<b>Ground type</b>	<b>Concentration</b>	<b>Layer</b>
ABB-14	381.6	105.6	0	100	Surface	0	0
ABB-14	381.6	105.6	10	90	no data	0	2
ABB-14	381.6	105.6	20	80	trichloroethane1700	1700	27
ABB-15	331.2	374.4	0	100	Surface	0	0
ABB-15	331.2	374.4	20	80	no data	0	2
ABB-15	331.2	374.4	22	72	trichloroethane150000	150000	49
ABB-16	240	62.4	0	100	Surface	0	0
ABB-16	240	62.4	20	80	no data	0	2
ABB-16	240	62.4	22	72	trichloroethane10	10	4

***Trichloroethane-April 1998***

<b>Borehole name</b>	<b>x (ft)</b>	<b>y (ft)</b>	<b>Depth (ft)</b>	<b>Elevation (ft)</b>	<b>Ground type</b>	<b>Concentration</b>	<b>Layer</b>
ABB-MW-1	-143.75	162.5	0	99.85	Surface	0	0
ABB-MW-1	-143.75	162.5	10.5	89.35	above WT	0	1
ABB-MW-1	-143.75	162.5	17	82.85	trichloroethane0	0	2
ABB-MW-6	268.75	353.13	0	100.78	Surface	0	0
ABB-MW-6	268.75	353.13	8	92.78	above WT	0	1
ABB-MW-6	268.75	353.13	15	85.78	trichloroethane0	1.4	2
ABB-B-10	211.25	708.3	0	100	Surface	0	0
ABB-B-10	211.25	708.3	9	91	above WT	0	1
ABB-B-10	211.25	708.3	14	86	trichloroethane100	84	13
ABB-12	379.2	268.8	0	100	Surface	0	0
ABB-12	379.2	268.8	20	80	no data	0	2
ABB-12	379.2	268.8	22	72	trichloroethane10000	10000	38
ABB-13	648	273.6	0	100	Surface	0	0
ABB-13	648	273.6	20	80	no data	0	1
ABB-13	648	273.6	22	72	trichloroethane0	0	2
ABB-14	381.6	105.6	0	100	Surface	0	0
ABB-14	381.6	105.6	10	90	no data	0	2
ABB-14	381.6	105.6	20	80	trichloroethane3300	3300	34
ABB-15	331.2	374.4	0	100	Surface	0	0
ABB-15	331.2	374.4	20	80	no data	0	2
ABB-15	331.2	374.4	22	72	trichloroethane100000	100000	48
ABB-16	240	62.4	0	100	Surface	0	0
ABB-16	240	62.4	20	80	no data	0	2
ABB-16	240	62.4	22	72	trichloroethane10	10	4

### Trichloroethane-May 1998

Borehole name	x (ft)	y (ft)	Depth (ft)	Elevation (ft)	Ground type	Concentration	Layer
ABB-MW-1	-143.75	162.5	0	99.85	Surface	0	0
ABB-MW-1	-143.75	162.5	10.5	89.35	above WT	0	1
ABB-MW-1	-143.75	162.5	17	82.85	trichloroethane0	1	2
ABB-MW-6	268.75	353.13	0	100.78	Surface	0	0
ABB-MW-6	268.75	353.13	8	92.78	above WT	0	1
ABB-MW-6	268.75	353.13	15	85.78	trichloroethane0	1	2
ABB-B-10	211.25	708.3	0	100	Surface	0	0
ABB-B-10	211.25	708.3	9	91	above WT	0	1
ABB-B-10	211.25	708.3	14	86	trichloroethane100	78	13
ABB-12	379.2	268.8	0	100	Surface	0	0
ABB-12	379.2	268.8	20	80	no data	0	2
ABB-12	379.2	268.8	22	72	trichloroethane7000	7300	35
ABB-13	648	273.6	0	100	Surface	0	0
ABB-13	648	273.6	20	80	no data	0	2
ABB-13	648	273.6	22	72	trichloroethane0	1	2
ABB-14	381.6	105.6	0	100	Surface	0	0
ABB-14	381.6	105.6	10	90	no data	0	2
ABB-14	381.6	105.6	20	80	trichloroethane3000	3500	31
ABB-15	331.2	374.4	0	100	Surface	0	0
ABB-15	331.2	374.4	20	80	no data	0	2
ABB-15	331.2	374.4	22	72	trichloroethane100000	100000	48
ABB-16	240	62.4	0	100	Surface	0	0
ABB-16	240	62.4	20	80	no data	0	2
ABB-16	240	62.4	22	72	trichloroethane5	5	3

### Trichloroethane-July 1998

Borehole name	x (ft)	y (ft)	Depth (ft)	Elevation (ft)	Ground type	Concentration	Layer
ABB-MW-1	-143.75	162.5	0	99.85	Surface	0	0
ABB-MW-1	-143.75	162.5	10.5	89.35	above WT	0	1
ABB-MW-1	-143.75	162.5	17	82.85	trichloroethane0	1	2
ABB-MW-6	268.75	353.13	0	100.78	Surface	0	0
ABB-MW-6	268.75	353.13	8	92.78	above WT	0	1
ABB-MW-6	268.75	353.13	15	85.78	trichloroethane0	1	2
ABB-B-10	211.25	708.3	0	100	Surface	0	0
ABB-B-10	211.25	708.3	9	91	above WT	0	1
ABB-B-10	211.25	708.3	14	86	trichloroethane100	100	13
ABB-12	379.2	268.8	0	100	Surface	0	0
ABB-12	379.2	268.8	20	80	no data	0	2
ABB-12	379.2	268.8	22	72	trichloroethane1200	1200	22
ABB-13	648	273.6	0	100	Surface	0	0
ABB-13	648	273.6	20	80	no data	0	2
ABB-13	648	273.6	22	72	trichloroethane0	1	2
ABB-14	381.6	105.6	0	100	Surface	0	0
ABB-14	381.6	105.6	10	90	no data	0	2
ABB-14	381.6	105.6	20	80	trichloroethane4100	4100	32

***(Trichloroethane-July 1998)***

ABB-15	331.2	374.4	0	100	Surface	0	0
ABB-15	331.2	374.4	20	80	no data	0	2
ABB-15	331.2	374.4	22	72	trichloroethane63000	63000	34
ABB-16	240	62.4	0	100	Surface	0	0
ABB-16	240	62.4	20	80	no data	0	2
ABB-16	240	62.4	22	72	trichloroethane0	1	2

***Trichloroethane-September 1998***

<b><i>Borehole name</i></b>	<b><i>x (ft)</i></b>	<b><i>y (ft)</i></b>	<b><i>Depth (ft)</i></b>	<b><i>Elevation (ft)</i></b>	<b><i>Ground type</i></b>	<b><i>Concentration</i></b>	<b><i>Layer</i></b>
ABB-MW-1	-143.75	162.5	0	99.85	Surface	0	0
ABB-MW-1	-143.75	162.5	10.5	89.35	above WT	0	1
ABB-MW-1	-143.75	162.5	17	82.85	trichloroethane0	1	2
ABB-MW-6	268.75	353.13	0	100.78	Surface	0	0
ABB-MW-6	268.75	353.13	8	92.78	above WT	0	1
ABB-MW-6	268.75	353.13	15	85.78	trichloroethane0	1	2
ABB-B-10	211.25	708.3	0	100	Surface	0	0
ABB-B-10	211.25	708.3	9	91	above WT	0	1
ABB-B-10	211.25	708.3	14	86	trichloroethane200	170	15
ABB-12	379.2	268.8	0	100	Surface	0	0
ABB-12	379.2	268.8	20	80	no data	0	2
ABB-12	379.2	268.8	22	72	trichloroethane2900	2900	34
ABB-13	648	273.6	0	100	Surface	0	0
ABB-13	648	273.6	20	80	no data	0	2
ABB-13	648	273.6	22	72	trichloroethane0	1	2
ABB-14	381.6	105.6	0	100	Surface	0	0
ABB-14	381.6	105.6	10	90	no data	0	2
ABB-14	381.6	105.6	20	80	trichloroethane2300	2300	30
ABB-15	331.2	374.4	0	100	Surface	0	0
ABB-15	331.2	374.4	20	80	no data	0	2
ABB-15	331.2	374.4	22	72	trichloroethane78000	78000	46
ABB-16	240	62.4	0	100	Surface	0	0
ABB-16	240	62.4	20	80	no data	0	2
ABB-16	240	62.4	22	72	trichloroethane0	1	2

***Trichloroethane-August 1999***

<b><i>Borehole name</i></b>	<b><i>x (ft)</i></b>	<b><i>y (ft)</i></b>	<b><i>Depth (ft)</i></b>	<b><i>Elevation (ft)</i></b>	<b><i>Ground type</i></b>	<b><i>Concentration</i></b>	<b><i>Layer</i></b>
ABB-MW-1	-143.75	162.5	0	99.85	Surface	0	0
ABB-MW-1	-143.75	162.5	10.5	89.35	above WT	0	1
ABB-MW-1	-143.75	162.5	17	82.85	trichloroethane0	1	2
ABB-MW-6	268.75	353.13	0	100.78	Surface	0	0
ABB-MW-6	268.75	353.13	8	92.78	above WT	0	1
ABB-MW-6	268.75	353.13	15	85.78	trichloroethane10	10	4
ABB-B-10	211.25	708.3	0	100	Surface	0	0
ABB-B-10	211.25	708.3	9	91	above WT	0	1
ABB-B-10	211.25	708.3	14	86	trichloroethane50	46	12

***(Trichloroethane-August 1999)***

ABB-12	379.2	268.8	0	100	Surface	0	0
ABB-12	379.2	268.8	20	80	no data	0	2
ABB-12	379.2	268.8	22	72	trichloroethane790	790	19
ABB-13	648	273.6	0	100	Surface	0	0
ABB-13	648	273.6	20	80	no data	0	2
ABB-13	648	273.6	22	72	trichloroethane0	1	2
ABB-14	381.6	105.6	0	100	Surface	0	0
ABB-14	381.6	105.6	10	90	no data	0	2
ABB-14	381.6	105.6	20	80	trichloroethane300	300	16
ABB-15	331.2	374.4	0	100	Surface	0	0
ABB-15	331.2	374.4	20	80	no data	0	2
ABB-15	331.2	374.4	22	72	trichloroethane85000	85000	47
ABB-16	240	62.4	0	100	Surface	0	0
ABB-16	240	62.4	20	80	no data	0	2
ABB-16	240	62.4	22	72	trichloroethane10	10	4

***Trichloroethane-January 2000***

<b><i>Borehole name</i></b>	<b><i>x (ft)</i></b>	<b><i>y (ft)</i></b>	<b><i>Depth (ft)</i></b>	<b><i>Elevation (ft)</i></b>	<b><i>Ground type</i></b>	<b><i>Concentration</i></b>	<b><i>Layer</i></b>
ABB-MW-1	-143.75	162.5	0	99.85	Surface	0	0
ABB-MW-1	-143.75	162.5	10.5	89.35	above WT	0	1
ABB-MW-1	-143.75	162.5	17	82.85	trichloroethane5	5	3
ABB-MW-6	268.75	353.13	0	100.78	Surface	0	0
ABB-MW-6	268.75	353.13	8	92.78	above WT	0	1
ABB-MW-6	268.75	353.13	15	85.78	trichloroethane5	5	3
ABB-B-10	211.25	708.3	0	100	Surface	0	0
ABB-B-10	211.25	708.3	9	91	above WT	0	1
ABB-B-10	211.25	708.3	14	86	trichloroethane5	6	3
ABB-12	379.2	268.8	0	100	Surface	0	0
ABB-12	379.2	268.8	20	80	no data	0	2
ABB-12	379.2	268.8	22	72	trichloroethane2400	2400	30
ABB-13	648	273.6	0	100	Surface	0	0
ABB-13	648	273.6	20	80	no data	0	2
ABB-13	648	273.6	22	72	trichloroethane5	5	3
ABB-14	381.6	105.6	0	100	Surface	0	0
ABB-14	381.6	105.6	10	90	no data	0	2
ABB-14	381.6	105.6	20	80	trichloroethane130	130	13
ABB-15	331.2	374.4	0	100	Surface	0	0
ABB-15	331.2	374.4	20	80	no data	0	2
ABB-15	331.2	374.4	22	72	trichloroethane29000	29000	40
ABB-16	240	62.4	0	100	Surface	0	0
ABB-16	240	62.4	20	80	no data	0	2
ABB-16	240	62.4	22	72	trichloroethane5	5	3

## ***APPENDIX V:***

### ***Contamination treatment techniques in site remediation: Soil vapor extraction and Air sparging***





## Appendix V: Contamination treatment techniques in site remediation: Soil vapor extraction and Air sparging<sup>1</sup>.

### V.1: Soil vapor extraction

Soil vapor extraction removes volatile organic components from the unsaturated zone by passing large volumes of air through the zone of contamination. Airflow through the spill is maintained by vacuum pumping in one or more wells. At the surface, treatment is usually required in order to remove contaminants from the air before it is released to the atmosphere. The method is one of the few alternatives to remove contaminants from the unsaturated zone, where pure organic liquids often occur at residual saturation. It also works with dissolved contaminants occurring in soil water or sorbed to soils, and in combination with the air sparging technique. Finally, an important feature of the method is that it is able to treat relatively large volumes of material with minimal disruption at the surface.

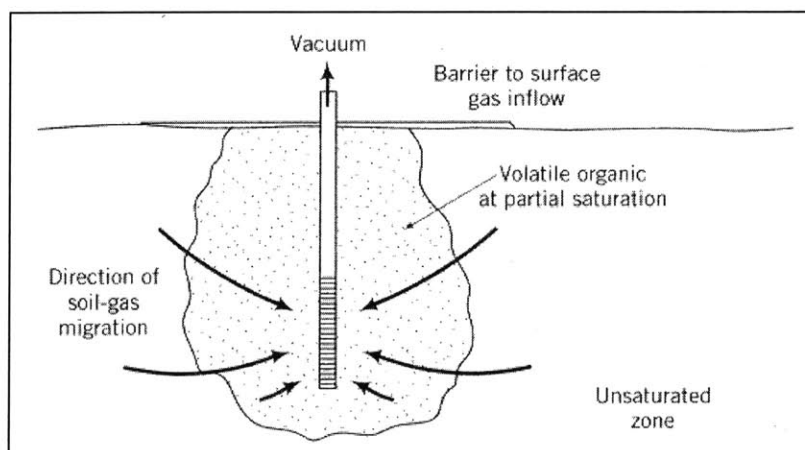


*Figure V.1: Principle of soil vapor extraction.*

**Mechanism:** Vacuum blowers in combination with soil-gas extraction wells are used to create airflow through the zone of contamination. The contaminants volatilize into this air stream (at concentrations dictated by their vapor pressure). The Volatile Organic

<sup>1</sup> Material taken from [8] "Physical and Chemical Hydrogeology".

Compounds (VOCs) carried to the well are removed and the air stream is cleaned up by carbon absorption or some type of thermal treatment (incineration or catalytic oxidation).

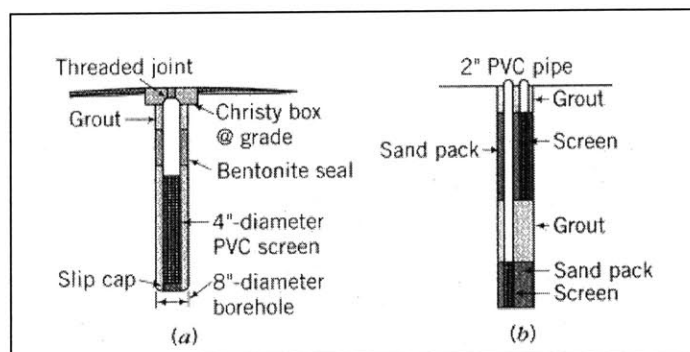


Figure V.2: Examples of extraction wells. (a) is a single well completion (from U.S. EPA, 1991). (b) is a multiwell completion.

For the soil vapor technique to work, the organic compound or the mixture of the organic compounds at the subsurface must be somewhat volatile. This means that the rate of volatilization into the moving air phase must be sufficiently large to reduce the total contaminant mass over a meaningful time frame. A rule of thumb for considering soil vapor extraction for a given contaminant is a vapor pressure greater than 0.015 atm. A list of contaminants that can be cleaned up using soil vapor extraction is given at Figure V.3.

<b>Volatiles:</b>	methanol
benzene	acetone
toluene	pyridine
xylenes	tetrahydrofuran
ethylbenzene	carbon tetrachloride
hexane	trichloroethane (TCA)
chloroform	<b>Semivolatiles:</b>
methylene chloride	chlorobenzene
tetrachloroethylene (PCE)	dichlorobenzene (DCB)
trichloroethylene (TCE)	trichloropropane
dichloroethylene (DCE)	<b>Hydrocarbons:</b>
ethyl acetate	gasoline
cyclohexane	jet fuel
methyl ethyl ketone (MEK)	diesel
methyl isobutyl ketone (MIBK)	kerosene
	heavy naphthas

From U.S. EPA (1989b).

Figure V.3: List of contaminants that can be cleaned up using soil vapor extraction.

## V.2: Air Sparging

Air sparging is a technique to recover volatile organic compounds, semivolatiles, chlorinated solvents and some petroleum compounds ( $C_3 - C_{10}$ ) from the saturated ground water system. Air is injected into the zone of contamination, it flows through channels and it forms an in-situ air stripping system, as volatile contaminants partition into the airflow. The contaminant-laden air arriving at the water table is then collected by soil vapor extraction techniques.

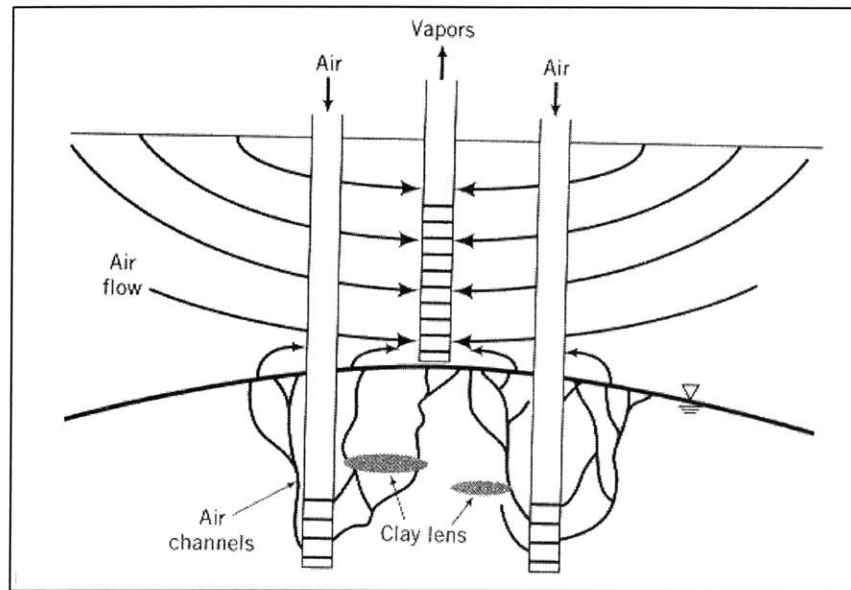


*Figure V.4: Principle of air sparging system*

**Mechanism:** Airflow occurs in channels. As soon as a sparging well is turned on, a pocket of pressurized air begins following the path of least resistance. This consists of media having the lowest air entry pressure, or lowest capillary pressure, thus the largest pore size (highest permeability). Lower permeability units are by-passed. Once air channels are established, they are maintained as long as the air-entry pressure is maintained. Important is that the airflow find its way to the unsaturated zone. The presence of low permeability layers may cause the formation of gas pockets and the lateral spreading of contaminants. Thus, geology should be considered before the application of the method.

Contaminants are removed because dissolved VOCs partition into the adjacent air phase. With time, the contaminant concentrations decrease adjacent to the air channel. In this way a concentration gradient is established, which promotes the further diffusion of contaminants towards the air channels.

A disadvantage of the method is that the addition of oxygen may promote biodegradation, but generally many VOCs are not biodegradable under oxic conditions (oxic ground conditions refer to ground conditions containing  $O_2$ ,  $NO_3^-$ ,  $MnO_2$ , etc; these have a tendency to remove electrons from organic compounds).